2011

DEVELOPMENT OF FREE-LABEL SENSING IN PLASTIC MICROFLUIDIC PLATFORMS USING PULSED STREAMING POTENTIALS (PSP)

Vera Fernando Luna
Virginia Commonwealth University

Fernando Luna Vera **2011**

Development of Label-Free Sensing in Plastic Microfluidic Platforms using Pulsed Streaming Potentials (PSP)

A dissertation submitted in partial fulfillment of the requirements for the degree of Doctor of Philosophy at Virginia Commonwealth University.

by

Fernando Luna vera

Director: Julio C. Alvarez

PhD, Chemistry Department

Virginia Commonwealth University

Richmond, Virginia

May, 2011

Acknowledgment

The author wishes to thank several people. I would like to thank my parents, Arturo Luna Lopez and Julia Vera Rey, for their love, support and patience during the past five years it has taken me to graduate. I would also like to thank Dr. Alvarez for his help with this project finding the economic resources and for providing an appropriate environment for free-thinking . I would like to thank additionally to my family for always caring and being aware of every little step I made in this journey. I would like to thank my friends who have been a tremendous support and always encouraged me to keep working even in the moments of highest weakness. And finally I want to thank to USA and VCU for giving me the opportunity to study my doctorate.

Table of content

Table of Illustrations

Abstract

DEVELOPMENT OF FREE-LABEL SENSING IN PLASTIC MICROFLUIDIC PLATFORMS USING PULSED STREAMING POTENTIALS (PSP)

By FERNANDO LUNA VERA, PhD

A dissertation submitted in partial fulfillment of the requirements for the degree of Doctor of Philosophy at Virginia Commonwealth University.

Virginia Commonwealth University, 2011

Major Director: Thesis / Julio C. Alvarez, PhD, Chemistry Department

This work deals with the development of a new label-free detection technique called Pulsed Streaming Potential (PSP). Its novelty relies on the adaptation of a classical electrokinetic phenomenon (streaming potential) into a tool which can evaluate molecular interplay in label-free fashion. Implementation of PSP to microfluidic platforms allowed the label-free sensing of binding events to plastic (modified and unmodified) surfaces. It was demonstrated the use of real time PSP in plastic microfluidic platforms for determination of kinetic parameters of the interaction of proteins and plastic surfaces. Moreover, initial change of PSP after adsorption of proteins showed to be proportional to the bulk concentration of proteins and it was used for quantification of Lysozyme in the nanomolar range. Several approaches were studied to manipulate the surface of microfluidic channels in order to improve selectivity of PSP through reduction of non-specific adsorption. These approaches included the fabrication of composite surface of polyacrilic acid (PAA) and polyethylene glycol acrylate (PEGA) on cyclic olefin copolymer microchannels, as well as adsorption of nanospheres on COC-PEGA channels.

1 Introduction

This chapter presents the motivations that led this investigation, the main objective and its relevance within the field of biosensing and free-label studies of protein interactions. A short historical perspective is also provided.

1.1 Need for label-free detection systems

A big part of modern biochemistry and its implications for human development, like medicines and disease control, are based on the realization that complexity involved in biological functions comes from the high diversity of precise and efficient interactions, from the atomic to the organism level. From that perspective, tools that allow the observation of specific molecular correspondences are of high importance because they can be used to unveil molecular pathways and key interactions.

In this work, a new methodology to observe and quantify such molecular interactions is investigated. Its innovation relies on the adaptation and use of a classical electrokinetic phenomenon (streaming potential) into a tool which can evaluate molecular interplay in label-free fashion.

In general, the assessment of complimentary interactions such as enzyme-substrate, antibody-antigen, DNA strands and drug-receptor has been well established and implemented during the last five decades. Historically, techniques involving chemical tagging were dominant before any label free method appeared as an alternative for assessment of such interactions. Radioactive and fluorescent labels, for example, have served not just as tool to pair complementary structures but also to allow accurate and selective quantification of relevant targets.

The concept of using molecular labels to report a specific interaction can be traced back to 1960 when Solomon Berson and Rosalyn Yalow described for the first time the Radio InmunoAssay (RIA) method.[1] This technique uses a radioactive iodine tag (Iodine-131 or 125) linked to a

recognizing agent (antibody or antigen) which reports the specific interaction by emission of radiation. Figure 1.1A-B shows the main steps used in a RIA analysis as well as the original result from Yalow showing the separation of a biological sample and its corresponding emission of radioactivity.

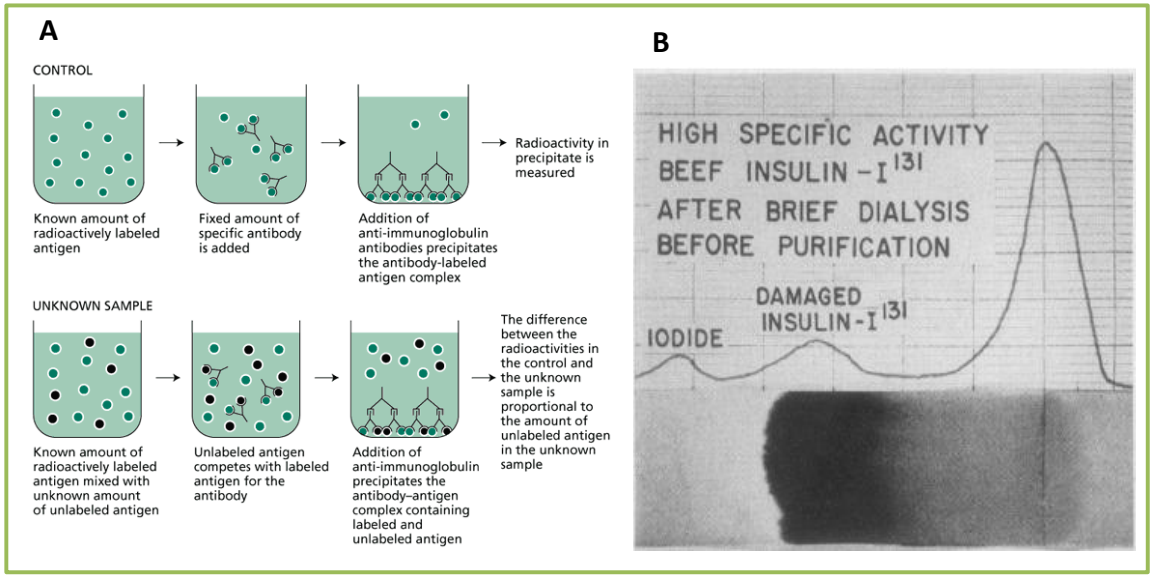

Figure 1.1. Radioactive Immuno-assay (RIA) and signal
A. Inmunoassay protocol (figure from Ref: [2]). **B**. Paper electrophoretic separation of a mixture of I^{131} labeled beef insulin after reaction with specific antibodies. Peaks from right to left represent: free I^{131} insulin, antibody bound I^{131} insulin and free I (Figure from Ref: [3]).

This method allowed for the reliable quantification of pM concentrations of important endogenous molecules for which the concentration was not known before, like insulin in serum. After its first report, RIA was extensively used to quantify peptides of high biological relevance like thyroxine (hormone from thyroid gland), somatostatin (growth hormone), enkephalins (Detection and control of noxious stimuli).[4] However, RIA represented a health risk for the experimenter because of the β and γ radiation released. This drawback implied huge investments in the construction of special facilities in order to handle radioactive materials. Nevertheless, the

importance of RIA was globally recognized by awarding its two creators with the 1979 Nobel Prize in physiology.

In the early 70's the use of new molecular labels came into play to address some of the RIA drawbacks. In 1971, Engvall and Perlmann published a paper on a technique known as Enzyme-Linked Immunosorbent Assay (ELISA). In this method an enzyme covalently attached to an antigen or antibody is used to catalyze the production of fluorescent or color absorbing molecules, which report the antibody-antigen interaction. Figure 1.2A depicts this concept and shows how capture, detection and tagged antibodies are allocated to detect the target protein by light absorption from tetramethylbenzidibe (TMB). Figure 1.2B shows the result of the ELISA analysis of a virus protein using HRP tagged antibody and o-phenylenediamine as reporting molecule.

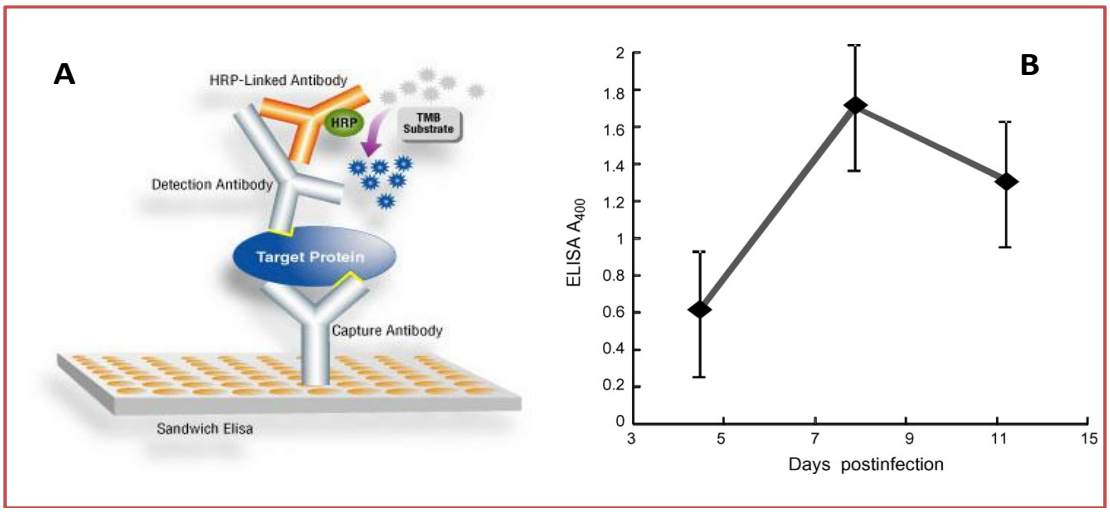

Figure 1.2. Enzyme-linked Immunosorbent Assay (ELISA). Format and signal.

A. Cartoon depicting a sandwich ELISA assay. A recognizing agent (antibody) is linked to the surface where target protein binds. Horse Radish Peroxidase (HRP) linked to a secondary antibody transform an appropriate substrate (3,3',5,5' tetramethylbenzidibe, TMB) in a colored product. Absorption corresponds with amount of target protein bound (copyright: www.wellsphere.com). **B**. Absorption at 400 nm of o-Phenylenediamine from an ELISA assay which used anti-avian influenza virus (H7N1) antibody (HRP tagged) collected from chicken plasma at different days after infection with AIV, as recognizing agent. The antibodies recognized the viral surface protein H7N1 HA1 (modified from Ref: [5]).

ELISA quickly became an essential tool, and its efficiency established its use for detection of viral agents like HIV, Hepatitis B, Rubella and Toxoplasmosis by screening for their corresponding antibodies in body fluids[6]. Additionally, using enzyme-based, non-radioactive tags conveyed the advantage of signal amplification. Since each linked enzyme can produce thousands of reporting molecules, very low detection limits were safely attainable, in the 10 pM range.[7]

However, portability and time of analysis are some disadvantages of methods that use molecular labels. ELISA, for example, is a time consuming procedure and requires skillful users. Commercial ELISA protocols employ three days of laboratory work involving steps for antibody coating, blocking of non-specific sites, washing, sample introduction, secondary antibody introduction and signal analysis.[8] Additionally, the signal producing step must be carefully optimized since some enzymes require cofactors like Mg^{2+} to work properly. Furthermore, quenching by interferences and self-quenching can easily happen.[9]

Obviously, labeled methods have been of enormous importance, but the ever growing search for faster, user-friendly, more cost-efficient technologies that are able to produce more valuable information have driven the recent development of the so called "label free" methods. Label-free technology has become promising and better suited to contemporary demands like for example, miniaturization, which has strong relationship with the development of point-of-care and warfare testing devices.

Label-free methods have a fundamental advantage over labeled ones: *they do not rely on a linked molecule to report interactions*. Instead, they use an inherent property of the query itself like

mass, dielectric constant or charge. This is advantageous because no tag has to be bind to a receptor or target prior to the analysis, which extensively reduces the time of analysis.

Additionally, label-free methods allow the option for real-time analysis, where the interaction of molecules or substrates can be studied versus time and without the potential complication of bias introduced by the tag itself. Some studies have shown, for example, that kinetic parameters obtained using tagged molecules can be seriously miss-estimated since the label itself can hinder or embolden interactions with receptors.[10] In reality, labeled methods require an extensive development to assure that the label does not block any important site on the recognizing agent used, such as antibodies.[10]

Real time analysis capabilities are of huge relevance for the pharmaceutical industry and the race for finding new drugs and therapeutic agents, since many medicines like anti-inflammatories[11], antidepressants[12] and antibiotics, amongst many others, use some sort of inhibitory mechanism of action. An inhibitory mechanism implies that the affinity of the therapeutic agent for a specific receptor, like cell membrane receptors, have to be studied and accurately estimated in order to ensure selectivity. Selectivity of a therapeutic agent for a receptor is a process that is performed in early stages of drug discovery and sometimes called "hit discovery".[13]

Therefore, modern label-free techniques of analysis like Surface Plasmon Resonance (SPR), Label-free internal reflection ellipsometry (LFIRE), Interferometry, Quartz Crystal Microbalance (QCM) and Electrical Impedance are gaining territory and acceptance as valuable tools to cope with current demands on molecular interaction and sensing investigation. Moreover, due to their potential advantages there is still a lot of interest in developing label-free methods.

This thesis deals with the development of an alternative and new label-free detection technique called Pulsed Streaming Potential (PSP). Its novelty relies on the adaptation and implementation of "streaming potential" to microfluidic platforms which allows the label-free sensing of binding events to plastic (modified and unmodified) surfaces. Additionally, it will be shown, that Pulsed Streaming Potentials have the prospective to be a general detection method for microfluidic platforms.

1.2 The leading question

For this work a leading question was formulated: *Can pulsed streaming potentials (PSP) be used as transduction systems for the label-free sensing of molecular interactions at the surface of microfluidic devices?* That is the principal aim of this work, the exploration of the ability of pulsed streaming potentials as a label-free transduction method in microfluidic platforms. As explained further in the following chapters, pulsed streaming potentials have several advantages over existing methods: for instance, the signal is a result of the pressure-driven flow which makes it very attractive for pressure actuated micro-devices.

Additionally, the instrumentation for these measurements does not require complicated equipment which could lead to portable and cost-effective biosensing devices.[14]

However, full application of pulsed streaming potential requires the demonstration of its ability to sense absorption of specific targets while controlling non-specific binding, as well as to demonstrate its ability to produce reliable information of target-receptor interaction.

1.3 Thesis outline

In Chapter 2 some background is provided dealing with the design and principal constituents of sensors. Special attention is placed on general guidelines for designing surfaces at sensing elements. Additionally, in Chapter 2 a survey of the current transduction methodologies used for label-free detection is provided. Chapter 3 presents the general instrumentation used to generate PSP including fabrication of microfluidic platforms. A general description of the benefits obtained from pulsed generation of streaming potentials is presented. Additionally, the use of non-dynamic PSP is shown for the cases of Self Assembled Monolayers on gold and Copper. In Chapter 4 the dynamic mode of PSP is introduced as well as its use for the study of non-specific adsorption of lysozyme on plastic microchannels. Chapter 5 describes the design and construction of a composite surface that reduces non-specific adsorption while providing selectivity to the real-time analysis of lysozyme through the immobilization of polyclonal antibodies to the sensing element. Finally, in Chapter 6 a new approach to improve selectivity is explored by construction of a dual COC-PEGA- nanospheres surface on the microchannel, where monoclonal antibodies can be bonded and used to detect Prostate Specific Antigen (PSA) by Pulsed Streaming Potentials.

1.4 References.

1. Lequin, R. M., Enzyme Immunoassay (EIA)/Enzyme-Linked Immunosorbent Assay. *Clin.Chem* **2005,** 51, (12), 2415-2418.
2. Taiz, L., Zeiger, E. Topic 19.3: Auxin Measurement by Radioimmunoassay. 2006.
3. Yalow, S. R., Solomon, A.B., Immunoassay of endogenous plasma insulin in man. *J.Clin Invest.* **1960,** 39, (7), 1157-1175.
4. Desiderio, D. M., *Liquid chromatography and mass spectrometry*. Elsevier Science Publishers: Amsterdam, 1984; Vol. 6.
5. Velumani, S., Du, Q., Fenner, J.B., Prabakaran, M., Wee, L.C., Nuo, L.Y., Kwang, J., Development of an antigen-capture ELISA for detection of H7 subtype avian influenza from experimentally infected chickens. *J.Virol.Methods* **2008,** 147, 219-225.
6. Engvall, Perspective on the historical note on EIA/ELISA by Dr. R.M. Lequin. *Clin.Chem* **2005,** 51, (12), 2225.
7. Giljohann, D. A., Mirkin, C.A., Drivers of bioadiagnostic development. *Nature* **2009,** 462, (26), 461-464.
8. Abcam, Direct Elisa Protocol. In http://www.abcam.com/ps/pdf/protocols/Direct%20ELISA%20protocol.pdf: 2009.
9. Wild, D., *The Immunoassay handbook.* 2 ed.; Nature Publishing Group: New York, NY, 2001.
10. Cooper, M. A., *Label-free Biosensors. Techniques and applications.* Cambridge University Press: Cambridge, UK, 2009.
11. Vane, J. R., Botting, R.M., Anti-inflammatory drugs and their mechanism of action. *Inflamm. res.* **1998,** Supplement 2, S78-S87.
12. Carvalho, L. A., Garner, B.A., Dew, T., Fazakerley, H., Pariente, C.M., Antidepressants, but not antipsychotics, modulate GR function in human whole blood: An insight into molecular mechanisms. *Eur. Neuropsychopharm* **2010,** 20, 379-387.
13. Shen, Y., Liu, J., Estiu, G., Isin, B., Ahn., Y-Y., Lee, D-S., Barabasi, A-L., Kapatral, V., Wiest, O., Oltvai, Z.N., Blueprint for antimicrobial hit discovery targeting metabolic networks. *PNAS* **2010,** 107, (3), 1082-1087.
14. Pu, Q., Elazazy, M.S., Alvarez, J.C., Label-free detection of herparin, streptavidin, and other probes by pulses streaming potentials in plastic microfluidic channels. *Anal. Chem.* **2008,** 80, (17), 6532-6536.

2 Label-free sensing basics

This chapter presents an introduction to the design of chemical sensors with special focus on the sensing surface. A general survey of the most relevant label-free methods of transduction is provided. Additionally, the concept of streaming potential is introduced.

2.1 Sensor design

2.1.1 What is a sensor?

A sensor is a device that evaluates and reports the magnitude of a physical property. It could be conceptualized as an assembly of several units that enable the generation of a response to a specific stimulus and its translation into a measurable signal which is displayed in a particular format. Necessary units or modules within a sensor comprise: a sensing element, a transducer and a display (Figure 2.1)

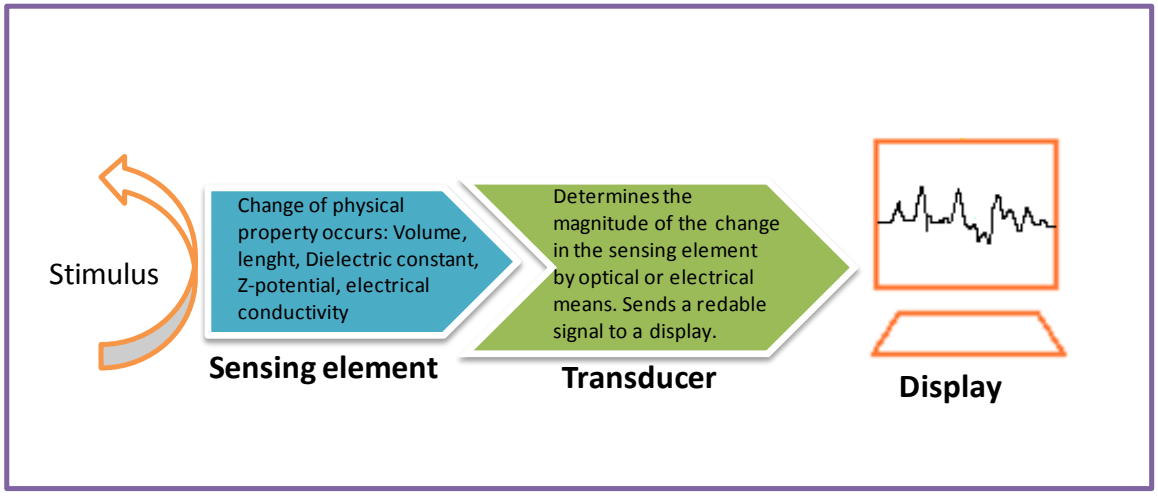

Figure 2.1. Sensor components and their role.

2.1.2 Sensing elements

Sensing elements are materials bearing a physical characteristic which changes, in a predictable way, due to the interaction with the physical property that is intended to be measured. As example, one can think of a humidity sensor that uses fibers as sensing elements (silk or human hair), which contract or expand due to the amount of vapor water present in the atmosphere. A 25 cm long hair can suffer an expansion up to 1.5 mm in the range of 1-100% relative humidity

(RH).[1] Then, by measuring the change in the length of the fiber the magnitude of RH can be estimated. In this case, the transducer will measure the expansion of the fiber.

In a label free sensor, molecular interactions and recognition of specific targets by their corresponding receptors are the initial stimuli to be studied which produce a change in the sensing element. In order to couple the recognition event with its transduction, most of label-free sensors use surfaces modified with specific receptors. Molecules like antibodies, enzymes, proteins, aptamers or molecularly imprinted polymers, which have a particular selectivity and high affinity, are the most desirable and common used receptors.

These recognizing agents are usually located on metallic, plastic or vitreous surfaces using either a covalent or non-covalent method. In the non-covalent approach, receptors are physically adsorbed by just putting the sensor surface in contact with a solution of receptors (antibodies, enzymes, etc). However, direct adsorption is often not ideal since receptors could become inactivated due to undesirable interactions with the surface. This is the case of bare gold on which surface proteins can denature due to the exposure of thiol groups to the metallic interface.[2] The high affinity of thiols for gold drives protein unfolding, which at the end leads to a loss of their recognition capabilities.[3, 4]

A covalent approach partially overcomes this problem since chemical groups located at the sensor surface can behave as spacers between the surface and the receptor, while providing a permanent link between sensing element and recognizing agent. Many chemical strategies have been developed to provide chemical functionality to surfaces and to use them to chemically

attach receptors to surfaces. [5, 6] Figure 4 shows some examples for common covalent approaches. Generally, different surface functionalities like: -OH, -COOH, -NH_2 (Fig 2.2A) are first activated (Fig 2.2B-C) to the nucleophilic attack of terminal amine and thiol groups in the molecules to be attached (Fig 2.2D). After formation of new bonds with the surface the desired receptors end up allocated at the solid interface (Fig 2.2E).

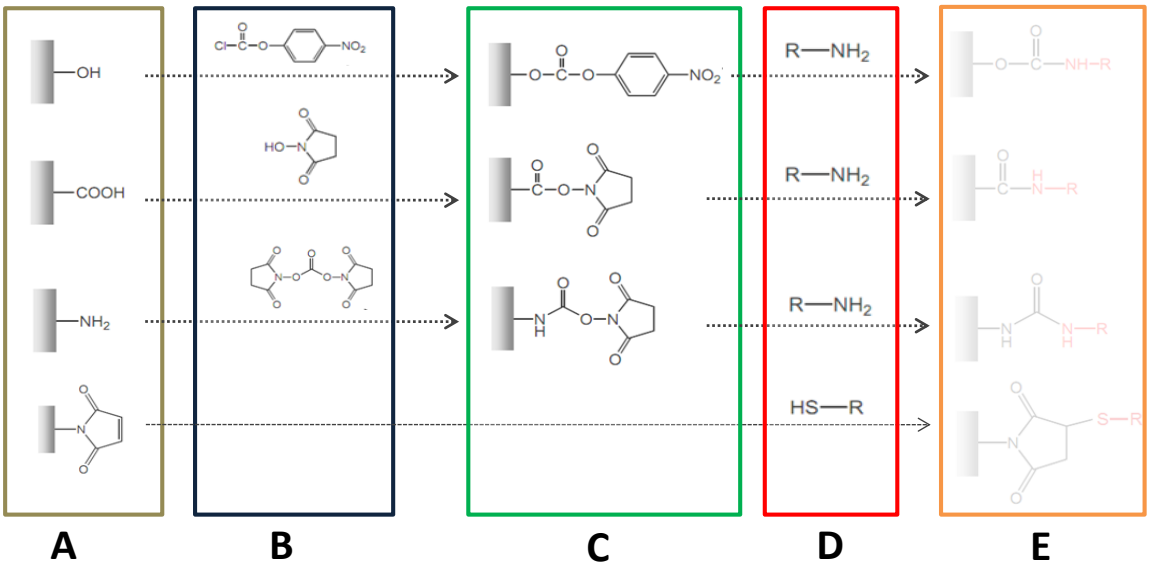

Figure 2.2. Covalent strategies for surface modification of sensing surfaces.

A.Sensor surface. Chemical groups produced by polymerization, adsorption, oxidation, etc, can be activated against receptor coupling. **B**. Activating agents. Good leaving groups **C.** Activated groups on the surface ready to be substituted by the receptor of choice. **D**. Chemical groups in the receptor (amino, carboxylic acid, thiols) interact with activated surface. **E.** Modified sensor surface ready to be used as sensing element.

2.1.3 Selectivity and sensing element

The ability of a sensing element to render information about a specific interaction when non-specific targets are present in the sample (selectivity) depends on several factors. The first is related to the exposure of receptor's recognition sites to the solid-liquid interface where analytes

adsorb. Here, the correct modification technique has to be performed or develop in order to avoid blocking of important recognition sites like the antigen binding fraction (Fab) in antibodies. Another factor to preserve selectivity is the avoidance of steric hindrance produced by a high density of receptors on the surface. This point stresses the need for the optimization of coupling conditions.

For label-free sensors a very important consideration to empower selectivity and performance is the reduction of non-specific adsorption (NSA). NSA is the adsorption of undesirable or unwanted analytes (interferences) on the sensor surface, which produces essentially large background signals. The influence of NSA can be better understood by considering the binding constants of interferences (K_i) and specific analytes (K_x) (equations 2.1 and 2.2) [7] :

$$K_{\mathrm{i}} = \frac{a_{\mathrm{si}}}{a_{\mathrm{s}} a_{\mathrm{i}}} \qquad (2.1)$$

$$K_{\mathrm{X}} = \frac{a_{\mathrm{sx}}}{a_{\mathrm{s}} a_{\mathrm{x}}} \qquad (2.2)$$

Where a_{si} and a_{sx} represent the activities of interference (i) and analyte (x) bound to the surface respectively, while a_{i} and a_{x} refer to the activities of free interferences and analyte. The range where the sensor responds linearly to the concentration of analyte, referred to as the dynamic range (D.R) can be represented as in equation 2.3:

$$D.R. = \frac{1}{K_{\mathrm{x}}} - K'_{\mathrm{i}} a_{\mathrm{i}} \qquad (2.3)$$

Where K'_i is the selectivity coefficient defined by equation 4:

$$K'_{\mathrm{i}} = \frac{K_{\mathrm{i}}}{K_{\mathrm{x}}} \qquad (2.4)$$

A well designed label-free sensor should provide a high selectivity (small K'_i). Nevertheless, from equation 2.4 it is evident that in order to attain good selectivity the best strategy is to effectively reduce the binding constant of the interferences (K_i) by reducing the activity of interferences bound to the surface (a_{si}), which involves reducing non-specific adsorption. Often, selectivity is intended to be achieved by increasing the affinity constant of the analyte (K_x). However, increasing the affinity constant results in the reduction of the dynamic range (equation 2.3), which implies that the sensor's effective analyte concentration range is narrowed.

2.2 Detection mechanisms of current Label-free techniques.

2.2.1 Optical sensors – Refractrometers.

Currently, Optical measurements are the most common means of detection, especially in microfluidic devices[8]. "Optical detection" refers to methods based on registering a change in a specific optical property. Perhaps the easiest and straightforward way is to register a change in the intensity of light due to absorption. For most optical label-free sensors there is a subjacent concept: *the change in light intensity is produced by a change in the refractive index of a surface.* [9]

The refractive index (η) is a measure of the speed of light in a specific medium. It is related with the relative dielectric constant, also known as the dielectric permittivity (ε_r), by equation 2.5:

$$\eta = \sqrt{\varepsilon_r} \qquad (2.5)$$

The refractive index of surfaces ($\eta_{surface}$) increases when molecules adsorb upon them, especially biological analytes like proteins, DNA and cells because these materials bear a greater dielectric permittivity than air or water. It is this increase in dielectric permittivity upon bio-molecules adsorption that causes a reduction of the propagation velocity of electromagnetic radiation than passes through the surface.[10]

Often a way to monitor a change in the dielectric constant is by generating an evanescent wave on the surface where adsorption of molecules takes place. This is performed by illuminating the surface, where adsorption occurs, with a p-polarized light beam. It is important to note that the evanescent wave is formed under the condition of total internal reflection. Total internal

reflection involves the use of a beam of light at a certain critical angle, which allows for all the light that hits the surface to be reflected back (Figure 2.3 A). Under these circumstances, the refractive index of the surface ($\eta_{surface}$) is greater than that of the medium in contact with it (η_{medium}). Critical angle (θ_c) and refractive index of the two mediums involved at the surface interface are related by equation 2.6:[11]

$$\theta_c = \sin^{-1}\left(\frac{\eta_{medium}}{\eta_{surface}}\right) \qquad (2.6)$$

Since ($\eta_{surface}$) increases after adsorption of molecules, θ_c decreases and the condition of total reflectance is no longer fulfilled and a net adsorption of light is obtained. Then, adsorption of biomolecules to the surface can be monitored by observing the change of the angle versus time or the change in absorbance, reflectance or transmission versus Time. This is the general mechanism of transduction for optical sensors based on changes in the diffraction index. For example, Figure 2.3 B shows the variation of absorbance versus time when different concentrations of *E.coli* absorb on an optic fiber modified with *E.coli* antibodies. Several label-free methods have emerged involving these techniques, which use essentially different surface and laser type configurations to produce the evanescent wave.

Some of these techniques are, Optical Waveguide Lightmode Spectroscopy (OWLS), where the interrogated surface is a planar waveguide coupled with an optical grating[12], Evanescent Wave Absorbance (EWA) which uses optical fibers[9, 13] and Tapered fiber-optic biosensors (TFOBS) that uses optical fibers but with special geometries.[14, 15] Other systems use a ring or liquid core optical ring resonator (LCORR). These rings are coupled with a waveguide used to shoot light

on the resonator where the condition of total reflectance is achieved and then modified by specific adsorption of analytes.[16, 17]

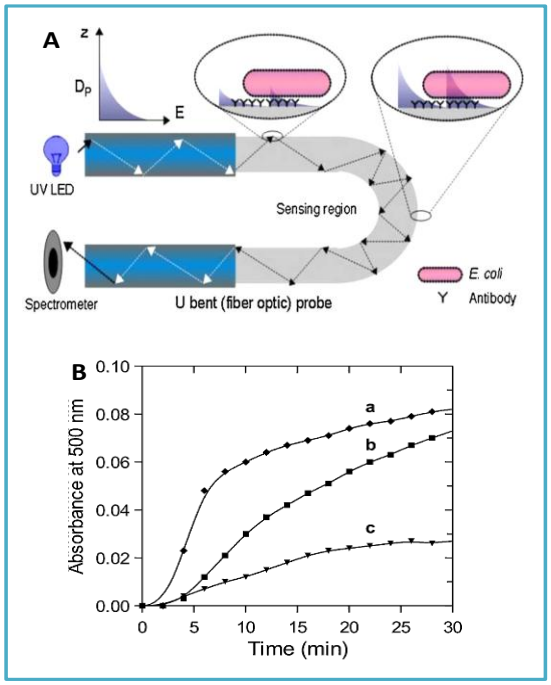

Figure 2.3. Optical transduction and evanescent wave generation.

A. Cartoon illustrating the concept of a light beam under total internal reflection mode. Light travels along an optic fiber producing an evanescent wave at the surface which interacts with adsorbed species.

B. Signal produced by adsorption of a: $1x10^7$, b: $1x10^6$ and c: $1x10^7$ UFC/mL of E.Coli on an bended optic fiber modified with anti-E.coli antibodies. Figures A and B taken from Ref: [13].

Some new systems use the change in refractive index upon attaching of molecules to register the change in the interference pattern (interferometers) rather than a change in the intensity or angle of the incident light.[18]

From a different and complimentary approach, the evanescent wave produced by light on a surface can be used to stimulate a secondary phenomenon. For example, if the surface that is illuminated is of metallic character (gold, silver or platinum) the electromagnetic character of the evanescent wave can interact with the electron plasma (charge density) and produce its collective oscillation at the interface metal/dielectric.[19] This coupling of interactions is the physical foundation for one of the most successful free-label methods based on optical detection, known as Surface Plasmon Resonance (SPR), Figure 2.4. The influence of SPR has been vast

with more than 10000 publications up to now and successful technologies in the market like Biacore® and Bio-Rad®.

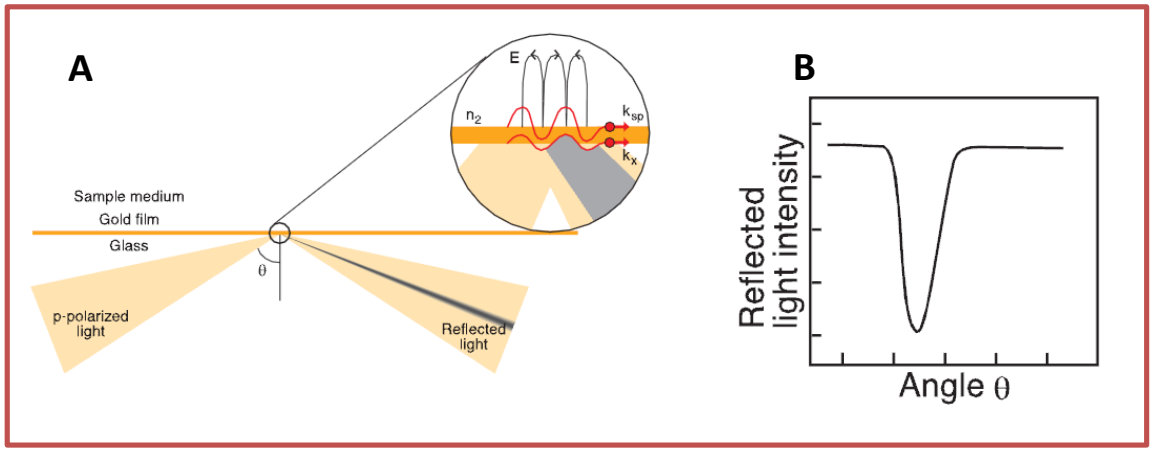

Figure 2.4. Surface Plasmon interaction with evanescent wave.

A. SPR (red lines) excited by a total reflected laser beam. Surface Plasmon enhances the evanescent wave (E) which interacts with adsorbed species on the gold surface. **B**. SPR is observed as a deep (quick reduction) in the reflected light. Figures taken form Ref:[20]

SPR is a surface based technique that was first demonstrated as a viable biosensing method in 1983 by Liedberg et al [19]. Liedberg used the well known phenomenon of plasmon resonance in a similar way to the previous methods explained above, by illumination of a metallic surface under total reflectance mode. When the angle of incident light is varied the percentage of reflected light changes, Figure 2.4. Conveniently, at the angle where total reflection occurs the plasmon resonates simultaneously (Fig 2.4). The sensing capability of this phenomenon relies then, in the fact the angle where total reflection takes place is highly sensitive to the layer thickness of the metallic surface and the refraction index of the interface respectively[21].

Using this finding, Liedberg showed that the layer thickness can change by adsorption of molecules adsorbing to the metallic surface. He found, for example, than a monolayer of adsorbed IgG can produce a shift of ~ 1º in the resonant angle.[19]

Moreover, some specific optical configurations made possible the classification of SPR as label-free technique. The milestone of these optical setups is the Krestschmann configuration, Fig 2.5A, in which a metallic thin film (50 nm) is deposited on the base of a glass prism.[22] A flow cell can be adapted to the prism so that the metallic interface is in continuous contact with a buffer solution where analytes are dissolved.

As the liquid runs, analytes become adsorbed to the metallic surface producing therefore a continuous change in the dielectric constant of the liquid-solid interface, the percentage of light reflected and the resonant angle. In this way, if a continuous surveillance of the reflectivity or the critical angle is conducted versus time, a sensorgram is obtained, which depicts the kinetic interaction of the analyte with the surface (Fig 2.5 B-C).

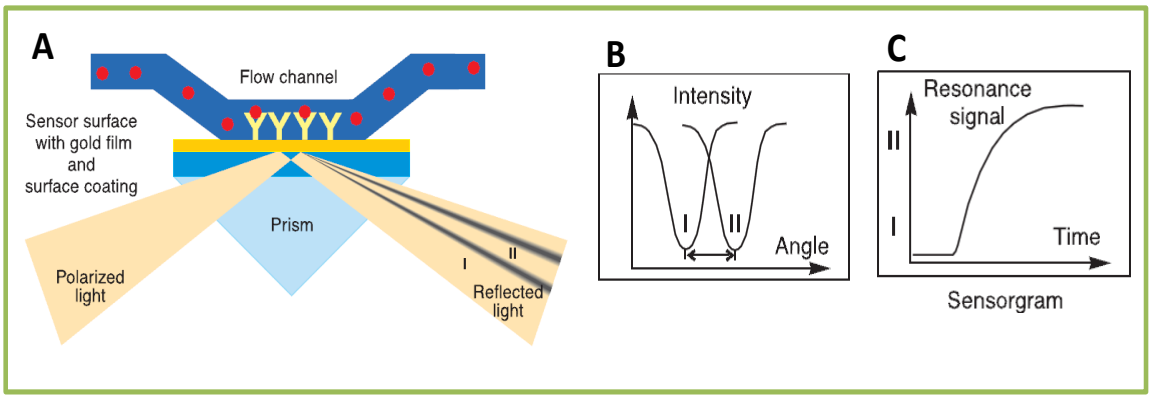

Figure 2.5. SPR transduction.
A. Kretschmann configuration and a fluidic cell transporting analytes. **B.** The angle where total internal reflection occurs is shifted from I to II by adsorption of analytes. **C.** Kinetic adsorption observed by following the shifting of critical angle. Figures taken from Ref: [20]

Optical transduction has also been used for binding events occurring on the miniaturized counterpart of a diving board that moves up and down at a regular interval, called: microcantilevers.[23] Microcantilevers are usually employed in Atomic Force Microscopy (AFM) to characterize surfaces. The ability of AFM to sense the pores, cavities, kinks and fine nano-structure of the outermost layer of materials is due to the capacity of microcantilevers to bend or deflect. Deflection in a cantilever happens by applying some stress (force) which produces its bending. By binding of a selective receptor to a cantilever, the deflection can be produced by adsorption of specific biomolecules[24] and monitored by the "optical lever" method or optical interferometry. In the former case, a laser beam strikes the cantilever surface (usually on a tungsten mirror attached to the surface) and the position of the reflected beam is monitored by a photo-detector. This scheme can monitor tiny displacements of the beam, on the order of 10^{-6}m. [25, 26]

2.2.2. Electrochemical sensors.

Sensors based on electrochemical transduction are usually referred as very suitable alternatives due to their low cost and uncomplicated instrumentation, advantages that make them appealing options for point-of-care diagnostics.[27] For example, even after many technological advances in sensor research and development, glucose biosensors, an amperometric based sensor, still account for approximately 85% of the current world market.[28]

One of the most popular label-free electrochemical techniques used is the so called Electrochemical Impedance Spectroscopy (EIS). This method uses the application of an alternating voltage (less than 10 mV) from a bi-potensiostat to an electrode in which surface affinity receptors are allocated. While the voltage is applied, the output current is registered.

Impedance ($Z(\omega)$) is then defined as the ratio between an incremental voltage (V_{AC}) at certain frequency (ω) and its correspondent change in current (I_{AC}):[27]

$$Z(\omega) = \frac{V_{AC}}{I_{AC}} \qquad (2.7)$$

EIS is performed using a conventional arrangement of three electrodes (working, reference and auxiliary) and a theoretical circuit for the interface solid/liquid can be devised in order to model the output signal (Figure 2.6A).

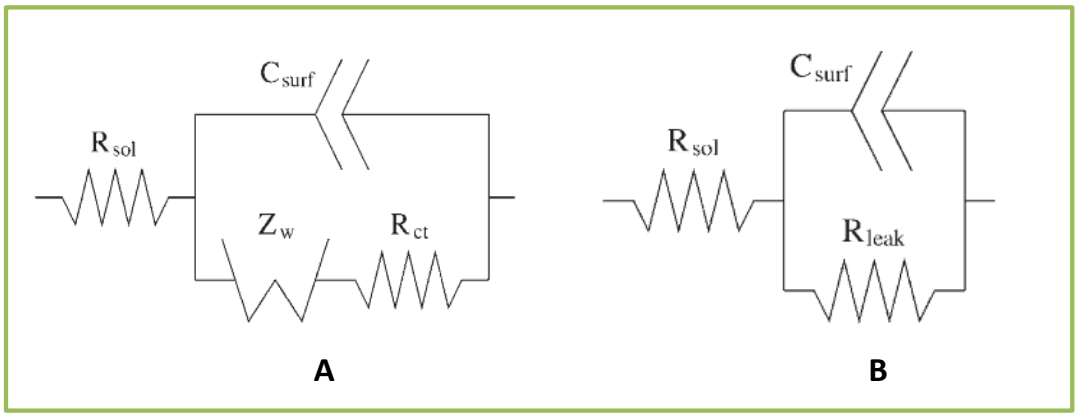

Figure 2.6. Common Circuits models for impedance measurements.
A. Circuit for faradic analysis . **B**. Circuit for non-faradic analysis.

Impedance measurements rely on an electroactive reporter which is oxidized or reduced on the electrode surface, like potassium ferrocyanide couple, $[Fe(CN)_6]^{3-/4-}$. The mechanism of detection in EIS is based on the change in the favorability for the electron transfer to occur between the reporter and the electrode (Figure 2.7). The ease of transfer is measured by the electron transfer resistance (R_{et}) parameter.[29] Conventionally, a decrease in the magnitude of R_{et} is produced because the bio-layer at the electrode surface grows in thickness after the target analyte binds the receptor.[30] Figure 2.7A shows $[Fe(CN)_6]^{3-/4-}$ as reporter for the detection of

thrombin on a surface modified with selective aptamers. The corresponding changes on R_{et} after different adsorption of thrombin are shown in Figure 2.7 B.

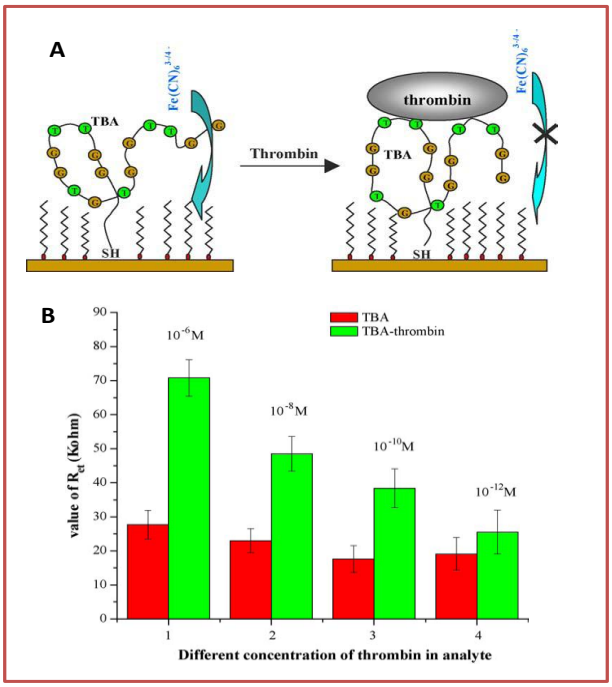

Figure 2.7. Electrochemical Impedance sensing.

A. A target molecule (thrombin) is recognized by an aptamer attached to the electrode sufarce. Target adsorption hinders the electron transfer of a mediator (potassium ferrocyanide) and then Impedance increases.

B. Change observed in the electron transfer resistance parameter (R_{et}) of the electrode depicted in A, upon exposure to variable concentrations of thrombin. Figures from Ref: [30].

When a redox reporter is used in EIS the output current comes from the transfer of electrons at the interface, which is known as a Faradaic process. Nevertheless, EIS can be performed in a non-faradaic or capacitive format in which no redox reporter is used. In this case the monitored current is the one coming from the discharge of the double layer at the electrode/liquid interface which behaves as a capacitor. For capacitive EIS the circuit model does not include the parameter R_{ct} (Figure 2.6B) and instead is the value of the capacitance between the electrode and the ions in solution C_{surf} which modulates the signal.[27] Conventionally, C_{surf} decreases upon binding of biomolecules because the binding causes an increment in thickness of the bio-layer attached to the electrode surface and acts as an insulating coating.[31]

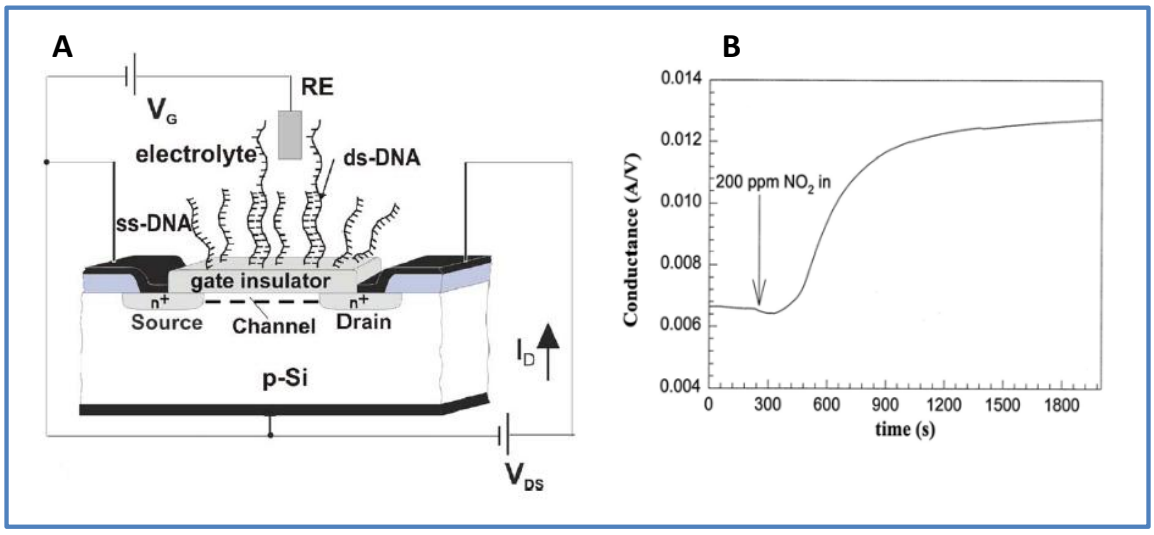

Figure 2.8. Field Effect Transistor (FET) detection.

A. FET system with specific receptors (DNA strands) on the gate insulator surface. A reference electrode (RE) in the solution generates a gate voltage (Vg) and allows the observation of the source-drain voltage (V_{DS}) from the semiconductor platform (p-Si). By measuring I_D (drain current) conductance can be estimated ($I_{D/}$ V_{DS}),figure from Ref: [32]. **B** Time dependence of the signal produced by the adsorption of NO_2 on a FET having walled carbon nanotubes (SWNT) as gate insulator. Figure from Ref: [33]

A change in capacitance is also used by another well known detection system called Field Effect Transistors (FET). Here, a change in the surface charge density is produced by selective adsorption of molecules on a gate isolator[32] which can be made of many different materials like carbon nanotubes[33], Si_3N4 [34] and organic thin films [35] amongst many others. Figure 2.8A shows an example of a FET configuration where DNA recognizing aptamers were attached to the gate surface. Figure 2.8B shows the signal produced after NO_2 adsorption on a FET sensor using modified nanotubes as sensing element.

Also, Differential Pulse Voltammetry (DPV)[36] , Squared Pulsed Voltammetry (SPV)[37], Square wave Voltammetry (SWV) and Cyclic Voltammetry (CV) have been used as label-free sensing techniques, using the inner redox ability of the target sensed. For example, proteins can be recognized and sensed by a selective substrate on the working electrode using their electroactive aminoacid residues.[36]

2.2.3. Acoustic Wave resonators

This transduction mechanism uses the generation of acoustic waves propagating on a sensing surface. The specific characteristics of these propagating waves (amplitude, velocity, frequency etc) can be affected by changes occurring on the surface, like the selective adsorption of biomolecules.[38] The physical concept behind an acoustic wave sensor relies on the finding that application of a periodic perturbation or stress to a solid results in a elastic deformation (strain), which travels as waves through the solid.[39] These are the so called acoustic waves, found in various forms, such as earthquake waves or human hearing.

A very common method of acoustic wave generation is the stimulation of piezoelectric materials like quartz (SiO_2), lithium tantalite ($LiTaO_3$) and lithium niobate ($LiNiO_3$).[40] Piezoelectric materials suffer a mechanical deformation when an electrical field is applied to them. So, by application of an alternating electrical field a periodical strain is created and the acoustic wave produced. In a very common setup (Quartz Crystal Microbalance, QCM) a fine slide of quartz cut by their optical axe is sandwiched between two gold layers which behave as electrodes. An electrical field is applied via the electrodes, which produces a parallel movement in opposite directions, of the gold surfaces, which become antinodes for the acoustic wave.[38] Figure 2.9A illustrates this concept.

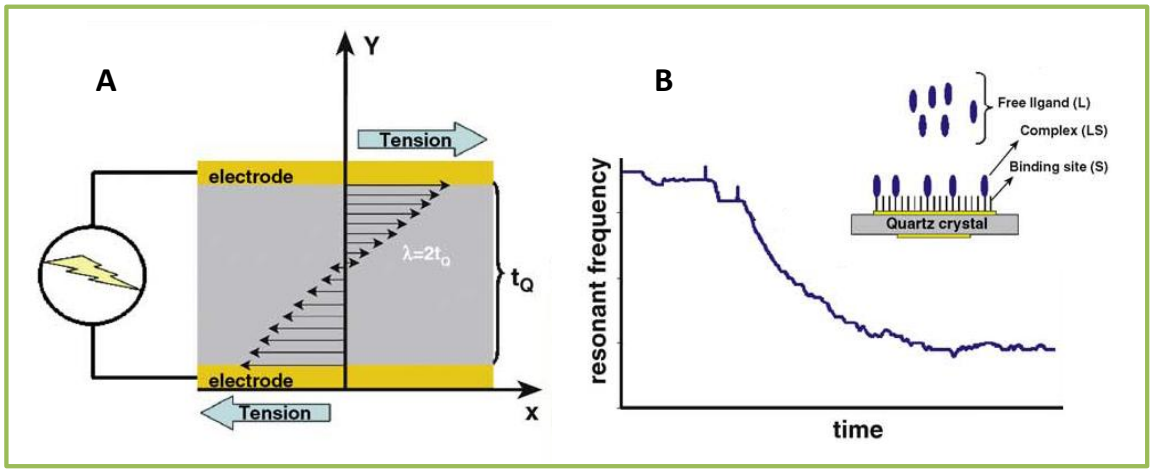

Figure 2.9. Quartz Crystal Microbalance transduction.

A. An acoustic wave is produced by a periodic deformation on a piezo-electric substrate (quartz). Deformation is caused by application of an electric field. **B.** Adsorption of molecules on the gold electrodes (which sandwich the quartz plate) produces a continuous change in the resonance frequency, f_0. Figures for A and B are from Ref: [38].

It turns out that the frequency of wave oscillation depends on its velocity of propagation which is highly dependent on the mass of crystal material (density). These corresponding relations are depicted in the well known Sauerbrey equation:[38]

$$\Delta f_o = -\frac{2}{\sqrt{E\rho}} f^2_o \frac{\Delta M}{A} \qquad (2.8)$$

Where Δf_0 is the change (shift) in resonant frequency, E is the Young modulus of the surface material, f_0 is the fundamental resonance frequency, ρ is the density and ΔM the change in mass.

So, the sensing capability of acoustic wave sensors comes from monitoring the change in the resonant frequency, which corresponds to a change in mass adsorbed. This basic mechanism has enabled the label free monitoring of binding kinetics[41] , cell adhesion[42] and bacteria quantification.[43] Figure 2.9 B shows an example of the change on the resonant frequency upon adsorption of biomolecules.

2.2.4. Calorimetric sensors

One of the most basic features of binding and recognition processes is heat exchange involved in their interaction.[44] Being an extensive property, the magnitude of heat released (Enthalpy) in an interaction depends on the amount of substrate that is able to interact with its complimentary counterpart.

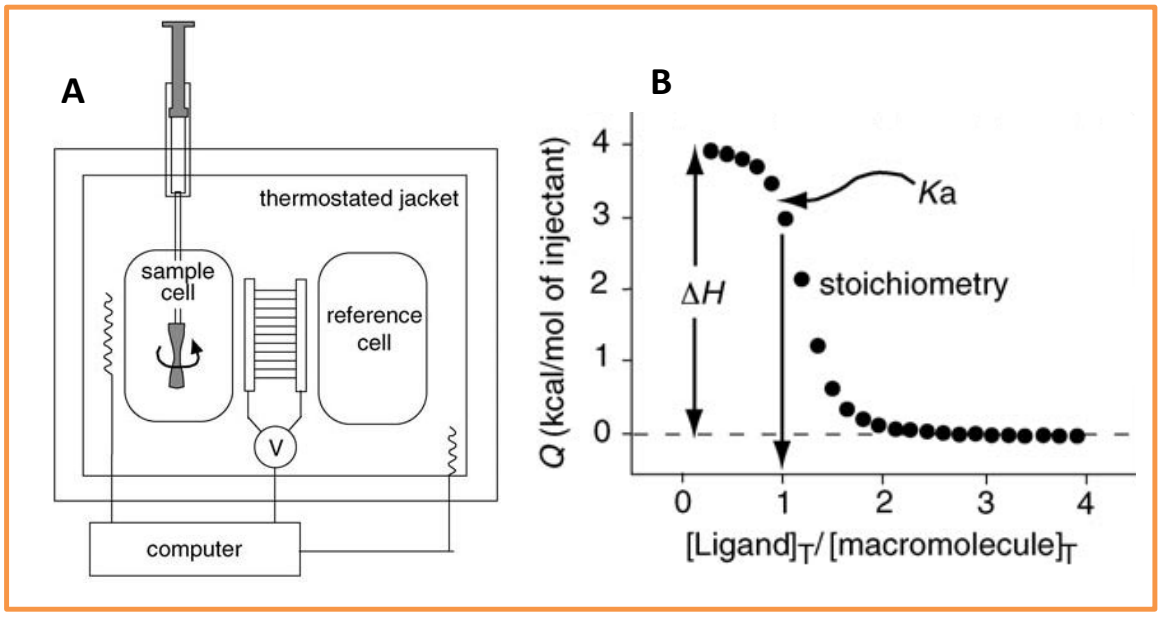

Figure 2.10. Isothermal Titration Calorimetry (ITC).

A. Diagram of the system used for ITC measurements. **B.** Characteristic response of a TIC experiment. Thermodynamic data like enthalpy and equilibrium constant (Ka) can be obtained from the isothermal plot. Figures A and B taken from Ref: [45] .

This is the principle of the technique called: Isothermal Tritration Calorimetry (ITC). In this method, consecutive volumes of target are added to a solution that contains a fixed amount of substrate. Detection of the binding event is made by quantifying the heat involved upon each addition of target.

An ITC experimental setup, as shown in Figure 2.10A, allows the injection of sample into a substrate containing chamber. The amount of heat produced or taken is calculated by the amount of current invested to maintain the temperature of the sample cell at the same temperature of a neighboring reference cell. Both cells reside on an adiabatic shield.

This technique allows the determination of thermodynamic data without the need of immobilizing the receptor to any surface. Additionally, thermodynamic information like Gibbs energy, entropy and heat capacity is possible to be estimated from the this methodology.[45] Figure 2.10B shows an example of a typical ITC experiment from which enthalpy is obtained after titration of the substrate with increasing amounts of ligand.

2.3 Streaming Potential

In this dissertation we attempt to implement a new method of transduction (pulsed streaming potential) which can detect in a label-free fashion, specific interactions at the solid-liquid interface of plastic microchannels. In order to understand how this work differentiates from the previous, the concept of streaming potential must be introduced.

Streaming potential is part of a broad set of effects called "electrokinetic phenomena" which involve the tangential motion of a fluid adjacent to a charged surface.[46] The surface charge needed for the observation of electrokinetic effects is spontaneously created at the solid - liquid interface due to ionization of surface groups or preferential adsorption of ionic species from the solution.

For example, in a substrate bearing silanol groups (-SiOH) at the surface, it is possible to create a negative charge by deprotonation of the –OH terminal groups when the surface is in contact with as solution of high pH. Then, if the surface is negatively charged, ions of opposite charge will be attracted and will create a gradient of positive charge. This distribution of ions at the interface defines the "electrical double layer" which comprises a tightly bound counter-ion layer, referred as the Stern layer, followed by a diffuse layer of ions that extends to the bulk solution as illustrated in Figure 2.12 (taken from Ref: [47]).

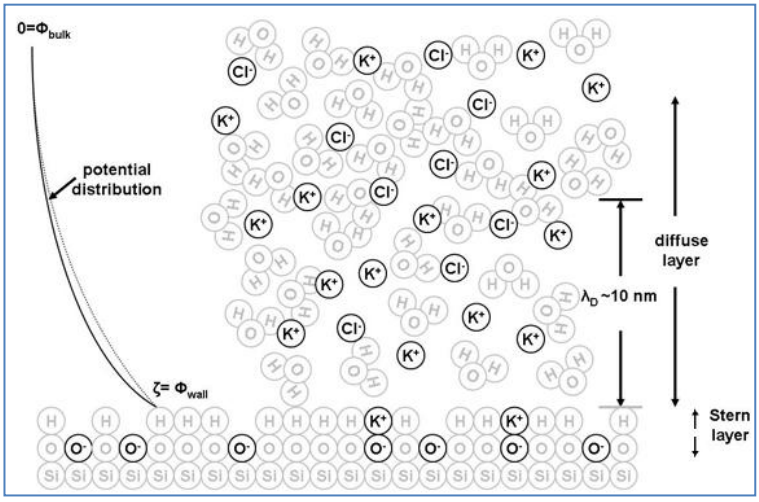

Figure 2.12. Double layer model. Distribution of charge at the solid-liquid interface.

This diffuse layer of ions is loosely retained at the surface and can be easily displaced. If the surface of interest is configured in the form of a capillary, a well packed column or membrane, the diffuse layer can be displaced by flowing liquid through at a set pressure. Therefore, by applying pressure those ions at the diffuse layer are transported forward, creating an overall gradient of charge along the capillary surface, membrane or column which is manifested as a potential difference at the outlets of the capillary. This potential difference is the so-called *streaming potential (E)* (Figure 2.13).

Streaming potential (E) is dependent on the characteristics of both phases, the liquid and the solid substrate, so variables like viscosity (η), conductivity (κ), applied pressure (P), zeta potential (ζ, potential between the Stern and diffuse layers) and some parameters like vacuum permittivity (ε_o) and dielectric constant (ε) determine the magnitude of E. The Smoluchowski equation relates all this variables (Equation 2.9):

$$E = \frac{\zeta P \varepsilon \varepsilon_o}{\eta \kappa} \qquad (2.9)$$

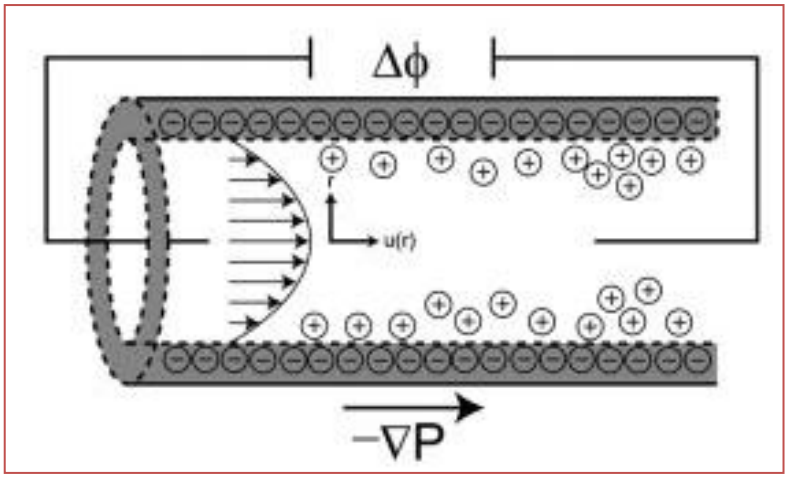

Figure 2.13. Streaming potential. Redistribution of ions after application of pressure in a micro channel.

Zeta potential (ζ), the parameter involved in equation 3, is a very important physical characteristic of materials, which provides information about the surface charge density. The estimation of ζ is of huge relevance since it controls the stability of colloidal systems and cell adhesion to surfaces, for example.[48, 49] Streaming potential has been extensively and principally used for the estimation of ζ in almost every possible substrate; plastic hydrophobic materials[50], gold[51], mica[52], SiO_2, TiO_2 and Al_2O_3 [53], PDMS[54], grafted polyelectrolites[55, 56], plasma deposited fluoropolymers[57], volcanic rocks[58] amongst many others.

Nevertheless, even though many other studies have used streaming potential for studying adsorptive processes like proteins on silica capillaries[59] or glass parallel plates [57], very few studies have been reported for the use of streaming potential as a general method for transduction of molecular interactions in a label free fashion.[60-62] Moreover, prior to this work no study had been reported in the coupling of streaming potential produced in a pulsed fashion as transduction mechanism in microfluidic platforms fabricated with plastic commodities.

In the next chapters the development of a methodology to generate and use pulsed streaming potentials in plastic microchannels, as a reliable transduction method will be presented. As well, the mechanisms for channel surface modification in order to allow the label-free detection of specific adsorption processes.

2.4 References.

1. Ha, T. T. N., An, D.K., Phong, P.V., Hoa, P.T.M., Mai, L.H., Study and performance of humidity sensor based on the mechanical-optoelectronic principle for the measurement and control of humidity in storehouses. *Sensor. Actuat. B-Chem* **2000,** 66, (1-3), 200-202.
2. Brewer, S. H., Glomm, W.R., Johnson, M.C., Probing BSA binding to citrate-coated gold nanoparticles and surfaces. *Langmuir* **2005,** 21, 9303-9307.
3. Johnsson, B., Lofas, S., Lindquist, G., Immobilization of proteins to a carboxymethyldextran-modified gold surfacefor biospecific interaction analysis in surface plasmon resonance sensors. *Anal. Biochem* **1991,** 198, 268-277.
4. Lofas, S., Johnsson, B., A novel hydrogel matrix on gold surfaces in surface plasmon resonance sensors for fast and efficient covalent immobilization of ligands. *J.Chem.Soc., Chem. Commun.* **1990**, 1526-1528.
5. Rusmini, F., Zhong, Z., Feijen, J., Protein immobilization strategies for protein biochips. *Biomacromolecules* **2007,** 8, 1775-1789.
6. Jonkheijm, P., Weinrich, D., Schroder, H., Niemeyer, C.M., Waldmann, H., Chemical strategies for generating protein biochips. *Angew.Chem.Int.Ed.* **2008,** 47, 9618-9647.
7. Janata, J., *Principles of chemical sensors*. 2 ed.; Springer: New York, US, 2009.
8. Mogensen, K. B., Kutter, J.P., Optical detection in microfluidic systems. *Electrophoresis* **2009,** 30, S92-S100.
9. Sai, V. V. R., Kundu, T., Deshmukh, C., Titus, S., Kumar, P., Mukherji, S., Label-free fiber optic biosensor based on evanescent wave absorbance at 280 nm. *Sensor. Actuat. B-Chem* **2010,** 143, 724-730.
10. Cooper, M. A., *Label-free biosensors. Techniques and applications.* 1 ed.; Cambridge University Press: Cambridge, UK, 2009.
11. Taitt, C. R., Anderson, G.P., Ligler, F.S., Evanescent wave fluorescence biosensors. *Biosens.Bioelectron* **2005,** 20, 2470-2487.
12. Voros, J., The density and refractive index of adsorbing protein layers. *Biophis. J.* **2004,** 87, 553-561.
13. Braradwaj, R., Sai, V.V.R., Thakare, Kamini., Dhawangale, A., Kundu, T., Titus, S., Verma, P.K., Mukherji, S., Evanescent wave absorbance based fiber optic biosensor for label-free detection of E.coli. *Biosens.Bioelectron* **2011,** 26, (7), 3367-3370.
14. Leung, A., Shankar, P.M., Mutharasan, R., Real-time monitoring of bovine serum albumin at femtogram/mL levels on antibody-immobilized tapered fibers. *Sensor. Actuat. B-Chem* **2007,** 123, 888-895.
15. Leung, A., Shankar, P.M., Mutharasan, R., A review of fiber-optic biosensors. *Sensor. Actuat. B-Chem* **2007,** 125, 688-703.
16. White, I. M., Zhu, H., Suter,J.D., Hanumegowda, N.M., Oveys, H., Zourob, M., Fan, Xudong, Refractometric sensors for lab-on-a-chip based on optical ring resonators. *IEEE. Sens. J.* **2007,** 7, (1), 28-35.

17. Suter, J. D., White, I.M., Zhu, H., Shi, H., Caldwell, C.W., Fan, X., Label-free quantitative DNA detection using the liquid core optical ring resonator. *Biosens.Bioelectron* **2008,** 23, 1003-1009.
18. Ymeti, A., Greve, J., Lambeck, P.V., Wink, T., van Hovell, S. WFM., Beumer, T.A.M., Wijn, R.R., Fast, ultrasensitive virus detection using a young interferometer sensor. *Nano.Lett.* **2007,** 7, (2), 394-397.
19. Liedberg, B., Nylander, C., Lunstrom, I., Surface plasmon resonance for gas detection and biosensing. *Sensor. Actuat.* **1983,** 4, 299-304.
20. Biacore, Surface plasmon resonance. *Technology note 1.* 2001.
21. Nylander, C., Liedberg, B., Lind, T., Gas detection by means of surface plasmon resonance. *Sensor. Actuat.* **1982/83,** 3, 79-88.
22. Liedberg, B., Editorial for Biointerphases in focus: Surface Plasmon Resonance-Plasmonics. *Biointerphases* **2008,** 3, (3), 1-2.
23. Vashist, S. K., A review of microcantilevers for sensing applications. *Journal of nanotechnology* **2007,** 3, 1-15.
24. Moulin, A. M., O'Shea, S.J., Badley, R.A., Doyle, P., Welland, M.E., Measuring surface-induced conformational changes in proteins. *Langmuir* **1999,** 15, 8776-8779.
25. Sepaniak, M., Datkos, P., Lavrik,N., Tipple, C., Microcantilever transducers: A new approach in sensor technology. *Anal. Chem.* **2002**, 569A-575A.
26. Lavrik, N., Sepaniak, M.J., Cantilever transducers as a platform for chemical and biological sensors. *Rev.Sci.Instrum* **2004,** 75, (7), 229-2253.
27. Daniels, J. S., Pourmand, N., Label-free impedandce biosensors: Opportunities and challenges. *Electroanal.* **2007,** 12, 1239-1257.
28. Newman, J. D., Turner, A.P.F., Home blood glucose biosensor: a commercial perspective. *Biosens.Bioelectron* **2005,** 20, 2435-2453.
29. Rodriguez, M. C., Kawde, A-N., Wang, J., Aptamer biosensor for label-free impedance spectroscopy detection of proteins based on recognition-induced switching of the surface charge. *Chem.Commun.* **2005**, 4267-4269.
30. Cai, H., Ming-Hung, L., Hsing, I-M., Label-free protein recognition using an aptamer-based impedance measurement assay. *Sensor. Actuat.* **2006,** 114, 433-437.
31. Gebbert, A., Alvarez-Icasa, Manuel., Stochlein, Walter., Schmid, R.D., Real-Time monitoring of immnuchemical interactions witha tantalum capacitance flow-through cell. *Anal.Chem* **1992,** 64, 997-1003.
32. Poghossian, A., Cherstvy, A., Ingebrandt, S., Offenhauser, A., Shoning M.J., Possibilities and limitations of label-free detection of DNA hybridization with fiel-effect-based devices. *Sensor. Actuat.* **2005,** 111-112, 470-480.
33. Hu, P. A., Zhang, J., Li, L., Wang, Z., O'Neill, W., Estrela, P., Carbon nanostructure-based field-effect transistors for label-free chemical/biological sensors. *Sensors* **2010,** 10, 5133-5159.
34. Sakata, T., Kamahori, M., Miyahara, Y., Immobilization of oligonucleotide probes on Si_3N_4 surface and its application to genetic field effect transistor. *Mat.Sci. Eng.C* **2004,** 24, (827-832).
35. Tanese, M. C., Fine, D., Dodabalpur, A., Torsi, L., Interface and gate bias dependence responses of sensing organic thin-film transistors. *Biosens.Bioelectron* **2005,** 21, 782-788.

36. Okuno, J., Maehashi,K., Kerman, K., Takamura, Y., Matsumoto, K., Tamiya, E., Label-free immunosensor for prostate-specific antigen based on single-walled carbon nanotube array-modified microelectrodes. *Biosens.Bioelectron* **2007,** 22, 2377-2381.
37. Reisberg, S., Piro, Benoit., Noel, V., Phan, M.C., DNA electrochemical sensor based on conducting polymer: dependece of the "signal on" detection on the probe sequence localization. *Anal.Chem* **2005,** 77, 3351-3356.
38. Ferreira, G. N. M., da-Silva, A-C., Tome, Brigitte., Acoustic wave biosensors: physical models and biological applications of quartz crystal microbalance. *Trends. Biotechnol.* **2009,** 27, (12), 689-687.
39. Janshoff, A., Galla, H.J., Steinem, C., Piezolectric Mass-sensing devices as biosensors-an alternative to optical biosensors? *Angew.Chem.Int.Ed.* **2000,** 39, 4004-4032.
40. Hoummady, M., Campitelli, A., Wlodarski, W., Acoustic wave sensors: desing, sensing mechanisms and applications. *Smart Mater. Struct.* **1997,** 6, 647-657.
41. Cooper, M. A., Singlenton, V.T., A survey of the 2001 to 2005 quartz crystal microbalance biosensor literature: applications of acoustic physics to the analysis of biomolecular interactions. *J.Mol.Recognit.* **2007,** 20, 154-184.
42. Modin, C., Stranne, A-L., Foss, M., Duch, M., Justesen, J., Chevallier, Andersen, L.K., Hemmersam, A.G., Pedersen, F.S., Besenbacher, F., QCM-D studies of attachement and differential spreading of pre-osteoblastic cells on Ta and Cr surfaces. *Biomaterials.* **2006,** 27, 1346-1354.
43. Su, X.-L., Li, Yanbin., A QCM immunosensor for *Salmonella* detection with simultaneous measurements of resonant frequency and motional resistance. *Biosens.Bioelectron* **2005,** 21, 840-848.
44. Saboury, A. A., A review on the ligand binding studies by isothermal titration calorimetry. *J. Iran. Chem. Soc.* **2006,** 3, (1), 1-21.
45. Velazquez-Campoy, A., Ohtaka, H., Nezami, A., Muzammil, S., Freire, E., *Isothermal Titration Calorimetry*. John Wiley&Sons, Inc.: 2004; Vol. Supplement 23, p 17.8.1-17.8.24.
46. Delgado, A. V., Gonzalez-Caballero, F., Hunter, R.J., Koopal, L.K., and Lyklema, J., Measurement and interpretation of electrokinetic phenomena. *Pure. Appl.Chem.* **2005,** 77, (10), 1753-1805.
47. Tandon, V., Bhagavatula, S.K., Nelson, W.C., Kirby, B.J., Zeta potential and electroosmotic mobility in microfluidic devices fabricated from hydrophobic polymers: 1. The origins of charge. *Electrophoresis* **2008,** 29, 1092-1101.
48. Richert, L., Boulmedais, F., Lavalle, P., Mutterer, J., Ferreux, E., Decher, G., Schaaf, P., Voegel, J-C., Picart, C., Improvement of stability and cell adhesion properties of polyelectrolyte multilayer films by chemical cross-linking. *Biomacromolecules* **2004,** 5, 284-294.
49. Tamada, Y., Ikada, Y., Cell adhesion to plasma-treated polymer surfaces. *Polymer* **1993,** 34, (10), 2208-2212.
50. Tandon, V., Bhagavatula, S.K., Nelson, W.C., Kirby, B.J., Transient ζ–potential measurements in hydrophobic, TOPAS microfluidics substrates. *Electrophoresis* **2009,** 30, 2656-2667.
51. Giesbers, M. J., Kleijn, Mieke., Stuart, M.A.C., The electrical double layer on gold probed by electrokinetic and surface force measurements. *J.Colloid.Interf.Sci* **2002,** 248, 88-95.
52. Zembala, M., Adamczyk, Zbigniew, Measurements of streaming potential for mica covered by colloid particles. *Langmuir* **2000,** 16, 1593-1601.

53. Zhukov, A., Integrated investigations of the electrosurface properties of nonaqueous disperse and capillary systems. *Adv.Colloid.Interface.Sci.* **2007,** 134-135, 330-345.
54. Chun, M.-S., Shim, M-S., Choi, N.W., Fabrication and validation of a multi-channel type microfluidic chip for electrokinetics streaming potential devices. *Lab.Chip.* **2006,** 6, 302-309.
55. Zimmermann, R., Birkert, O., Gauglitz, G., Werner, C., Electrosurface phenomena at polymer films for biosensor applications. *Chem.Phys.Chem.* **2003,** 4, 509-514.
56. Dukhin, S. S., Zimmermann, R., Werner, C., Electrokinetic phenomena at grafted polyelectrolyte layers. *J.Colloid.Interf.Sci* **2005,** 286, 761-773.
57. Werner, C., Korber, H., Zimmermann, R., Dukhin, S., Jacobasch, H-J., Extended electrokinetic characterization of flat solid surfaces. *J.Colloid.Interf.Sci* **1998,** 208, 329-346.
58. Hase, H., Ishido, T., Takakura, S., Hashimoto, T., Sato, K., Tanaka, Y., ζ potential measurements of volcanic rocks from Aso caldera. *Geophys.Res.Lett* **2003,** 30, (23), HL2 1-HL2 4.
59. Norde, W., Rouwendal, E., Streaming potential measurements as a tool to study protein adsorption kinetics. *J.Colloid.Interf.Sci* **1990,** 139, (1), 169-176.
60. Miyabayashi, A., Mattiasson, B., A dual streaming potential device used as an afinity sensor for monitoring hybridoma cell cultivations. *Anal. Biochem* **1990,** 184, 165-171.
61. Koch, S., Woias, P., Kudlich, E., Zimmerer, B., The ISFET-based measurement of the streaming potential as a novel biosensor principle. *Sensor. Actuat.B.* **1996,** 34, 289-294.
62. Glad, C., Sjodin, Karin., Mattiasson, Bo., Streaming potential-a general affinity sensor. *Biosensors* **1986,** 2, 89-100.

3 Signal generation and non-dynamic measurements

This chapter deals with the fabrication of the instrument which allows the production of Pulsed Streaming Potentials (PSP) in plastic microchannels. A discussion about the method used for estimation of the PSP magnitude is provided. Furthermore, the use of PSP as tool to investigate adsorption processes is tested for three specific cases, which were carried out sequentially: polymerization of a positively charged hydrogel, electroless deposition of copper and gold and adsorption of thiols and tartaric acid.

3.1 Introduction

Many of the processes occurring on surfaces are regulated by their surface charge. Bacterial adhesion on quartz particles, for example, is inhibited at the typical pH of sandy ground water due to the negative charge on both, bacteria and quartz surfaces. However, the bacteria adhesion increases with the content of Iron (III) oxide (Fe_2O_3) in clay particles, which adds positive charge to their surface and promotes the adsorption of negative charged species. [1, 2] This dependency on surface charge for the modulation of adsorptive processes has made surface charge evaluation one of the principle pieces of information for surface characterization.

The most commonly used method to estimate the surface charge character in particulate materials, fibers, soft and hard surfaces is the Zeta potential (ζ). Additionally, by evaluation of ζ it is possible to estimate characteristic parameters like the isoelectric point (pI), which refers to the pH where the net charge at the surface becomes zero, as well as other features like the influence of the kind of electrolytes involved in membrane fouling.[3, 4]

Zeta potential is conventionally evaluated using some electrokinetic phenomenon, like electrophoretic mobility, streaming current or streaming potential. For the case of non-particulate materials streaming potential is the tool of choice. Conventional devices used for streaming potentials generation apply a tangential flow of a buffer on the sample's surface. This tangential flow is normally produced by application of pressurized gas, like nitrogen, into a buffer reservoir from which the liquid is pushed into a sample holder. The magnitude of positive pressure produced is monitored by a gauge connected in line with the system.[5, 6]

The main point of a streaming potential device is to record the potential generated by displacement of the diffuse layer at the liquid-solid interface due to the tangential flow. This potential is typically measured by placing indicator and reference electrodes at the inlet and outlet of the flow cell or capillary.

Herein, a new approach to generate and produce streaming potentials is presented. The main difference with other works relies on the use of pulses of pressure instead of a continuous or oscillating flow.[7] Additionally, the system has been designed to easily fit microfluidic disposable chips fabricated in plastic polymers in which chemical modification can be performed using photo-polymerization, electrode-less deposition or passive adsorption. The suitability of the whole system to investigate surface interactions is evaluated in two adsorptive processes: the formation of a positively charged polymer and self assembled layers of acid and basic thiols on gold and copper modified Cyclic Olefin Copolymer microchannels.

3.2 Experimental Section

3.2.1 Streaming potential device.

The device developed to measure pulsed streaming potentials (PSP) is made by assembling three different modules: 1. Pressure module, which allows controlled application of negative pressure to the microchip and collection of waste liquid after measurements, 2. PSP generation module which holds the sample (microchannels), uses electrodes and a voltage follower circuit to allow the accurate measurement of the Pulsed Streaming Potential (PSP). 3. Data acquisition and control module that employs a data acquisition card and a Lab View virtual instrument (VI) to send the signal to a PC, record and process data generated, as well as control the pressure applied to the PSP generation module. A complete description of the construction of the three modules and their assembly is provided in supplementary information 1.

3.2.2 Plastic Microfluidic chips

Microchannels on plastic surfaces were made by the wire imprinting technique reported elsewhere[7] and depicted in figure 3.1. Rectangular 2 x 5 cm plates of Cyclic Olefin Copolymer (COC) (Ticona Inc, Florence, KY) were produced by injection molding by Proto Labs (Maple Plain, MN). A stainless steel wire of 0.005 inches in diameter (127 μm) and cut in pieces of 4 cm long (Small Parts, Miami Lakes, FL) was used to imprint microchannels on COC plates by sandwiching a piece between a COC plate and a two glass microslides using four binder clips (Figure 3.1A). This assembly was heated up to 120 ºC for 20 minutes inside a chromatographic oven. The same process was followed for another COC plate but using no wires (Figure 3.2 B). Both assemblies were taken out of the oven, cooled down and the wires were peeled off using

small tweezers. On the plates where no wires were imprinted two holes of ~ 4 mm in diameter were drilled separated by 3 cm from each other. These two holes make the outlet and inlet of the chip. Both COC plates were sonicated in ethanol for 15 minutes and then dried for 20 minutes at 60 ºC in a conventional oven. Cleaned and dried plates were assembled together by matching the holes of one chip with the microchannel in the other and by sandwiching these two pieces between glass slides and clamped with 4 binder clips (Figure 3.1C). The assembly was place in on 82 ºC chromatographic oven for 20 minutes in order to fuse the two plastic pieces together and seal the whole chip. Finally, the chips are cleaned by passing ~ 500 µL DI water through the channels.

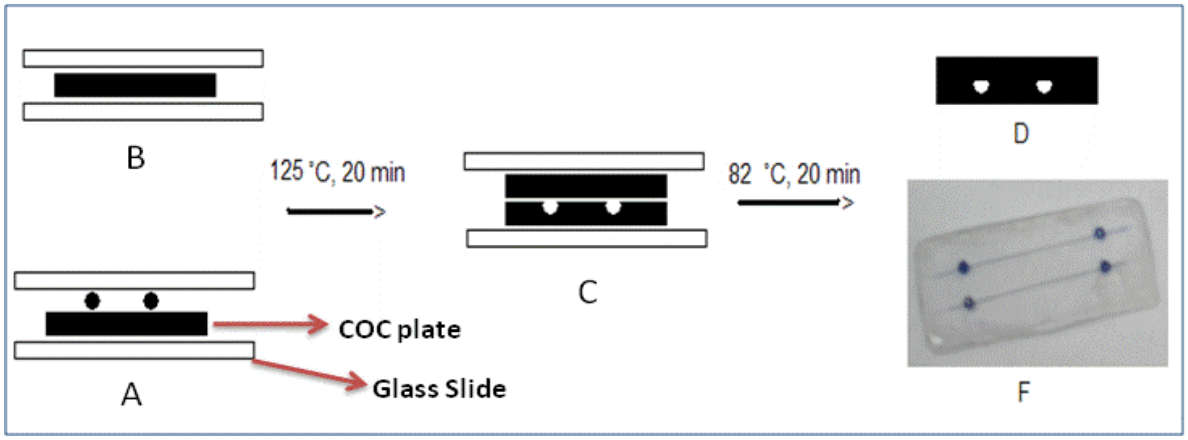

Figure 3.1. Fabrication of microchips by wire imprinting.
Front view of **A**. Wires sandwiched between two glass slides and COC plate. B. COC plate sandwiched between two glass slides, C. Both COC plates put together and sandwiched again, after wires are peeled off. D. Microchip with microchannels. F. Top view of a microchip after fabrication.

3.2.3 Modification of microchannel surface and open COC plates by photopolymerization of N-[3-(dimethylamino)propyl]methacrylamide. (COC-R_3N)

N-[3-(dimethylamino)propyl]methacrylamide (NDMA) and benzophenone (BP) were products of Sigma-Aldrich (St. Louis, MO). A polymeric, positively charged layer containing surface

amine groups was produced by polymerization of NDMA inside Cyclic Olefin Copolymer microchannels using a monomer solution of 10% V/V of NDMA + 0.1% W/V of benzophenone in DI water; BP was dissolved in a small portion of acetone prior to being mixed with the monomer. The monomer solution was then filtered using filter grade 1 acquired from Whatman and degassed for 15 minutes by application of vacuum. Microchannels were filled with degassed monomer mixture and illuminated for 15 minutes at 5 cm from the light source using a Super Spot MK III UV lamp equipped with a flexible light guide (Lesco, Torrance, CA). The irradiation power, 1.5 W/cm^2 at the end of the light-guide was measured with a calibrated SuperSpot intensity meter from (Lesco, Torrance, CA). After NDMA polymerization, microchannels were removed from the UV-light chamber and cleaned by flowing DI water and dried later with an air stream.

The same monomer solution (10 % V/V NDMA + 1% W/V BP), filtered and degassed was used to photolithographically produce a pattern of lines on open rectangular COC plates. To this end, ~ 0.5 mL of monomer solution were put on top of a 2 x 5 cm rectangular COC and it was cover with a quartz photomask containing the line pattern. To level the distance between the COC plate and photomask two pieces of wire of 127 µm in diameter were used as spacers. The whole group of COC plate and photomask was irradiated for 10 minutes with UV light using the same conditions as used for polymerization inside microchannels. After polymerization the plates were cleaned with DI water and dried using an air stream.

3.2.4 Electroless deposition of copper inside microfluidic channels and open COC plates. (COC-R_3N-Cu)

Copper (II) sulfate pentahydrate ($CuSO_4$), tetraazadodecane, triethanolamine, dimethylaminoborane and palladium (II) chloride ($PdCl_2$) were acquired from Sigma-Aldrich.

A layer of metallic copper was produced on *COC-R_3N* modified channels and open plates, using a copper electroless plating bath. First, an aqueous solution of 0.01 M $PdCl_2$ was applied inside modified channels and on open COC plates for 1 hour to activate the surfaces to copper reduction. Excess of solution was removed by washing with DI water and channels and plates dried in an air stream after activation was completed.

The electroless plating bath was an aqueous solution of 0.032 M $CuSO_4$, 0.04 M tetraazadodecane, 0.3 M Triethanolamine and 0.04 M Dimethilaminoborane. This solution was left inside Pd^{2+} activated microchannels and on activated open *COC-R_3N* plates for two hours until a clear metallic aspect was observed, after which plates and channels were cleaned with copious water and dried in air stream.

3.2.4 Electroless deposition of gold inside COC microfluidic channel (COC-R_2N-Au).

Potassium gold (III) chloride ($KAuCl_4$), sodium sulfite ($NaSO_3$) and formaldehyde 37% (CH_2O) were all products from Sigma-Aldrich. Two aqueous solutions were prepared by dissolving 47.55 mg of $KAuCl_4$ and 126 mg of $NaSO_3$ in 1 and 3 mL of DI water respectively. The gold chloride solution was then poured into the sulfite solution and the diluted 5 mL with DI water. This order of addition is important for the solution stability since any other sequence of addition will produce its rapid decomposition (reduction). A gold electroless plating bath was prepared immediately before of its use by mixing 1 mL of the gold - sulfite solution with 150 µL of

formaldehyde 37%. The resultant solution was introduced into *COC* microchannels and left inside overnight. After a metallic appearance is developed channels were washed thoroughly with DI water and dried in an air stream.

3.2.5 Self assembly of thiols and tartaric acid.

L-tartaric acid, cysteine, 4-aminophenol and 4-mercapto benzoic acid were all products from Sigma-Aldrich. Adsorption of tartaric acid on *COC-R_3N-Cu* microchannels was carried out by leaving a 1.1 mM L-tartaric acid aqueous solution inside metalized channels for 12 hours. After this time, the channels were cleaned with water and its pulsed streaming potential determined.

A similar procedure was used to modify *COC-Au* microchannels with thiols. Adsorption of 10 mM 4-mercaptobenzoic acid (4-MBA) and 10 mM 4-aminothiophenol (4-ATP) in 95% ethanol where also done in separated channels, using 24 hours of contact between the solution and the *COC-Au* microchannels. After completion of the adsorption time surfaces were washed with ethanol and dried in an air stream.

In a separate experiment, 10mM 4-mercapto benzoic acid in 100% ethanol was adsorbed on a *COC-Au* microchannel and its pulsed streaming potential measured at 0.5, 2, 5, 8, 20 and 24 hours of adsorption, using a pH 8.5 phosphate buffer solution. Each time, the microchannel was washed with absolute ethanol before the streaming potential was measured. After each determination, a new solution of 4-MBA was introduced inside the channel and left until the next measurement.

3.2.6 Pulsed Streaming Potential measurements.

Surface modification steps carried out in steps 3.2.2 to 3.2.4 were characterized by observation of the change in pulsed streaming potential (PSP) after formation of each new layer inside

microchannels. In order to produce PSP, phosphate buffer solutions with variable pH (3–11) and approximately constant conductivity (~185µS/cm) were flowed in pulsed fashion through each microchannel using the PSP device built in 3.2.1.

3.3 Results and discussion.

3.3.1 Pulsed Streaming Potential Generation

Assembly of the three modules (Pressure application, PSP generation and Data acquisition) produces an instrument which enables the generation of Pulsed Streaming Potentials by the application of negative pressure pulses on COC microfluidic chips with automatic controlled solenoid valves (Figure 3.2).

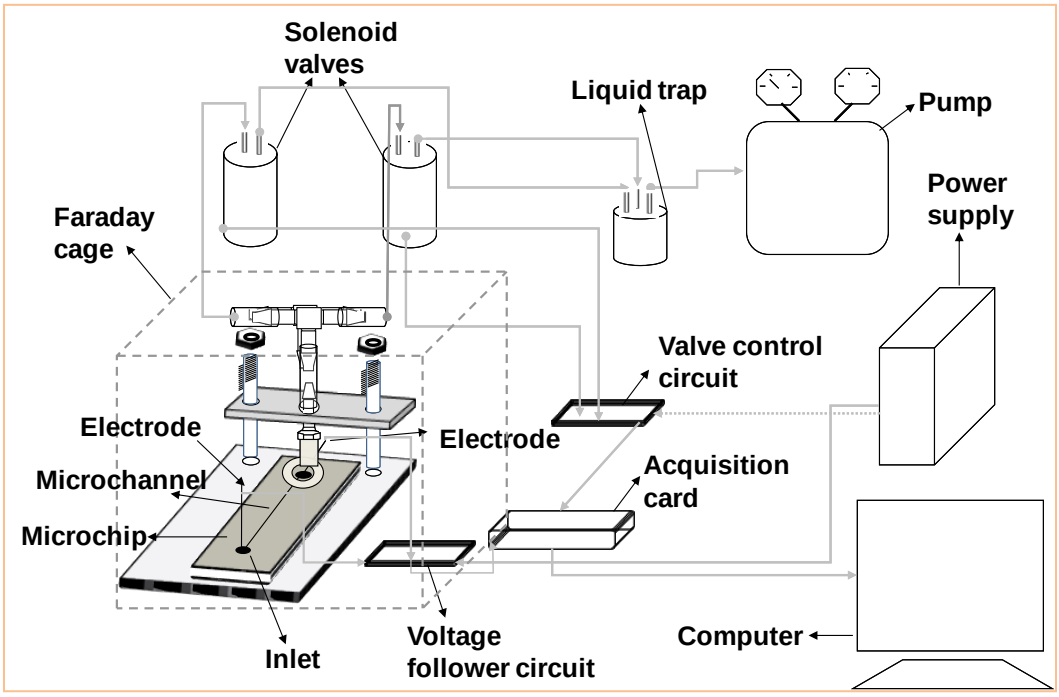

Figure 3.2. Schematic illustration of the Instrument for generation and acquisition of Pulsed Streaming Potential

The instrument is controlled by a software programmed in LabView which allows the control over 4 different variables: time delay for filling of the microchannel with sample (channel fill time), solenoid valve opening and closing delay (T open and T close) and the number of cycles used. These controls can be manipulated through the graphical interface shown in Figure 3.3

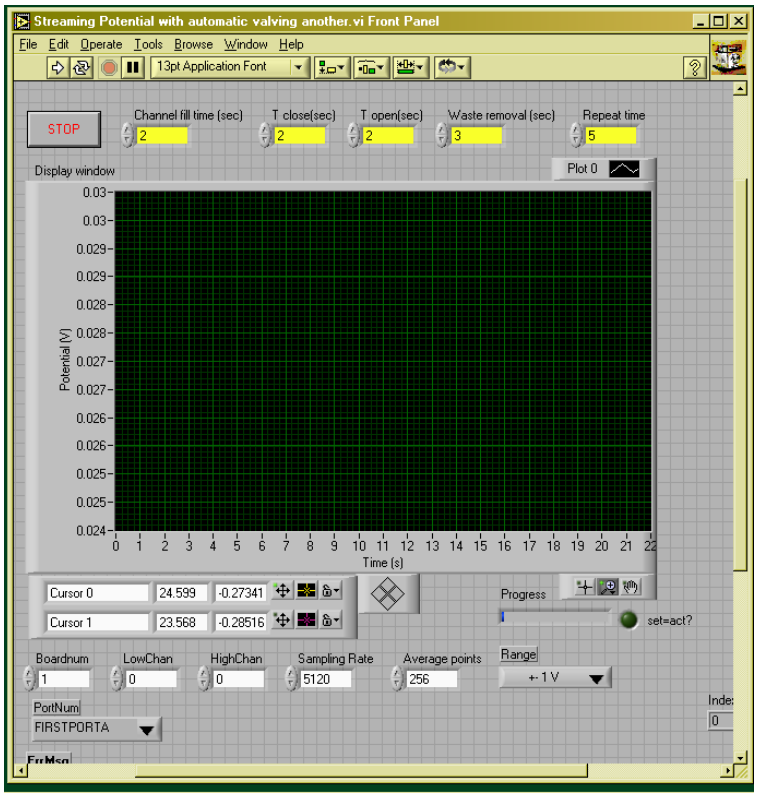

Figure 3.3. Front panel of the Labview program for pressure control of the Pulsed Streaming Potential instrument.

Operation of the device involves positioning a microchip on the holder and manual feeding of the sample by placing some drops (~ 200 µL) on top of the inlet. The two platinum electrodes located at the inlet and at the clamped washer on the outlet are connected to the voltage follower circuit (Figure 3.2). Conditions for the run are set on the graphic interface changing the "T close" and "T open", which will determine the frequency in which the pulses of negative pressure are applied. By clicking on the start button and after the vacuum pump is turned on, a series of pressure cycles begin; the sample is constantly sucked into the microchannel for the time established in "T open", then the solenoid valve closes and remains closed for time set in "T close". This cycle "on-off" is repeated as many times as set on the field "repeat time" (Figure

3.3). After the number of cycles is completed a secondary valve opens for the time set on the field “waste removal” to take away the liquid accumulated at the outlet and send it to the liquid trap where waste liquid is accumulated.

Streaming potentials are generated and sensed on the microchannel by electrodes allocated at its ends. Each time that the solenoid valve turns off, the pressure difference between outlet and inlet drops to zero, therefore the separation (gradient) of loosely held charge along the channel is no longer maintained and the potential drops to the rest potential of the electrodes until the valve turns “on” again and produces a new pulse of pressure and potential (Figure 3.4).

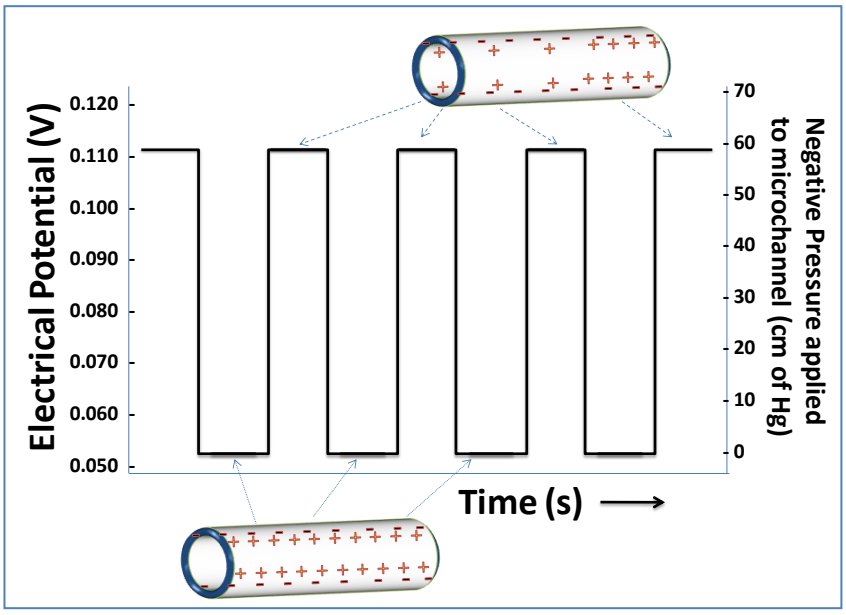

Figure 3.4. Generation of pulses of potential by pulsing the pressure applied through microchannels.

3.3.2 Evaluation of Pulsed Streaming Potential Magnitude.

By pulsing the pressure an electrical potential step is created. The initial level of the step corresponds to the point when a zero pressure difference exists between each end of the

microchannel ends (0 cm of Hg in Figure 3.4). At that moment the potential reported by the electrodes can be associated to the difference in the equilibrium potential for both platinum electrodes allocated at the microchannels ends. In real situations this initial potential changes with time since polarization may occur at the electrodes. For example, Figure 3.5 depicts how the initial base potential, potential when the valves are closed (zero pressure), changes with time for four different cycles in a pristine COC microchannel containing phosphate buffer.

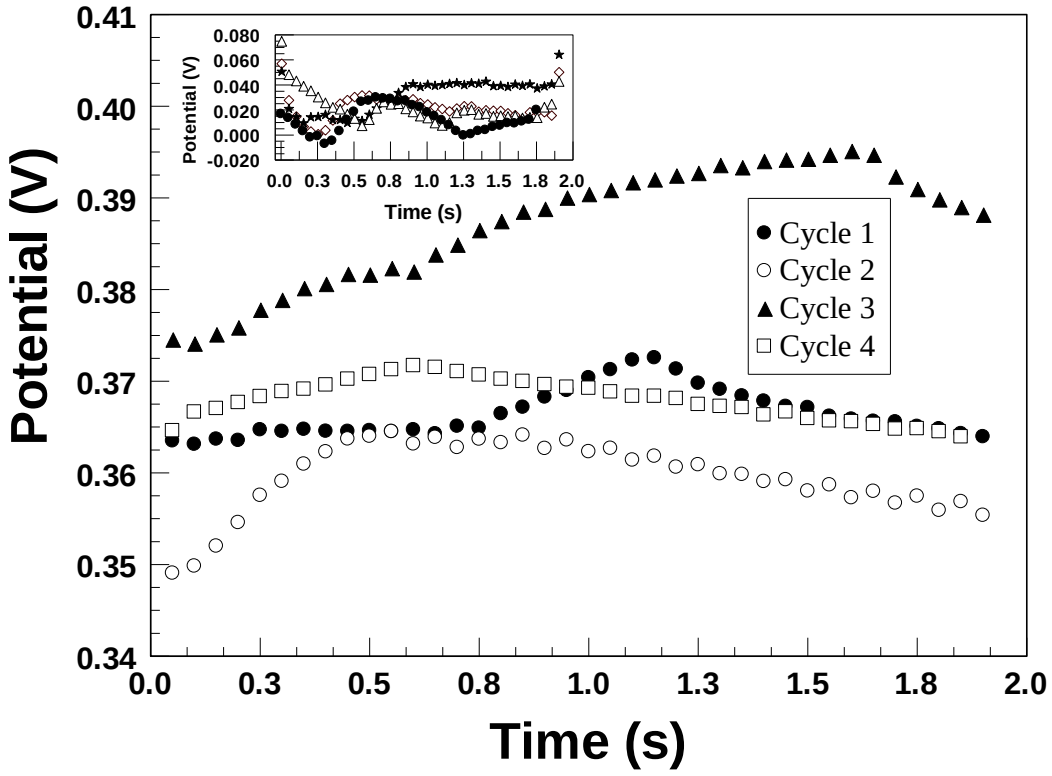

Figure 3.5. Potential drift over time for platinum electrodes in a COC microchannel when pressure is 0 cm Hg and at 60 cm Hg (inset) for four "on-off" cycles. Phosphate buffer solution pH 7.1 and 185 µS/cm was flushed inside channels when the valves are open (inset).

When the valves are open (up to 60 cm of Hg) the potential jumps to a value which should correspond with the true streaming potential since this is the moment when the liquid flows

through the microchannel. However, this potential is not stable either and varies with time too. The inset in the Figure 3.5 shows the variation of the potential during the time when the valves are open. This potential drift, when the valves are open and close, is the expected behavior when no reference electrodes are used. Under these conditions, determination of the streaming potentials magnitude becomes intricate since they drift with time even for the same set of conditions and same microchannel.

The advantage of pulsing the pressure comes with the possibility to evaluate the difference between the electrical potential observed when liquid is not moving (closed valves) and when it is flowing (open valves) or what this investigation calls *Pulsed Streaming Potentials (PSP).* As shown below this difference turns out to be reproducible and insensitive to the potential drift, which makes reference electrodes unnecessary.

The procedure of PSP estimation is carried out by a software module written in LABVIEW which calculates a regression line from a selected range of time series data point obtained when liquid is stopped and when is flowing. The aim of finding a regression line is to select a consistently representative point or potential for the each series. These representative potentials are the last on the non-flowing series and the first on the liquid flowing series. To estimate these two values, the time corresponding with the moment when the valves are open is introduced as independent variable in each regression line. In this way the potentials in flowing and non-flowing situations are found for the exact same moment (Figure 3.6). Using this methodology each representative potential for each series will have the same value without regard of how the potentials drift with time. The Pulsed Streaming Potential (E) refers then to the difference of the potentials found in the two regression lines. This concept is depicted in Figure 3.6.

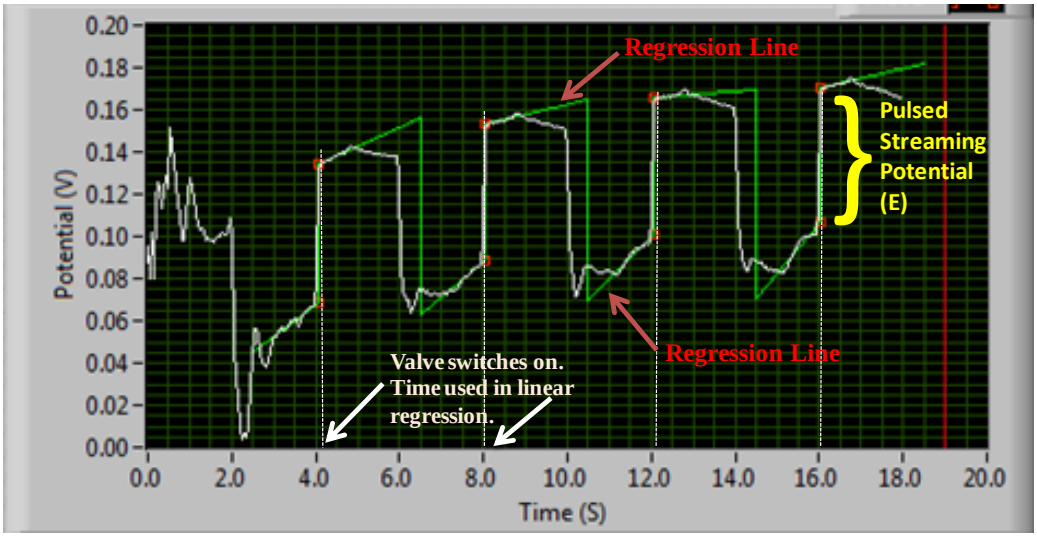

Figure 3.6. Calculation of Pulsed Streaming Potentials magnitude through the use of linear regression of time series data points.

Interestingly, Pulsed Streaming Potentials are reproducible and usually show relative standard deviation (RSD) < 1% between cycles when adsorptive processes have reached the equilibrium. For the four cycles showed in Figure 3.6, for example, the values of SPS obtained are: -0.06518, -0.06394, -0.06454 and -0.06474 V which produces an average value of -0.0646 V and a RSD of 0.79%. This RSD values is very low, taking into account the huge drift of the potentials in the valleys and at the top of the pulses (Figure 3.6).

PSP is then a potential difference and it is related to the streaming potentials since flowing liquid is involved in its estimation. However, these PSP's behave effectively as streaming potentials since their magnitude depends on the pressure applied, as expected from the Smoluchowski relation (equation 2.9, section 2.3)[7] therefore they could be used for evaluation of changes occurring at the solid-liquid interface of microchannels.

3.3.3 Pulsed Streaming Potential in evaluation of polymer formation.

Cyclic Olefin Copolymer (COC) surface characterization was performed by evaluation of PSP produced in microchannels when different pH buffer solutions where flowed through (Figure 3.7). Results show for COC that only at pH 3.1 the PSP was positive and then the potential decreases to negative values as the pH increases. Conductivity, temperature, viscosity and pressure where maintained constant through the whole set of buffer used. So, variations obtained are likely to be due principally to changes in the ζ potential after interaction between the solution and the surface.

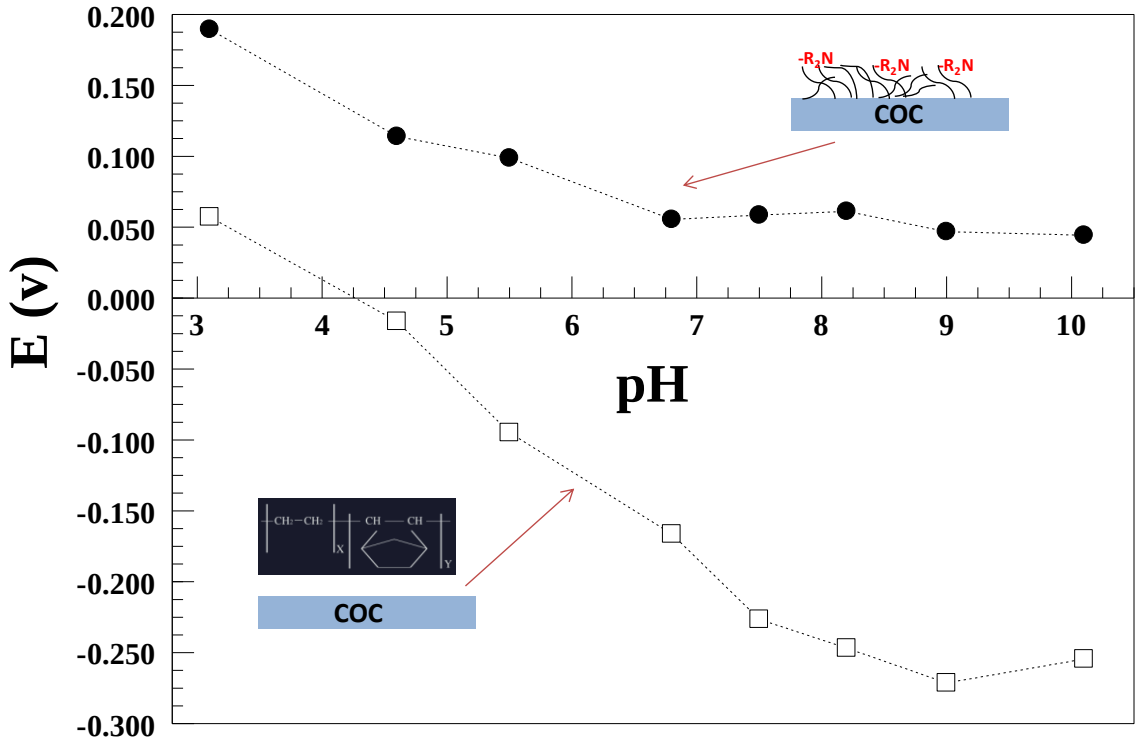

Figure 3.7. Pulsed Streaming Potential (E) for pristine and NDMA modified COC microchannels. Phosphate buffers of ~ 1.5 mM of variable pH and ~ 200 µS cm-^{1} flowed through microchannels at 60 cm Hg in cycles of 2 seconds of flow and 2 seconds of stopped liquid.

The sign of PSP is an indication of the charge character of the COC surface. This means, from Figure 3.7, that above pH 3.1 COC becomes negatively charged and that character increases until approximately pH 8.2 where the PSP plateaus. This result indicates that the non-polar character of COC, since it is a cyclic alkane (inset in Figure 3.7), is not an impediment for development of a negatively charge interface. This behavior has been corroborated several times for different researchers and it is explained as a consequence of the selective adsorption of hydroxyl groups on ice-like structured water held at the surface due to formation of "dangling hydrogen bonds".[8,9]

In order to produce an extreme change on the COC surface charge NDMA was polymerized using photografting. In this method, the rapid growth of the NDMA polymer occurs at the COC plastic substrate where hydrogen is first abstracted and later radical species are generated and used to attach NDMA acrylate groups.[7] Attachment of NDMA to the COC surface functionalizes the surface with tertiary amines (-R_2N), which eventually induces a positive charge at the interface due to the easy protonation of the amine groups. Figure 3.7 shows how after NDMA polymerization Pulsed Streaming Potentials become positive along the range of pH's studied. This finding demonstrates how PSP are related with the surface charge as well as the ability of PSP to sense the reversal of the charge after ternary amine coating. Moreover, the profile of potentials shows how the positive charge is depleted when pH becomes higher, which is related to the neutralization of protonated amines due to the increase of base. However, the results show that even at pH 10 the surface remains positive which implies that not all charged species on the surface are being neutralized and that an isoelectric point of the modified surface exist beyond pH 10.

3.3.4 Metallization of plastic microfluidic channels and adsorption of thiols and tartaric acid.

The new chemical functionality produced on COC after NDMA photografting was used later to carry on a second surface modification which involved the electroless production of metallic copper on the microchannel surface. Electroless deposition refers to the reduction of a metallic ion on a surface without the use of electrical current.[10] This implies that the source of electrons is a reducing agent present in the electroless bath. In this case the electroless plating bath contains Cu^{2+}, which will be reduced at the *COC-R_2N* surface. However, since a reducing agent is in solution the kinetics of the reaction must be manipulated to foster the reduction of Cu^{2+} at the surface and retard this process in the solution. To this end, a chelating agent was introduced in the formulation (tetraazadodecane) which stabilizes Cu^{2+} and also a catalytic layer of Pd^{2+} was preadsorbed on *COC-R_2N.* [11]

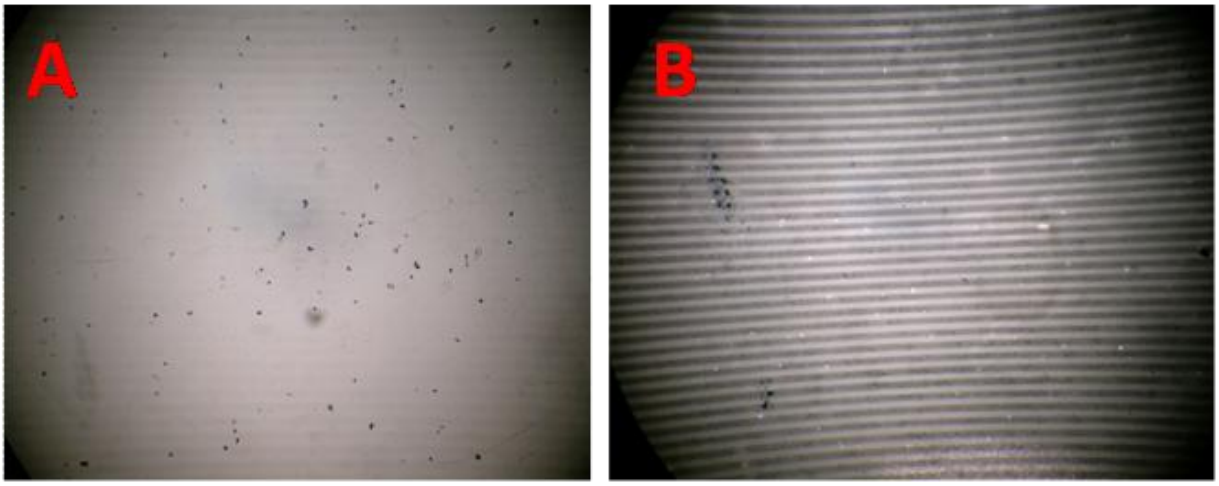

Figure 3.8. Electroless copper deposition on *COC-R_2N open plates.*
COC open plates were modified by photo-polymerization of N-[3-dimethylamino)propyl]-methacryl amide, (15 min UV illumination). Electroless bath was applied for 50 seconds of exposition in plates without (A) and with (B) preadsorbed Pd^{2+}.

The mechanism of reaction involves the early reduction of Pd^{2+} to Pd^{0} on the surface and subsequent reduction of Cu^{2+} by Pd^{0}. [12] This mechanism should lead to the selective reduction of copper in those spots where palladium was pre-adsorbed. In this case, tertiary amines allocated on *COC-R_2N* where used to selectively adsorb palladium by using their electron donor capability to complex Pd^{2+}. Figure 3.8 presents two examples of electroless copper deposition on *COC-R_2N*. In both examples NDMA was polymerized into a pattern of lines. Figure 3.8A shows a COC plate where Pd^{+2} was not pre-adsorbed prior to the application of the copper electroless bath. In this case, results show the very faded appearance of the patterned lines, which corresponds with deposition of some copper. Conversely, in Figure 3.8B where Pd^{+2} was pre-adsorbed, a clear deposition of copper was observed after just 50 seconds of contact with the electroless bath. The dark lines on Figure 3.8B correspond to localized reduction of copper which occurred on top of patterned NDMA. Clear regions between lines are pristine COC where no polymer was grafted.

The same procedure of metallization after polymer grafting was used to modify COC microchannels. Electroless plating produced a clearly distinguishable layer of metallic appearance inside microchannels with a resistance of 379 MΩ. Pulsed Streaming Potentials were used to characterize copper modified surfaces. Table 1 shows the PSP (E (mV)) obtained at different pH before and after plating.

As observed before, *COC-R_2N* produced a positive value of PSP for the whole range of pH. However, when copper is deposited a huge depression of the signal occurs and the potentials are reduced. For example, the PSP values at pH 3.4 are 140 mV for *COC-NH_2*, yet on *COC-NH_2-Cu* the value is only 8 mV. Likewise, at pH 10.2 the PSP value decreases from 31mV to -1mV.

Table 3.1. Pulsed Streaming Potentials for COC-R_2N microchannels before and after electroless copper deposition.

pH	***E for COC-R_2N (mV)***	***E for COC-R_2N-Cu (mV)***	***E for COC-R_2N-Cu-TarAc (mV)***
3.4	140 ± 70	8 ± 4	23 ± 2
4.9	75 ± 6	0.7 ± 0.9	3.8 ± 0.3
6.8	47 ± 7	0.4 ± 0.5	-14.0 ± 0.3
8.5	46 ± 9	0.5 ± 0.6	-19.5 ± 0.4
10.2	31 ± 3	-1 ± 2	-30.0 ± 0.3

This reduction of positive charge can occur since copper deposition proceeds preferentially at surface exposed amine groups, where Pd^0 was first formed; So, when copper is reduced at those activated sites neutral Cu^0 hides the positive charges on R_2NH^+ which become no longer available to build surface charge at the double layer. Another aspect to consider is that metallic layers often develop an amphiphillic character due to the surface hydration which leads to the formation of accessible surface hydroxyls, as shown in equations 3.1 and 3.2:[13]

$$-MOH_2^+ \rightarrow \text{-}MOH + H^+ \quad (3.1)$$

$$-MOH \rightarrow -MO^- + H^+ \quad (3.2)$$

This acid-basic like behavior is in fact observed in the copper layer formed inside microchannels. Table 3.1 shows for the *COC-R_2N-Cu* system positive values of PSP, from ~ 8 mV to ~ 0.5 mV in the range of 3.4 to 8.5 of pH, with a buffer region between 4.9 and 8.5 where the PSP changed an average only 0.3 mV. This trend is in agreement with the deprotonation of metallic hydroxyl groups (equation 3.1). Moreover, at pH 10.2 the PSP reaches an average value of -1 mV and

represents a total inversion of the charge, probably due by the building of a net negative charge density from deprotonated –MOH (equation 3.2). This finding demonstrates how the surface charge can be modulated and characterized by PSP via coating with a metallic surface on a positively charged polymer.

Additional chemical modification was carried out on the *COC-R_2N-Cu* substrate using the well known ability of tartaric acid (2,3-dihydroxybutanedioic acid) to produce self assembled monolayers (SAM) on copper surfaces.[14] Table 3.1 shows pulsed streaming potentials after adsorption of tartaric acid on copper modified microchannels. Tartaric acid has a pK_2 = 4.3 which implies that above this pH most of the molecules are deprotonated and negatively charged. This fact is in accordance with the results obtained which show a new profile of PSP versus pH where a negatively charged surface above pH 4.9 is developed after tartaric acid adsorption (Table 3.1). Additionally, PSP below pH 4.9 show an increment towards positive values when compared with *COC-R_2N-Cu.* This is likely due to protonation of groups brought to the surface by tartaric acid, like –OH and –COOH, which in general provide a higher density of positive charge than just the mere –M-OH existing in the unmodified copper layer.

In additional experiments further demonstration of the ability of PSP to sense changes at the surface of microchannels was performed. Here, pristine COC microchannels were metalized with gold using an electroless method. Moreover, on the gold layer thiols of basic and acid character were adsorbed independently. In this case, PSP characterization reveals a huge dependence of the surface charge with the pH (Table 3.2) for the plastic microchips covered with gold (*COC-Au*).

Table 3.2. Pulsed Streaming Potentials for COC microchannels metalized with gold (COC-Au) and after adsorption on 4- aminothiophenol (COC-Au-4ATP) and 4-mercaptobenzoic acid (COC-Au-4MBA)

pH	***E for COC-Au (mV)***	***E for COC-Au-4ATP (mV)***	***E for COC-Au-4MBA (mV)***
3.1	120 ± 1	3 ± 1	100 ± 9
6.9	-13 ± 4	-0.7 ± 0.1	-60.6 ± 0.5
10.6	-90 ± 3	-0.6 ± 0.2	-110 ± 7

This is possibly a result of a non-uniform and incomplete metallization of the COC underlying substrate. This inefficient metallization of the COC produces pin-holes which are prone to hydroxyl adsorption which in the end reproduces the ion adsorption pattern characteristic of pristine COC (Figure 3.7), as observed in monolayers of alkanethiols on gold films deposited on glass.[15]

Values of Pulsed Streaming Potentials for COC-gold modified with 4-aminothiophenol (4-ATP) manifest the lack of the titration behavior and relatively no change of the surface charge above pH 6.9. Development of this plateau is possibly due because a layer of amine terminated molecules was formed on the gold surface which is not as dense as required to reverse the charge exhibited by the *COC-Au* system. Moreover, results at pH 6.9 show that the hydroxyl concentration was enough to deprotonate most of pending amine groups, which leaves the control of the charge to some uncovered gold and *COC* spots which itself develop a tiny but negative charge. This fact is attributed to the concept that Pulsed Streaming Potentials are able to sense the *net charge density* of the surface, which is the result of the sum of all the negative and positive charges at a certain moment.

When 4-thiobenzoic acid is adsorbed, carboxylic groups are allocated at the *COC-Au* surface. Table 3.2 shows that the potential for *COC-Au-4MBA* at pH 3.1 is less positive after than before 4-MBA adsorption. However, at pH 6.9 this situation is reversed, and an extreme decrease in the PSP is observed. These results can be explained by thinking about the *charge density* at the two states before and after adsorption. *COC-Au* develops an observable positive charge (~120 mV) at pH 3.1 most likely due to adsorption of protons following the same mechanism explained in equation 3.1. This adsorption of protons by *COC-Au* results in a system which is able to allocate more positive charge and then a more positively dense surface than *COC-Au-4MBA* (~100mV), which is in agreement with the smaller pKa of carboxylic acid when compared with alcohols (-M-OH). At pH 6.9 the *COC-Au* surface shows a small PSP (~ 13 mV) which reveals an incipient deprotonation (equation 3.2) that builds a net negative charge density. However, the carboxylate modified surface (*COC-Au-4MBA)* is deprotonated at pH 6.9, and a higher negative PSP is observed, -61mV. This is due to the acidic character of 4-MBA, which has an isoelectric point of 4.9. [16]

3.3.5 Variation of the Streaming Potential with time for the adsorption of 4-mercaptobenzoic acid.

In the previous experiments, Pulsed Streaming Potentials were used to evaluate the surface before and after adsorption processes. In each case, the adsorption was evaluated after a period long enough to assure that the equilibrium was achieved. For example, in the case of thiol adsorption final characterization was performed after 24 hours, after which a well ordered monolayer should be achieved and equilibrium with solution obtained.[17] For the case of 4-mercaptobenzoic acid adsorbing on *COC-Au* modified microchannels an extra experiment was

performed where the surface was evaluated by PSP at different times along the adsorption process. Figure 3.9 shows the results of the PSP evaluation at 0.5, 2, 5, 8, 20 and 24 hours of adsorption. Each time the thiol solution was flowed away and microchannel cleaned with absolute ethanol prior to PSP measurements. In this sense, Pulsed Streaming Potentials obtained correspond with the bound species after each period when the reaction was stopped.

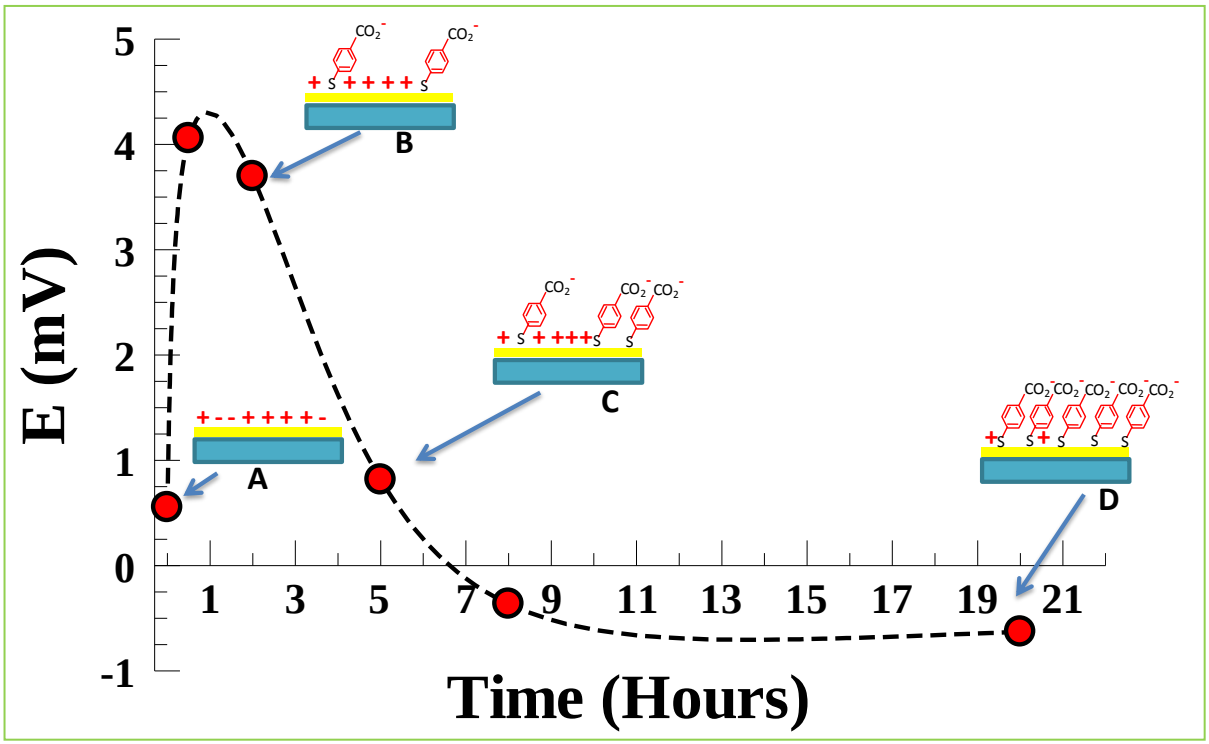

Figure 3.9. Adsorption of 10 mM 4-mercaptobenzoic acid on gold metallized COC microchannel evaluated by pulsed streaming potentials at different times of adsorption. PSP was evaluated with a phosphate buffer pH 8.5 and ~ 200 µS/cm. Absolute ethanol was used as solvent.

The increase of the PSP observed in the first two hours can be rationalized following the idea of a change in the charge density. The initial value of the metallized channel is 0.554 mV indicating a net positive charge population (inset A, Figure 3.9). In the early stage of SAM formation the negative charges transported by the 4-MBA sit on the gold surface and set a lower density of negative charge than the one on the pristine gold surface. This decrease in the negative charge density at the gold surface produces the total effect of increasing the positive charge

population, since now fewer negative charges are available to neutralize the positive ones on the gold layer (inset B, figure 3.9).

After 5 hours the density of 4-MBA becomes greater and builds up higher negative density, after molecules suffer processes of interchange, torsion and reordering (inset C, Figure 3.9).[17] Finally by the eighth hour, the density of negative charges is enough to reverse the sign of the observed PSP. Beyond 8 hours the surface seems to reach a stable density manifested by a plateau of potential around ~ -0.628 mV (inset D, Figure 3.9).

3.4 Conclusions

A system which enables the generation, recording and measurement of streaming potentials by means of pulses of pressure has been developed. The use of pulses produced by application of negative pressure, avoids the need of reference electrodes due to the irrelevance of electrical potential drift to the estimation of the streaming potential magnitude. The design of the device allows the analysis of any surface that can be configured in a micro-channel format. Pulsed Streaming Potentials (PSP) are demonstrated to be useful to sense the changes at the solid-liquid interface of plastic microchannels after occurrence of different adsorptive processes like polymerization, metal deposition and assembly of monolayer.

Estimation of the surface interactions was possible through the evaluation of the Pulsed Streaming Potential change when two different states where compared: the initial and final estate of the surface after adsorption. This kind of surface evaluation is useful to estimate global changes but is still not able to give information about adsorptive processes in real time since each buffer used to evaluate the PSP were different than those used to produce the adsorption event. So, when the potentials are evaluated there is not an adsorptive process happening.

It was additionally proposed that pulsed streaming potentials respond to the global charge density which corresponds to the sum of negative and positive species allocated at the surface. Methods were also demonstrated and developed in order to modify plastic microchannels by photo-polymerization and electroless deposition of gold and copper.

3.5 References

1. Li, B. L., B.E., Bacterial adhesion to glass and metal-oxide surfaces. *Colloid. Surface. B.* **2004,** 36, 81-90.
2. Ryan, J. N., Elimelech, M., Ard, R.A., Harvey, R.W., Johnson, P.R., Bacteriophage PRD1 and silica colloid transport and recovery in an Iron oxide-coated sand aquifer. *Environ. Sci. Technol.* **1999,** 33, 63-73.
3. Shim, Y., Lee HJ., Lee, S., Moon, SH., Cho, Jaeweon, Effects of natural organic matter and ionic species on membrane surface charge. *Environ. Sci. Technol.* **2002,** 36, 3864-3871.
4. Chun, M., Park, W.C., Time evolution of electrokinetic flow-induced streaming pontential and flux in dead-end and cross-flow filtration of colloids through nanopores. *J. Membrane. Sci* **2004,** 243, 417-424.
5. Parreira, H. C., Automatic recording apparatus for measurements of streaming-potentials. *J.Coll. Sci.* **1965**, (20), 1-6.
6. Marsden., S., Two phase streaming potentials. *Proceeding, 12th Workshop on Geothermal Reservoir Engineering (January)* **1987**, 147-151.
7. Pu, Q., Elazazy, M.S., Alvarez, J.C., Label-free detection of heparin, streptavidin, and other probes by pulsed streaming potentials in plastic microfluidic channels. *Anal.Chem* **2008,** 80, (17), 6532-6536.
8. Zangi, R., Engberts, JBFN., Physisorption of hydroxyde ions from aquous solution to a hydrophobic surface. *J.Am.Chem.Soc.* **2005,** 127, 2272-2276.
9. Tandon, V., Kirby., J.B., Zeta potential and electroosmotic mobility in microfluidic devices fabricated from hydrophobic polymers: 2. Slip and interfacial water structure. *Electrophoresis* **2008,** 29, 1102-1114.
10. Liu, S., Li, JR., Jiang, L., Surface modification of platinum quartz crystal microbalance by controlled electroless deposition of gold nanoparticles and its enhancing effect on the HS-DNA immobilization. *Colloid. Surface. A.* **2005**, (257-258), 57-62.
11. Jagannathan, R., Krishnan, M., Electroless plating of copper at low pH level. *J.Res.Develop* **1993,** 37, (2), 117-123.
12. Charnonner, M., Alami., Romand, M., Electroless plating of polymers: XPS study of the initiation mechanisms. *J. Appl. Electrochem* **1997,** 28, 449-453.
13. Duval, J., Lyklema,J., Kleijn, J.M., Leeuwen, H.P., Amphifunctionally Electrified Interfaces: Coupling of Electronic and Ionic Surface-Charguing Processes. *Langmuir* **2001,** 17, 7573-7581.
14. Switzer, J. A., Kothari, H.M., Poizot, P., Nakanishi, S., Bohannan., E.W., Enantiospecific electrodeposition of a chiral catalyst. *Nature* **2003,** 425, 490-493.
15. Schweiss, R., Welzel, P.B., Werner, C., Knoll, W., Dissociation of surface functional groups and preferential adsorption of ions on self-assembled monolayers assessed by streaming potential and streaming current measurements. *Langmuir* **2001,** 17, 4304-4311.
16. Hiramatsu, H., Osterloh, F.E., pH-Controlled Assembly and Disassembly of Electrostatically Linked CdSe-SiO_2 and Au-SiO_2 Nanoparticle Clusters. *Langmuir* **2003,** 19, 7003-7011.
17. Love, J., Estroff, L.A., Kriebel, J.K., Nuzzo, R.G., Whitesides, G.M., Self-assembled monolayers of thiolates on metals as a form of nanotechnology. *Chem. Rev* **2005,** 105, 1103-1169.

Supplementary information 1

Construction of streaming potential machine

1. Module 1- Pressure.

1.1 Materials

An oil free pressure vacuum pump (model No. 2522B-01) was a product of Welch Vacuum Technology (Skokie, IL). A 50 mL centrifuge tube was obtained from Fisher Scientific (Pittsburgh, PA). Straight Thru Connectors, 500 Series Barbs 3/16"ID Tube (*part number* D1-ST074-05), Elbow Connectors Classic Barbs 3/16"ID Tube (*part number F1-EL042-05)* and Straight Barbed, 1/16" Tubing ID 10-32 UNF Pipe Thread (*part number TFN-BAM062/1032)* were products from Small Parts (Miami Lakes, FL). Solenoid valves, stainless steel 3 ways 12 VDC (*part 01380-01)* and 2 way normally closed 12 VDC (*part number 05684-1)* were acquired from Cole Parmer (Vernon Hills, IL). All electronic components, Transistor NPN 30V (*part number 497-3106-5-ND),* 1K ohm resistor (*part number 1.0KH-ND),* rectifier 1A 200 V DO-41 (*part number 1N4003-TPMSCT-ND),* connector terminal female 18-24AWG (*part number WM1008-ND),* rectangular Header Male Pin *(number part* 929647-02-36-ND) and prototype bread boards were purchased through Digi-Key (Thief River Falls, MN). 1 mL disposable syringes were purchased from Becton Dickson and Company (Franklin Lakes, NJ). Cable for connections between components, alligators clips, rosin core solder and light-emitting diodes (LEDs), green and yellow, were obtained from a local Radio Shack store. Pressure flexible tubing was purchased from local stores.

1.2 Construction:

1.2.1 Valve control circuit.

A. Locate the electronic components as described in Figure 1S inserting the legs of each component in the holes of the prototype breadboard:

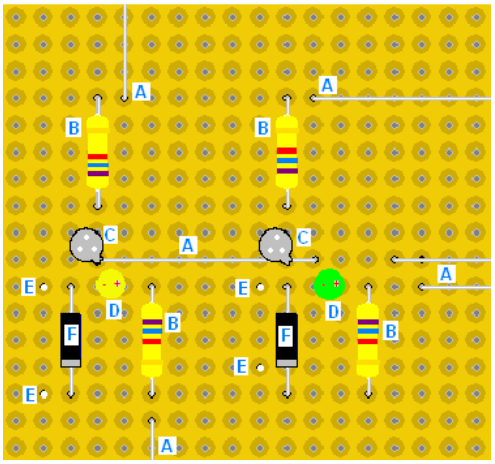

Figure 1S. Valve control circuit. *A*. Connection cables, *B*. Resistor 1 K ohm, *C*. Transistor NPN 30 V, *D*. LED (negative terminal refers to the shortest leg), *E*. Male pin, *F*. Rectifier 1A.

B. After all components have been located at the right place they have to be soldered to the prototype breadboard. Use conventional rosin core solder and a soldering iron to make the right connections by soldering the terminals on the back side of the board as described next. Use the terminal component guide shown in Figure 2S as a guide:

- Connect terminals 1 and 3.
- Connect terminals 2 and 7.
- Connect terminals 9 and 10.
- Connect terminals 8, 15, 16 and 19 together.
- Connect terminals 20 and 21.

- Connect terminals 17, 18, 22, 33, 25, 26 and 30 together.
- Connect terminals 4 and 6.
- Connect terminals 5 and 12.
- Connect terminals 14, 11, 31 and 32.
- Connect terminals 13, 23, 24 and 27 together.
- Connect terminals 28 and 29.

C. After all components have been soldered, attach one female connector 18-24AWG to each male pin (E, in figure 1S) using tweezers to fasten the female connector clamps around the male pins.

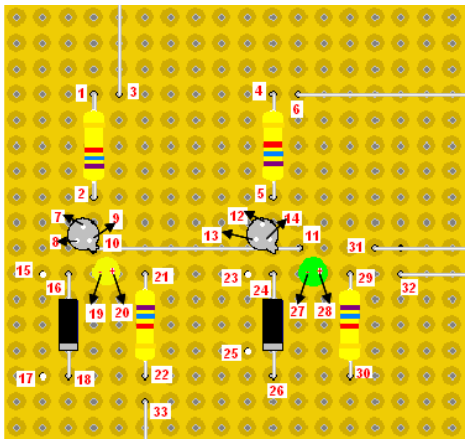

Figure 2S. Component connection guide for valve control circuit. Each number represents a terminal of a component or connecting cable. Terminals not labeled in connecting cables should be left free (unconnected) for connections with other modules.

1.2.2. Liquid trap

A. A 50 mL plastic test tube is used to fabricate a liquid trap. Make three holes in the cap of the plastic tube using a drill press. Two of these three holes should allow clearance for a straight thru connector and elbow connector pass tightly though the cap. A third hole will hold the barrel reservoir of a 1 mL plastic syringe cut at the 0.7 mL mark. Complete the attachment of the

connectors to the cap by applying epoxy glue around the holes and the connectors in order to seal any possible leak when the pressure is applied. The liquid trap should look like in Figure 3S when complete.

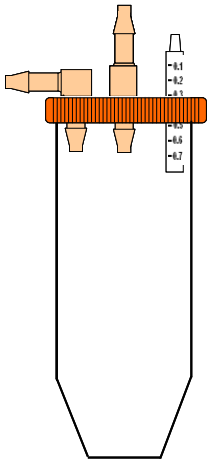

Figure 3S. Lateral view of the liquid trap made using a 50 mL plastic tube and connectors on its cap.

1.2.3. Connecting the pressure system

A. Connect appropriate diameter tubing from the vacuum outlet of the oil free pressure pump to the straight thru connector of the liquid trap.

B. Link the barrel reservoir on the cap to the outlet located at the edge of the normally closed 12 VDC solenoid valve by using appropriate diameter tubing. Attach another 10 cm piece of tubing to the second outlet of the solenoid valve and leave it unconnected.

C. Screw one Barbed 1/16" Tubing ID 10-32 UNF Pipe Thread into each of the side outlets of the stainless steel 3 way 12 VDC solenoid valve. Over each outlet of the valve, located on the sides, the label shows a number 1 or 2. Connect the elbow connector of the liquid trap cap to the

outlet valve number 1. A plastic tip maybe required to be inserted inside the tubing end to make this connection, given the small diameter of the valve outlet connector.

D. Connect the black cables of the stainless steel 3 ways 12 VDC solenoid valve to the female connectors at the positions 23 and 25 illustrated in figure 2S (it is not important which cable goes to which female connector).

E. Connect the green cables of the normally closed 12 VDC solenoid valve to the female connectors at the positions 15 and 17 as illustrated in figure 2S (it is not important which cable goes to which female connector).

2. Module 2 - SP generation Module

2.1 Materials.

A ¼" thick acrylic sheet was obtained from Small Parts (Miami Lakes, FL). 0.5 mm diameter silver wire was purchased from Alfa Aesar (Ward Hill, MA), syringe needles (25G 5/8) was a product from Becton Dickson and Company (Franklin Lakes, NJ). PTFE #30 thin wall tubing (*Part number 06417-11)* was obtained from Cole Parmer (Vernon Hills, IL). A 1/16" thick polycarbonate sheet (*Part number* SPC-0062-C), A Barbed Tubing Connector Tee 3/16" x 3/16" x 3/16" Tubing ID (*Part number TFN-BT187)* and Straight Barbed 3/16" Tubing ID 1/4-18 NPT Pipe Thread (*part number TFN-BAM125/18)* were purchased from Small Parts (Miami Lakes, FL). All electronic components: ceramic capacitor 0.1 µF (*Part number 445-2634-ND)*, capacitor 3.3 µF 63V (*Part number 565-2262-1-ND)*, JFET operational amplifier 8DIP linear (*Part number 296-1780-5-ND)*, 8 pin solder tail dip socket (*Part number A-400-ND)* and resistor 470 ohms 1/4W 5% tolerance (*Part number 470QBK-ND)* were acquired from Digi-Key (Thief

River Falls, MN). A metallic box (*Part number BW-98)* was purchased from Mier Products Inc (Kokomo, IN). Alligator clips and cable for connecting components were purchased from a local Radio Shack store. Pressure flexible tubing was acquired from local stores.

2.2 Construction.

2.2.1 Voltage follower

A. Locate all electronic components as described in Figure 4S inserting the legs of each component in the holes of the prototype breadboard.

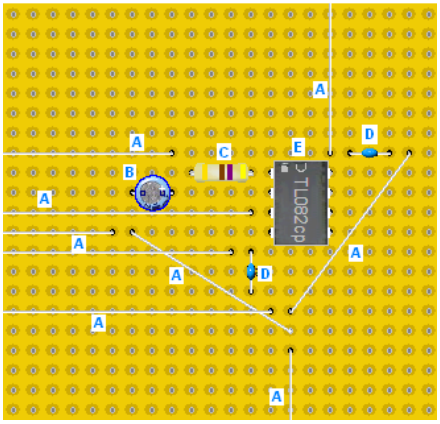

Figure 4S. Voltage follower circuit. *A.* Connection cables, *B.* Capacitor 3.3 µF, *C.* Resistor 470 ohms, *D.* Ceramic capacitor 0.1 µF, *E.* JFET operational amplifier.

B. After all components have been located use conventional rosin core solder and a soldering iron to make the right connections by soldering the terminals on the back side of the board as described next. Use the terminal component guide shown in Figure 5S:

- Connect terminals 1, 2 and 10 together.

- Connect terminals 9, 17 and 18 together.

- Connect terminals 3 and 4.

- Connect terminals 5 and 6.

- Connect terminals 7 and 8.

- Connect terminals 16, 19, 20, 21 and 22 together.

- Connect terminals 13, 14 and 15 together.

- Connect terminals 11 and 12.

C. Tie alligators clamps to the free terminals of the connecting cables coming from positions 12 and 20. Attach, along with the alligator, a new piece of connecting cable to one from position 20. To the free end of this new cable tie an alligator clamp, which will connect the circuit to ground.

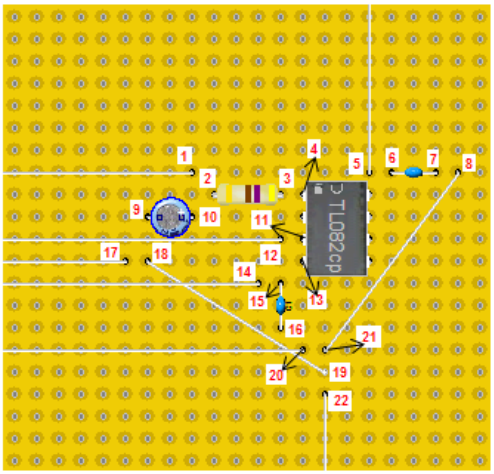

Figure 5S. Components connection guide for voltage follower circuit. Each number represents a terminal of a component or connecting cable. Terminals not labeled in connecting cables should be left free (unconnected) for connections with other modules.

2.2.2 Microchip Holder

A. The microchip holder is shown in Figure 6S. To make the bottom plastic section, cut one piece of 5 x 6 cm of acrylic plate from a ¼" thick acrylic sheet and drill four holes (~ 0.4 cm diameter) at each corner (Figure 7S-b). Pass two long screws and two short ones through the holes (Figure 7S-a).

B. The top plastic section of the holder is made by cutting a piece of 2.0 cm x 5 cm of acrylic plates from a ¼" thick acrylic sheet (Figure 7S-c). Drill two holes on each corner to let the long screws pass through. Drill a third hole (~ 0.8 cm diameter) in the middle of the piece to let the straight sarbed 3/16" Tubing ID 1/4-18 NPT Pipe Thread go through the piece and be linked with the tee connector using a piece of plastic tubing (Figure 7S-a).

C. Cut an acrylic piece of 1.5 cm x 5.0 cm from a 1/16" thick polycarbonate sheet and use it to make the electrode holder. Drill a hole at one corner of the piece (~ 0.4 cm diameter) to insert one of the long screws. At 1.5 cm from the first hole drill 10 consecutive holes (~ 0.2 cm diameter each) separated from each other by approximately 0.15 cm (Figure 7S-d).

D. Insert the tip of a syringe needle (25G 5/8) inside a portion of PTFE #30 thin wall tubing of 7.5 cm long. Introduce the tubing through the Tee and the Straight Barbed 3/16" connectors (Figure 6). Adjust tightly the plastic end of the needle to the tee connector to prevent any leaks upon applying pressure.

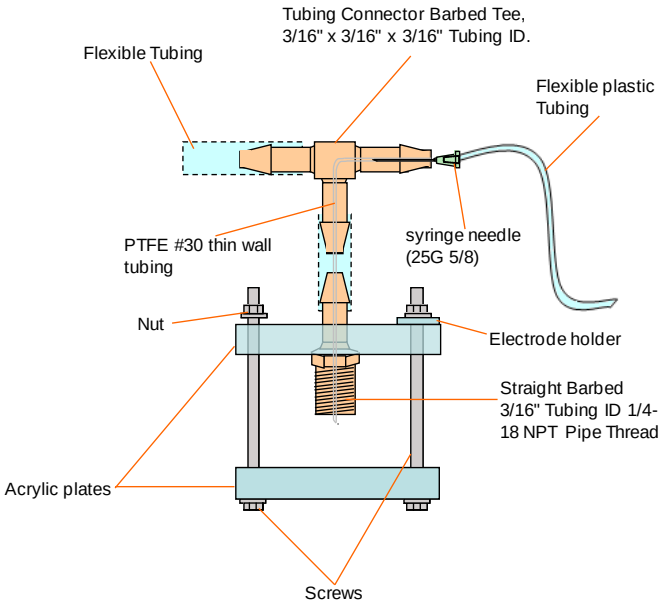

Figure 6S. Schematic illustration of the microchip holder front view.

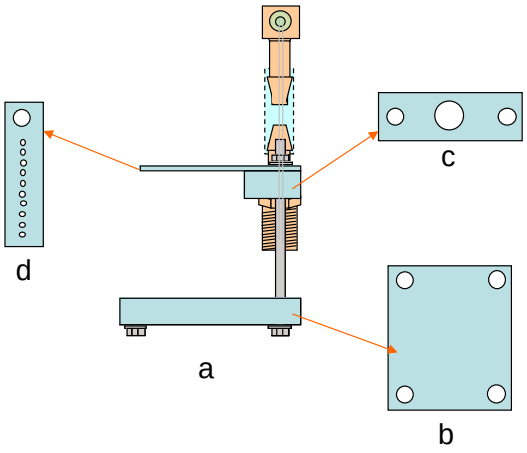

Figure 7S. Schematic representation of the lateral view of the microchip holder (a). Top view of the bottom plastic section (b). Top view of the top plastic section (c). Top view of the electrode holder (d).

E. Assemble all the parts to have a layout similar to that shown in Figure 6. Put a nut at the top end of each long screw to keep all pieces in place.

2.2.3 Faraday cage

F. At one of the front sides of the metallic box drill 5 holes which will allow connections of the microchip holder with other modules. Drill a hole of 0.5 cm, three little, of 0.2 cm and one of 1.0 cm as shown in Figure 8S.

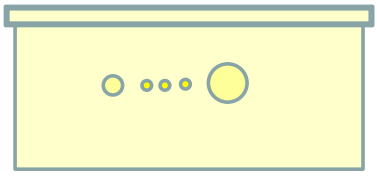

Figure 8S. Metallic box that contains microchip holder and acts as faraday cage.

G. Locate the microchip holder and the voltage follower circuit inside the metallic box. Attach a piece of approximately 5 cm long of silver wire to the alligator clamp of the free terminal from position 12 (Figure 5S). Attach one the alligators from position 22 to the metallic box (ground), leave the other unconnected. Leave the remaining terminals from cable connectors out of the box through the outlets located at the bottom of the metallic box.

3. Module 3 - Data acquisition and control

3.1 Materials

Lab View Developer suit version 8.5.1 was obtained from National Instruments Corp. (Austin, TX). A data acquisition card (*Part product USB-1208 FS)* was a product of Measurement Computing (Norton, MA). A HiPro HP-M1854F3P power supply was purchased from Beach Computers (Satellite Beach, FL). A conventional computer with RAM higher than 516 Mb was used.

3.2 Construction.

3.2.1 Connecting data acquisition card.

A. Install Labview on the computer following directions from the manufacturer.

B. Connect the data acquisition card to an USB port on the computer. Install the software *InstaCal* using the CD that comes with the acquisition card. Use *InstaCal* to install the acquisition card.

3.2.2 Installing Virtual instruments

A. In the computer, on the C disk, open a new folder and name it "Streaming potential". From the CD labeled as "virtual instruments for streaming potential" copy the folder named "LabView code" into the new one named "Streaming potential". The "LabView code" folder contains two virtual instruments "Streaming Potential with automatic valving.vi" and "Streaming potential calc from data file.vi", which control the solenoid valves and allow data processing, respectively. Block diagrams for those virtual instruments are shown in Figures 9S and 10S.

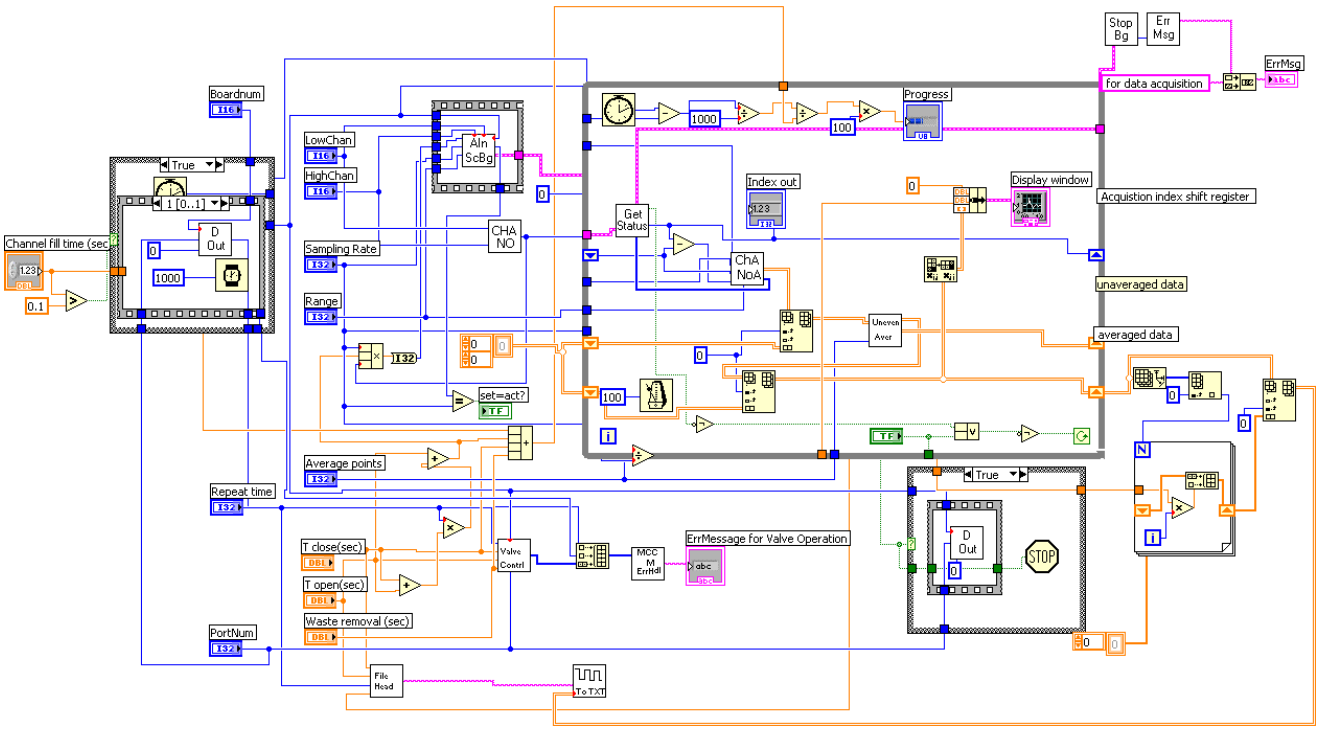

Figure 9S. Block diagram for the virtual instrument "Streaming potential with automatic valving.vi".

B. Verify that the file "Das16.llb" is in the location C:/program files/National instruments/LabView7.0/menu/Universal Library. If the file is not in that location, copy it from C:/program files/National instruments/LabView8.5/menu/Universal Library/ and paste it in the right place.

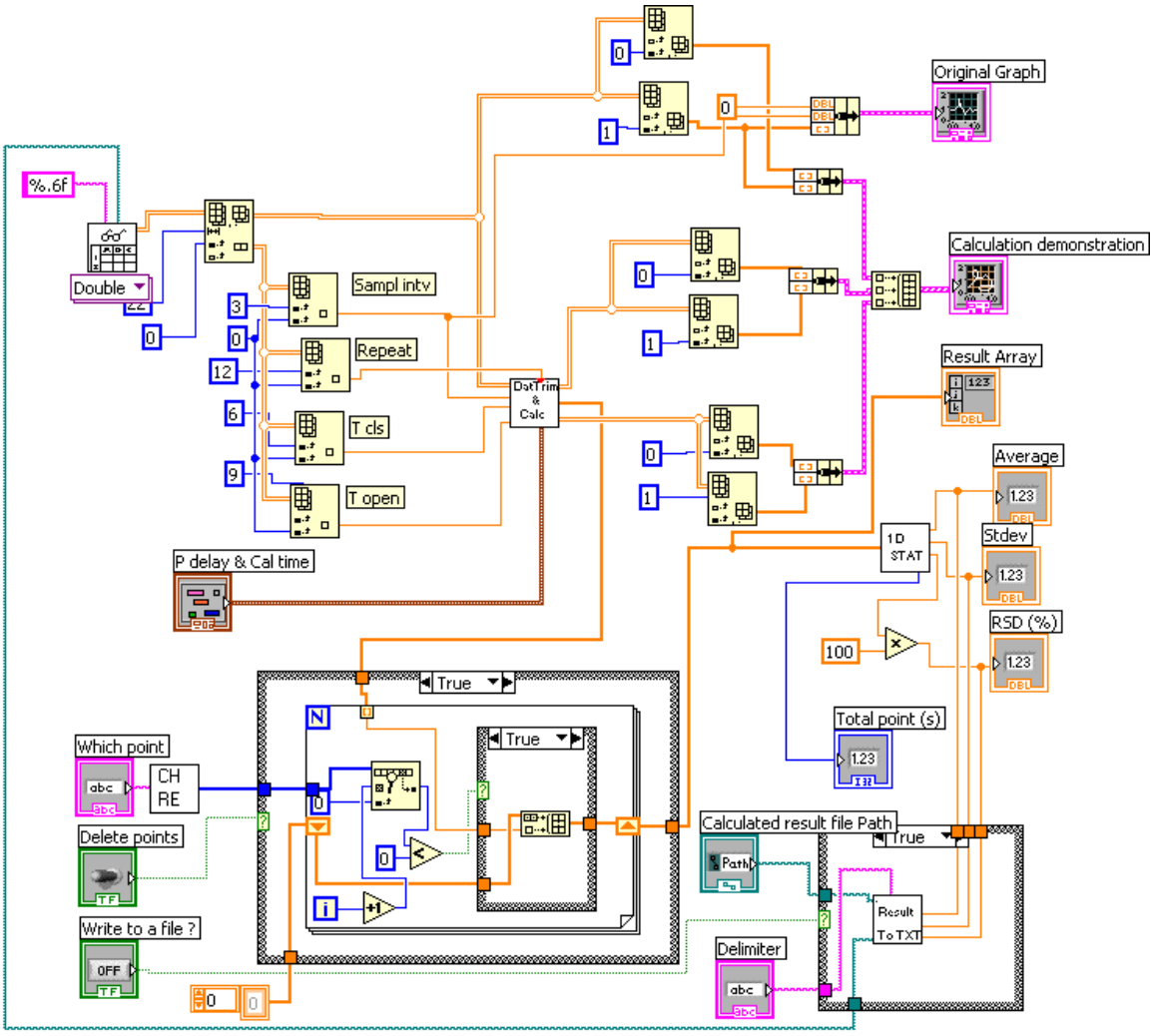

Figure 10S. Block diagram for the virtual instrument "Streaming potential calc from data file.vi"

4.0 Assembling the modules

A. Connect the valve control circuit with the acquisition card:

- Free terminal from position 3 to socket No 24 of acquisition card.
- Free terminal from position 6 to socket No 21 of acquisition card.
- Free terminal from position 31 to socket No 31 of acquisition card.

B. Connect the power supply to an electric outlet. Localize the group of inlets on the power supply labeled as P6. Hold the P6 connector with the label facing you and insert free terminals Numbers 32 and 33 from the valve control circuit as described in Figure 11S.

C. Connect the 10 cm piece of tubing from the normally closed 12 VDC solenoid valve to the needle (25G 5/8) already inserted in one side of the tee of the microchip holder (Figure 5). Use the 0.5 cm hole drilled on the metallic box to bring the tubing to the microchip holder.

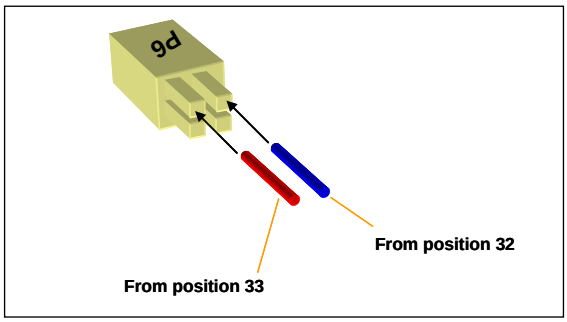

Figure 11S. Connections for the valve control circuit to power supply.

D. Attach the stainless steel 3 way 12 VDC solenoid valve to the external part of the metallic box using the 0.2 cm holes and wrapping wire. Connect the outlet number 2 of the solenoid valve (section *1.2.3 C*) to the free side of the tee connector of the microchip holder using appropriate flexible tubing (Figure 6S). A plastic tip may need to be inserted inside the tubing end to make it fit in the small diameter of valve outlet elbow.

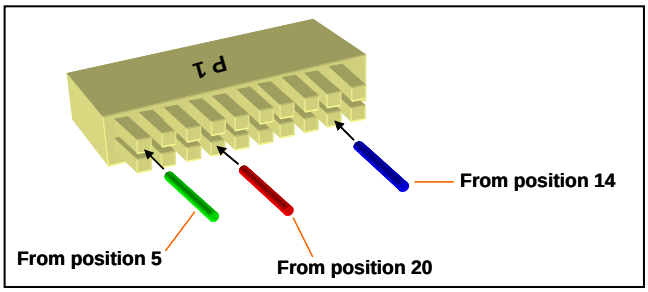

Figure 12S. Connections for the voltage follower circuit to power supply.

E. Connect voltage follower circuit with the acquisition card:

- Free terminal from position 17 to socket No 2 of acquisition card.
- Free terminal from position 1 to socket No 1 of acquisition card.

F. Localize the group of inlets on the power supply labeled as P1. Hold the P1 connector with the label facing you and insert free terminals No 32 and 33 from the voltage follower circuit as described in Figure 11.

G. Electrical power is supplied to all system by placing a small piece on cable between the two sockets located at the right of the cable from position 14 on P1. (Figure 11).

H. After all modules have been assembled the instrument is ready to use by placing a microchip at the microchip holder, turning on the oil free pump and using the virtual instruments installed on the computer.

4 Real time detection with Pulsed Streaming Potentials

In this chapter real-time measurements of Pulsed Streaming Potentials are presented. Results of the applications of this methodology for the quantification of proteins and estimation of kinetic parameters are shown.

4.1 Introduction

In Chapter 3 the use of Pulsed Streaming Potentials (PSP) to sense the changes in surface charge occurring at solid surfaces upon adsorption of molecules was explained. However, the methodology used previously allows the sensing of changes at the interface only when no adsorptive species are present in the solution used to produce the PSP. This feature restricts the PSP measurements to non-dynamic cases and impedes the observation of real-time adsorption and the behavior of PSP with time. In this chapter, an approach to monitor adsorption processes in real time using PSP is reported, which allows the investigation of the whole process of adsorption, from the initial stages to the saturation of the surface. Moreover, desorption processes are able to be observed as well, which in combination with the adsorption phase allows the estimation of kinetic parameters of the interaction adsorbent-surface.

The key factor and major advantage that allows the use of PSP for kinetic analysis of the charge interactions on the microchannel surface in real-time is the incorporation of an "injector" to the Pulsed Streaming Potential device. This injector maintains a constant supply of sample and allows continuous recording of the PSP versus time.

As a proof of concept of the real-time measurements, the protein lysozyme (Ly) was selected**.** Lysozyme has been shown to adsorb non-specifically on different surfaces.[1-4] Several features of the protein-surface interaction are studied, like the effect of phosphate buffer on the adsorption kinetics of Ly was studied also on COC microchannels. Lysozyme is an enzyme that is part of the innate protection system present in secretions such as tears, saliva and mucus to protect the body from bacteria.[5]

This new methodology of real-time evaluation of PSP is very relevant within the field of microfluidics where there has been success in coupling microscale platforms like microchips and microarrays with well established detection methods like laser induced fluorescence[6-8], impedance-conductance[9-11], amperometry[12] and voltammetry[13, 14]. However, these techniques are often based on complex optics, lasers, potentiostats and in general bulky instrumentation that do not conform well to the overall goal of miniaturization.

Most current detection methods rely on the use of an ex-situ excitation signal that produces a response that is generally proportional to the surface or bulk concentration of flowing or attached analytes in the microfluidic device. In this light it is very desiderable to have an in-situ produced signal, label free and susceptible to be miniaturized, that could avoid any external bulky instrumentation used to detect target molecules bound to the device surface.

4.2 Experimental Section

4.2.1 Chemicals

Two times crystallized and dialyzed lysozyme was purchased from Worthington biochemical corporation (Lakewood, NJ). NaCl 99.5%, NaH_2PO_4 and Na_2HPO_4 were from Merck (San Diego, CA).

4.2.2 Streaming Potential Acquisition.

The measurements were performed in semicircular microchannels (~100 μm wide x ~47 μm height x ~3 cm long) fabricated as described previously[15, 16].

4.2.3 Lysozyme Adsorption Kinetics.

Two different series of Ly solutions were prepared. One set contained Ly at 7.0, 17, 35, 53, 70, 210 and 350 nM in DI water (MilliQ grade) with NaCl 5.0 mM and a conductivity of 544 ± 10μS/cm. The second set of solutions contained the same concentrations of Ly (from 7.0 – 350 nM) plus 1.5 mM phosphate. Because the conductivity of the Ly solutions with buffer had lower conductivity than the solutions with NaCl 5.0 mM, aliquots of NaCl 50 mM were added to adjust the conductivity to 544 ± 10μS/cm, however the final concentration of NaCl in the buffer solutions never exceeded ~3.5 mM. The pH of all solution was 6.4 ± 0.1. Before injecting Ly solutions, each microchannel was conditioned for at least 200 s with Ly-free solutions containing NaCl and/or phosphate buffer. Every data point reported corresponds to an average for the same solution in two different microchannels. The values of streaming potential recorded at certain

time (E_t), were divided by the streaming potential value of the protein-free solution (E_b) which was flowed prior to each Ly injection. Therefore, the corrected E_c is equal to E_t / E_b so that the first value of E_c is 1 and for pristine COC is plotted with a negative sign arbitrarily assigned to indicate the charge of this material at pH 6.4 (see below). Fitting of experimental data to kinetic equations were made using the Levenberg-Marquadt method included in the math module of PSI-Plot version 8.83 (Poly software International, Pearl River, NY).

4.2.4 Inhibition of protein adsorption

A 2% v/v Polyethylene glycol sorbitan monolaurate (Tween 20) solution was prepared in DI water and its conductivity adjusted to 540 µS cm-1 with addition of NaCl 50 mM. Tween 20 solution was flowed through a microchannel during 900 seconds, followed by surface washing with free surfactant solution for 450 seconds. Then, adsorption of lysozyme 70 nM in DI water occurred for 700 seconds followed by surface washing with free protein solution for 350 seconds

4.3 Results and discussions.

4.3.1 Real-time Pulsed Streaming Potentials for evaluation of dynamic adsorption processes.

Figure 4.1 shows the new approach for sample introduction developed in this work using a plastic micropipette tip attached to the inlet of a COC microchannel. This plastic reservoir acts as on-line injector that allows the introduction of finite volumes of sample followed by blank solution to monitor adsorption and desorption processes in real time. The microchannel is usually a semicircular conduit (~3 cm×~120 µm×~50 µm) connected to a suction pump through the outlet as depicted in Figure 4.1.

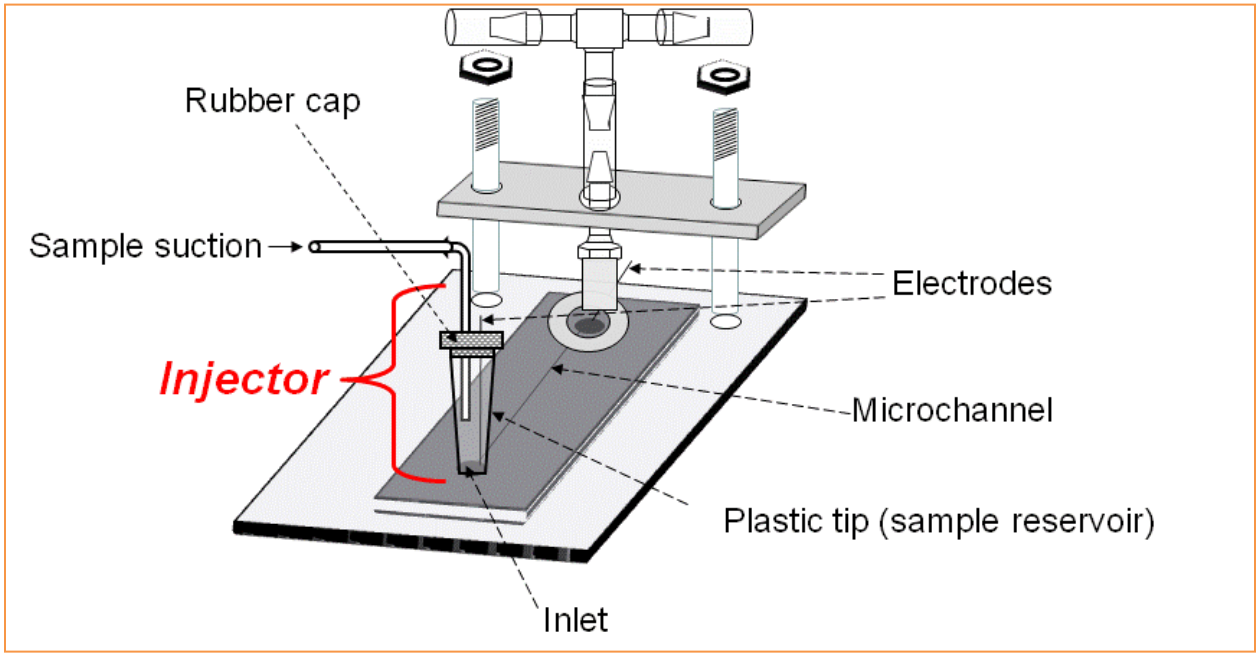

Figure 4.1 Plastic reservoir acting as injector on the inlet of a COC microchannel

Another aspect that makes the present approach unique with respect to previous work on streaming potentials[17-26] is the pulsed nature of the pressure-driven flow which is used to mitigate the electrochemical drift of the electrodes.[15] This allows the measurement of E with non-reference electrodes without the need of special electrolytes to stabilize the electrode potentials[15].

Figure 4.2 shows the variation of the pulsed streaming potential for a COC microchannel when injecting Ly solution 350 nM into an ongoing stream of blank solution at pH 6.4. Prior to the injection, the pulses are displayed in negative direction to illustrate the negative character of the pristine COC surface at this pH. [15, 23, 25, 26] Because the isoelectric point, pI, for Ly is 11.1, [27] its net charge at neutral pH is positive, therefore, adsorption of Ly would render a positive charge on the COC surface.

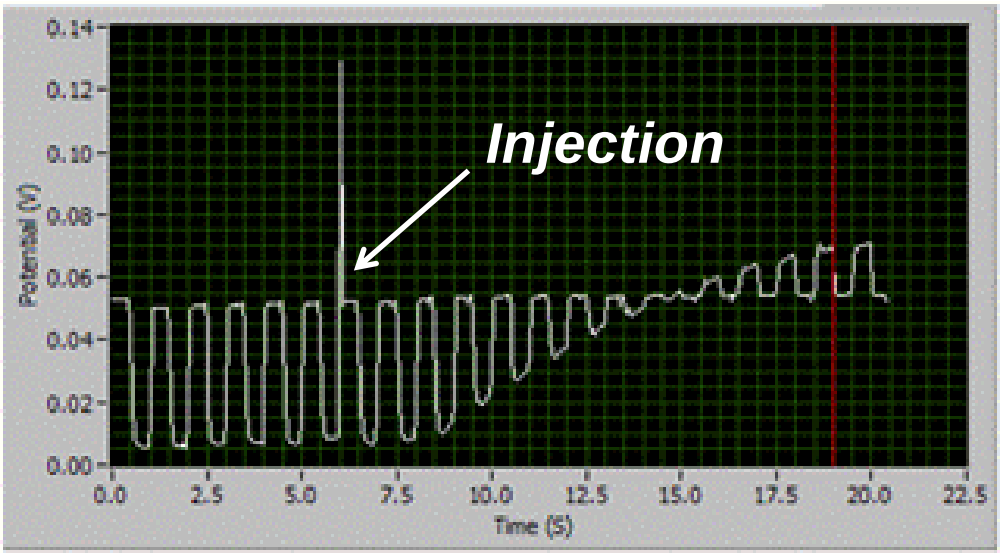

Figure 4.2. Pulsed streaming potential response showing the injection of lysozyme 350 nM.

This is confirmed by the gradual decrease of the negative pulse magnitude and the subsequent increase of the pulse in the opposite direction after Ly injection (Figure 4.3). Spectroscopic evidence on open COC plates has also confirmed the tendency of other proteins to adsorb non-

specifically on COC. [16] Surveillance times longer than 20 seconds allow the observation of adsorption/desorption profiles similar to the ones obtained by surface plasmon resonance (SPR).[28, 29]

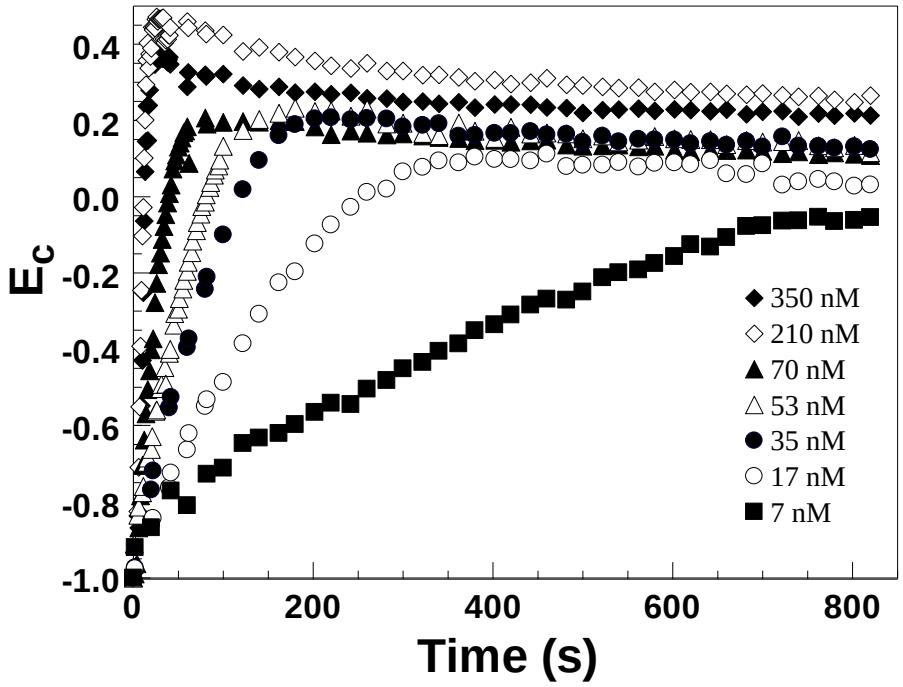

Figure 4.3 Time profile of Ec at different concentrations of Ly in 5.0 mM of NaCl pH 6.4 no phosphate buffer; all solutions was 544 ± 10 µS/cm.

To evaluate the effect of the concentration on the adsorption kinetics on pristine COC, solutions with Ly ranging from 7.0 to 350 nM in 5.0 mM of NaCl were injected. The time profiles over 800 s are displayed in Figure 4.2. The corrected E_c (see experimental section) is arbitrarily plotted with a negative sign to indicate the charge of pristine COC at pH 6.4 (Figure 4.2).[15,16]

The charge of COC under these conditions have been attributed to oxygenated functionalities created during the molding of the plastic which involves melting temperatures in aerobic conditions and also non-specific adsorption of anions.[16, 23, 25, 26, 30, 31]

The concentrations above 70 nM show a very rapid increase of the streaming potential with a maximum followed by a small decrease of the signal that levels off at longer times. This behavior known as "overshooting", has been explained as conformational reorganization or spreading of molecules on the surface.[32-35] For Ly, overshooting has been observed in adsorption on both hydrophobic and hydrophilic substrates.[36-38] Because the streaming potential is directly related to the surface charge density,[39] the reduction of E_c after the maximum at the initial stages of adsorption, could be rationalized as a decrease in the number of positive charges exposed to the liquid-solid interface. This interpretation is compatible with adsorption models which suggest that during reorganization, Ly adopts a "side on" configuration that hides some of the positive charges from the solid-liquid interface.[37, 38, 40]

To investigate variables that could affect the kinetics of Ly adsorption, the effect of phosphate buffer was considered given that phosphate is one of the most common anions and its adsorption on hydrophobic plastic surfaces has been suggested previously.[30, 31] However, it has also been said that phosphate anions in mM concentrations are unlikely to adsorb[31] and recently it has been suggested that surface charge is dominated by hydroxyl adsorption even in the presence of phosphate.[41]

Figure 4.4 shows time profiles for the same concentrations of Ly as in Figure 4.2 but with phosphate buffer 1.5 mM at pH 6.4. In the presence of phosphate, slower reversal of charge is observed during Ly adsorption when compared to the same concentrations of Ly without phosphate buffer.

Furthermore, for solutions above 210 nM overshooting is appreciably lessened and the E_c maximum is lower. For instance, at 17 nM of Ly in pure NaCl solution, ~244 seconds are

needed to reverse the negative surface charge of the pristine COC. In contrast, the presence of phosphate at 17 nM of Ly still renders a negative surface charge after ~800 seconds.

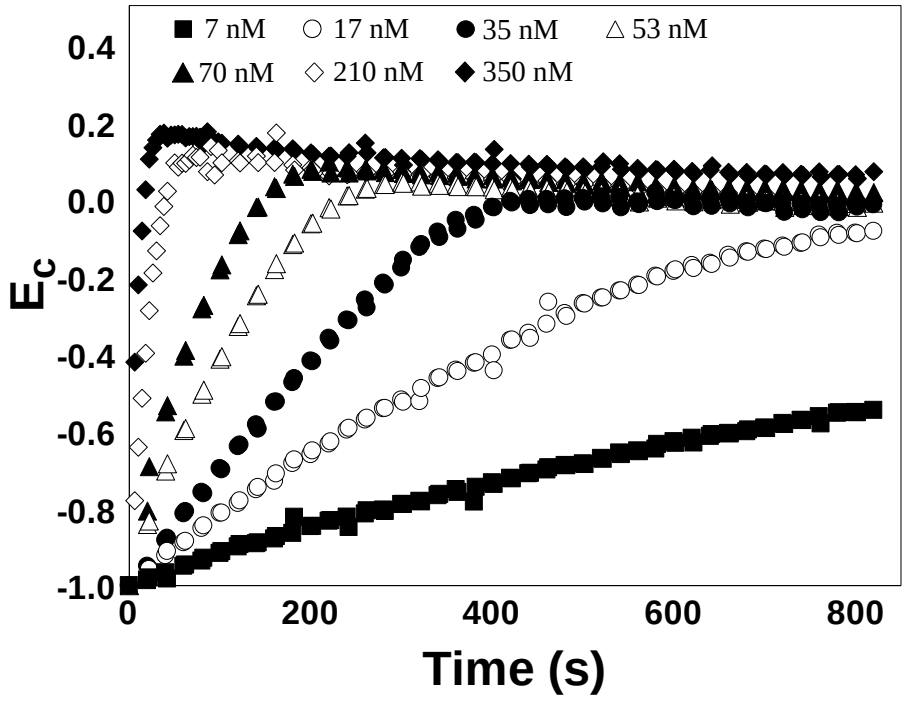

Figure 4.4 Time profile of Ec at different concentrations of Ly in 1.5mM buffer phosphate pH 6.4 and NaCl to adjust conductivity; the conductivity of all solutions was 544±10 µS/cm.

Similar trends are observed for the other concentrations of Ly tested. It appears as if the positive surface charge brought in by Ly adsorption and detected by streaming potential is less when phosphate ions are present. This process could occur through charge neutralization of some amino acids by phosphate ions,[42, 43] or through a decrease in the electrostatic attraction between Ly and the COC surface as result of the overall reduction of the protein's positive charge.[44] By the same token, if the absorbed Ly carries less positive charge, the lateral repulsion between neighboring molecules should be lower and the reduction of overshooting may be explained.

This kind of ion-binding interaction has been brought up as explanation for the shift of electrophoretic mobility of Ly and the reduction of its charge number in phosphate medium[44, 45].

To further support this point, experiments with incremental additions of phosphate buffer were performed at constant pH and conductivity. Figure 4.5 shows how despite increasing the concentration of phosphate buffer from 1.5 to 3.0 and 4.5 mM, the adsorption kinetics of a 70 nM solution of Ly did not change. This is an indication that 1.5 mM of phosphate is enough to saturate the ion binding capacity of the adsorbed Ly which reduces its overall positive charge and causes a slower reversal of the COC negative charge as Ly adsorbs.

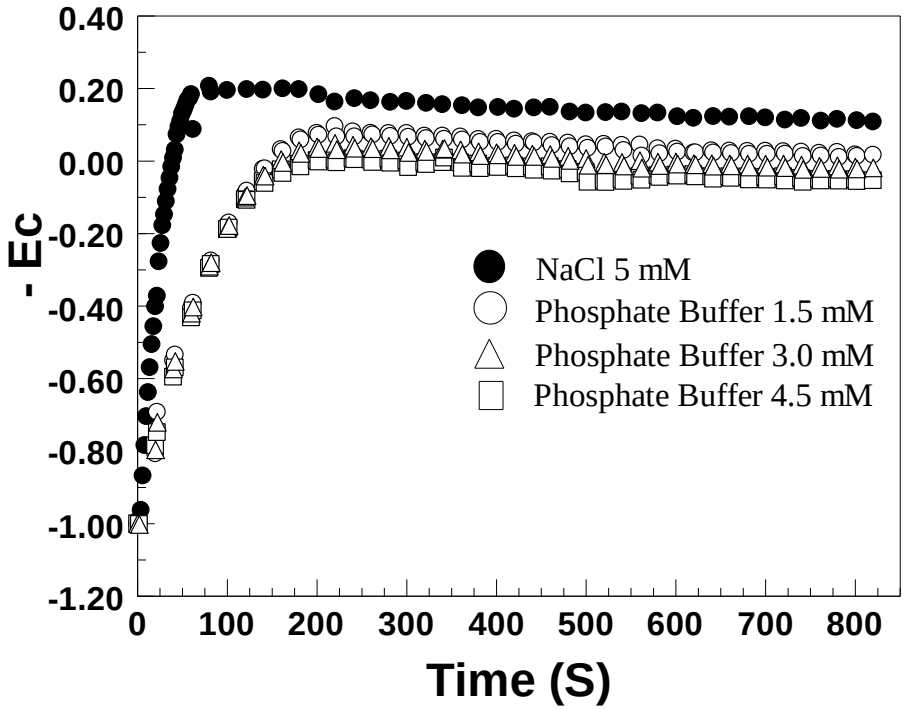

Figure 4.5 Time profile of Ec for 70 nM of Ly in 5.0 mM of NaCl at different concentrations of phosphate buffer pH 6.4; the conductivity of all solutions was in the 544 ± 10 μS/cm.

4.3.2 Real time Pulsed Streaming Potentials as quantification method.

To illustrate the potential of this method for quantification of proteins, a simple adsorption model represented by Equation 4.1 can be used. The protein in solution indicated by Ly_{free} can be

adsorbed on the surface, Ly_{ads}, according to the forward rate constant k_i and vices versa through k_{-i}. If it is assumed that any adsorption of Ly will lead to a change in the surface charge, which in turn determines the streaming potential E_c, the time variation of E_c, dE_c/dt, can be expressed in terms of the concentrations and the rate constants (Equation 4.2).

(4.1) $$Ly_{free} \underset{k_{-i}}{\overset{k_i}{\rightleftharpoons}} Ly_{ads}$$

(4.2) $$\frac{dE_c}{dt} = k_i[Ly_{free}] - k_{-i}[Ly_{ads}]$$

(4.3) $$\left(\frac{dE_c}{dt}\right)_i = k_i[Ly_{free}]$$

At the initial stages of adsorption when $[Ly_{free}] >> [Ly_{ads}]$, the second term in Equation 4.2 can be dropped and $(dE_c/dt)_i$ becomes a linear function of the bulk [Ly] (Equation 4.3) with k_i accessible from the slope of a plot of $(d E_c/dt)_i$ vs. [Ly] (Figure 4.6).

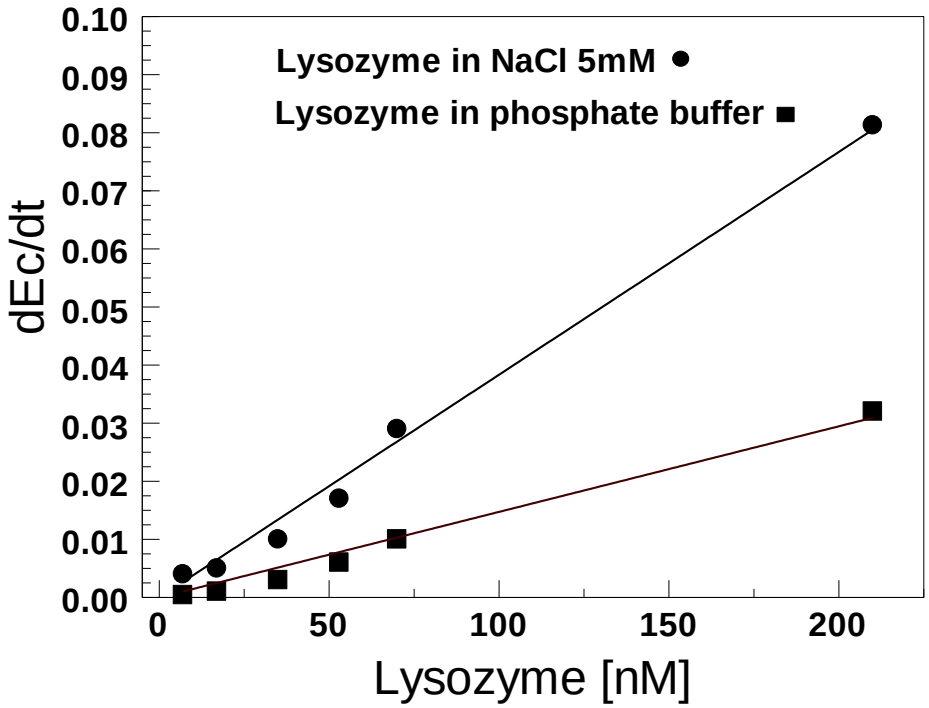

Figure 4.6 Plots of (dEc/dt)i as a function of [Ly] with two different electrolytes pH for both solutions was 6.4.

These graphs were constructed with the slope values, $(dE_c/dt)_i$, determined from the linear regions of the time profiles of E_c vs. t. The $(dE_c/dt)_i$ values and corresponding correlation coefficients of linearity obtained for the first 60 s of adsorption at different concentrations of Ly are listed in Table 4.1.

Table 4.3 Linear regression results for Ec vs t data points taken from the first 60 s of adsorption in Figure 4.3. The fit was made to the equation Ec = m t + b, where m is the slope given by (dEc/dt)i and b is the intercept with the ordinate. The correlation coefficient of linearity is r^2. The same approach was done for the first 60 s of Figure 4.3 to obtain the data points in Figure 4.6 corresponding to the measurements in the presence of phosphate buffer.

Lysozyme Concentration	**dE/dt (x 10^3)**	**b**	**r^2**
7 nM	0.82	-1.00	0.94
17 nM	1.91	-1.00	0.99
35 nM	3.22	-1.01	0.99
53 nM	6.53	-0.98	0.99
70 nM	9.68	-0.97	0.98
350 nM	31.06	-0.97	0.99

The k_i values also reflect the effect of phosphate ions which reduce the positive charge brought in during Ly adsorption. Therefore, a smaller variation of $(dE_c/dt)_i$ when increasing the bulk [Ly] indicates that the protein is less effective in changing the streaming potential or reversing the negative charge of COC during adsorption. For instance, k_i in the presence of phosphate was estimated to be 1.4×10^{-4} which is lower than the value determined in the absence of phosphate ions, 3.9×10^{-4} $(nM\ s)^{-1}$. The k_i value can also be used as calibration parameter to estimate [Ly] in samples of unknown concentration. Once $(dE_c/dt)_i$ is determined from the linear region of the adsorption kinetics for the unknown sample, [Ly] is calculated from Equation. 4.3

Since a value of $(dE_c/dt)_i$ can be found per each adsorption profile, at each concentration, it is possible to calculate the value of k_i with only one calibration point (equation 4.3). Table 4.2 shows a list of [Ly] values that were calculated using k_i found using only the initial adsorption of 70 and 53 nM Ly, in NaCl and phosphate respectively. Each [Ly] calculated is for a point in a series of solutions prepared with known concentration of Ly

Table 4.4. Calculated concentrations of lysozyme from k_i obtained from "one –point" calibration.

Value expected (nM)	Value calculated in NaCl (nM)	Value calculated in Phosphate (nM)
7	10	4
17	12	9
35	24	27
53	41	53
70	70	88
210	196	283

Despite the significant error involved, the calculated values fall within the same order of magnitude of the actual concentrations of Ly. This approach with analytical potential is only valid at the initial stages of adsorption because the signal is linearly related to the bulk concentration of Ly (Eq. 4.3) as it should be when the adsorption is limited by mass transport[46], and is an indication of the viability of the method to perform "one-point" calibration.

4.3.3 Estimation of dynamic parameters from real-time Pulsed Streaming Potentials

To show that pulsed streaming potentials can be used to study adsorption and desorption events in real time, an injection of Ly 70 nM, followed by protein-free solution was monitored over time. Figure 4.7 shows the time variation of corrected E_c values for Ly in NaCl 5.0 mM with no buffer phosphate (open squares) and 1.5 mM of phosphate buffer (open circles) at pH 6.4. The dashed and solid lines represent fits to exponential equations adopted from SPR kinetic analyses based on a bimolecular model of interaction with the surface.[29]

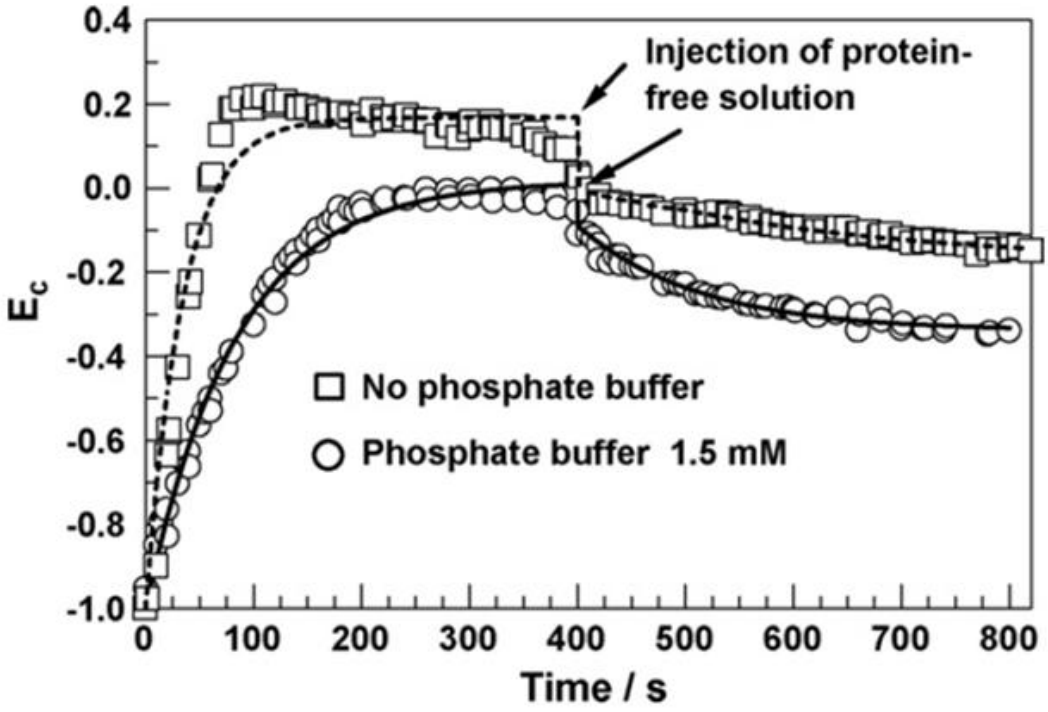

Figure 4.7. Time response of streaming potential for a solution of Ly 70nM showing adsorption and desorption phases; Conductivity of all solutions was 544 ± 10 S/cm. Dashed and solid lines represent fits to Eqs. (5) and (6)

The expressions for the adsorption and desorption phases are given by Equations 5 and 6 respectively. E_c is the corrected streaming potential signal, E_∞ is the signal at equilibrium ($t = \infty$), E_0 is the signal at t = 0, and k_a and k_d are the adsorption and desorption rate constants.

(4.4) $$E_c = E_\infty(1 - e^{-(k_a[Ly]+k_d)t}) + E_0$$

(4.5) $$E_c = E_\infty(e^{-k_d t}) + E_0$$

All the isotherms in Figures 4.4 and 4.5 were subjected to fitting with Equation 4.4 and the values for the exponential term k_a [Ly] + k_d at each Ly concentration are shown in Table 4.3. These values were plotted against [Ly] and k_a was estimated from the slope for adsorption of Ly with and without phosphate present. In principle k_d could be estimated from the intercept of this plot as well but it is not considered accurate, therefore Equation.4.5 is used instead with the assumption that re-adsorption of the analyte does not occur.[29, 47]

Table 4.5 Fitting to Eq. (5) at different Ly concentrations.

10^{-9} [Ly] (Mol L^{-1})	**(k_a [Ly] + k_d)**	
	With phosphate	**No phosphate**
7.0	2.40×10^{-7}	4.00×10^{-7}
17	1.00×10^{-6}	6.80×10^{-3}
35	4.36×10^{-3}	1.38×10^{-2}
53	9.98×10^{-3}	1.97×10^{-2}
70	1.58×10^{-2}	4.16×10^{-2}
210	5.54×10^{-2}	1.17×10^{-1}

Because this simple adsorption model does not consider surface reorganization nor lateral interactions, the overshooting observed for the data without phosphate buffer is not well represented by the fit, however the rest of the data is. The estimated values of k_a (3.2×10^5 s^{-1} M^{-}

^{1}) and k_d (8.9 x 10^{-3} s^{-1}) for Figure 4.7, can also be used to calculate an adsorption equilibrium constant K_{eq}, knowing that $K_{eq} = k_a / k_d$, 3.6 x 10^7 M^{-1}. Since the rate constants are not corrected for mass transport effects, they may be under or overestimated.[29]

Nevertheless, relative comparisons of conditions that affect the adsorption kinetics are valid. For example, k_a estimated from fitting to Eq. 5 and 6, for 70 nM of Ly in the absence of phosphate was found to be higher (5.9 x 10^5 s^{-1} M^{-1}) whereas the value of k_d was lower (3.3 x 10^{-3} s^{-1}). This effect on both rate constants could be explained as an overall increase in the attraction between Ly and the negative COC surface as a result of the unshielded positive charge of Ly when no phosphate ions are present.

Additionally, the data corresponding to the time when the equilibrium of adsorption is achieved in the plots Ec versus time, can be fitted to a model isotherm. Figure 4.8 shows the values of Ec at 300 seconds of adsorption, from figures 4.3 and 4.4 at each concentration studied. Dotted lines correspond to the fitting with the model in equation 4.7

(4.7)
$$Ec = \frac{KC(A-B)}{1+KC} - B$$

A and B represent empirical constants, C (M) is the concentration and K (M^{-1}) is a pseudo equilibrium constant which captures the essence of the adsorptive process at the equilibrium, when Ec remains unchanged beyond `~ 300s of adsorption. The relation of this K with the K_{eq} obtained from $K_{eq} = k_a / k_d$ can be observed in Table 4.4, which reviews the constants obtained for both methods. This results show that both methodologies produced very similar values, which is complementary evidence that real-time streaming potentials can be used to evaluate

equilibrium constant of the adsorption process. Moreover, the methodology of using the Ec values when equilibrium is reached, eliminates the need for the evaluation of desorption phase and then it could be advantageous since "no re-adsorption" assumption has to be done.

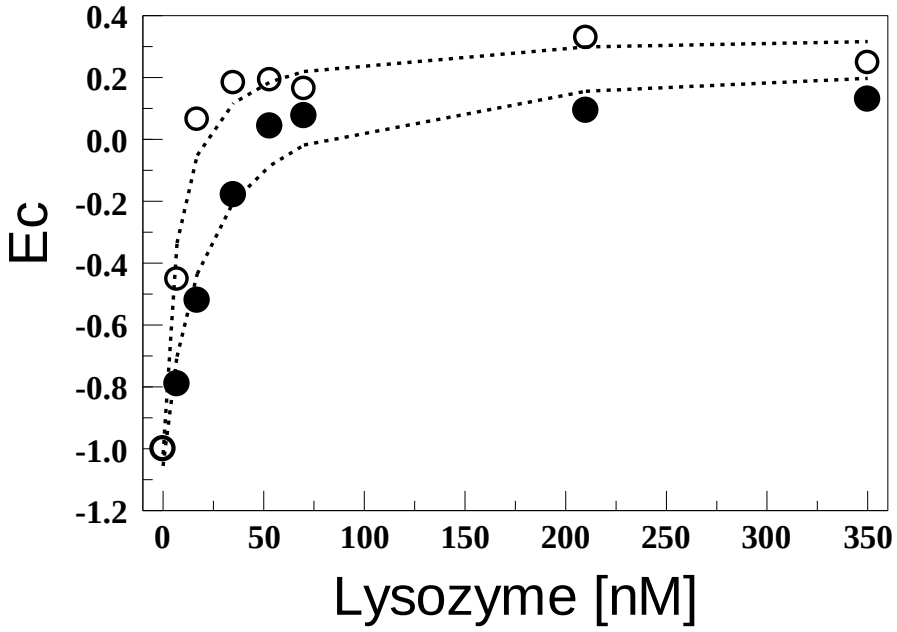

Figure 4.8 Isotherms obtained at the equilibrium of adsorption (~ 300 seconds) of lysozyme on COC channels, in phosphate buffer (black circles) and in NaCl 5 mM (open circles). Broken lines represent fitting of the data with the model in equation 4.7.

Table 4.6. Equilibrium constants for the adsorption of lysozyme on Cyclic Olefin Copolymer, with and without presence of phosphate buffer, calculated by two different models using normalized Pulsed Streaming Potentials (Ec).

	K from isotherm model	**Keq from kinetic model**
Phosphate Buffer	$5.2 \times 10^{7}\ M^{-1}$	$3.6 \times 10^{7}\ M^{-1}$
No Phosphate buffer	$1.4 \times 10^{8}\ M^{-1}$	$1.8 \times 10^{8}\ M^{-1}$

4.3.4 Inhibition of adsorption by blocking the surface

Since the adsorption of lysozyme on COC is dependent on the electrostatic interaction between protein and surface, as shown by the effect of the phosphate buffer, a great inhibition of the protein adsorption can be expected if the surface is modified with a coating which produces an almost non-charged interface. Poly-alcohols are good candidates to inhibit the electrostatic interaction since alcohol groups do not have a strong acid-based behavior.

To show inhibition of lysozyme adsorption, polyethylene glycol sorbitan monolaurate (Tween 20) was adsorbed, before lysozyme, on the COC microchannel surface and its adsorption followed by real-time Pulsed Streaming Potentials. In Figure 4.9 the first 1350 seconds show the adsorption-desorption phases for Tween 20. The adsorption phase show how when Tween 20 is attached to the surface Ec reaches values close to zero (0.05), as expected for a molecule with no ionizable groups (see inset in Figure 4.9) which produces an small amount of counterions located at the interfacial double layer. Introduction of free Tween buffer at ~ 900 seconds produced a fast reduction of Ec due to the washing out of excess Tween 20. At 1350 seconds, when the surface has achieved a value of ~ 0.6, lysozyme 70 nM was introduced.

When lysozyme is introduced on the microchannel coated with Tween 20, the surface charge is never reversed and Ec increases only from -0.60 to -0.38 and then it reverts back to -0.56 after washed with protein-free solution. This is a strong evidence that most of the lysozyme that was attached to the Tween 20 modified surface, leaves the substrate after the desorption phase. For uncoated COC after washing with protein-free solution, Ec is considerably different from the pristine surface, indicating that protein is irreversible attached. This considerations show that pre-adsorption of polyalcohols is a way to inhibit lysozyme attachment to the COC surface.

Moreover, this result shows that real-time Pulsed Streaming Potentials are an easy way to evaluate the antifouling properties of coatings.

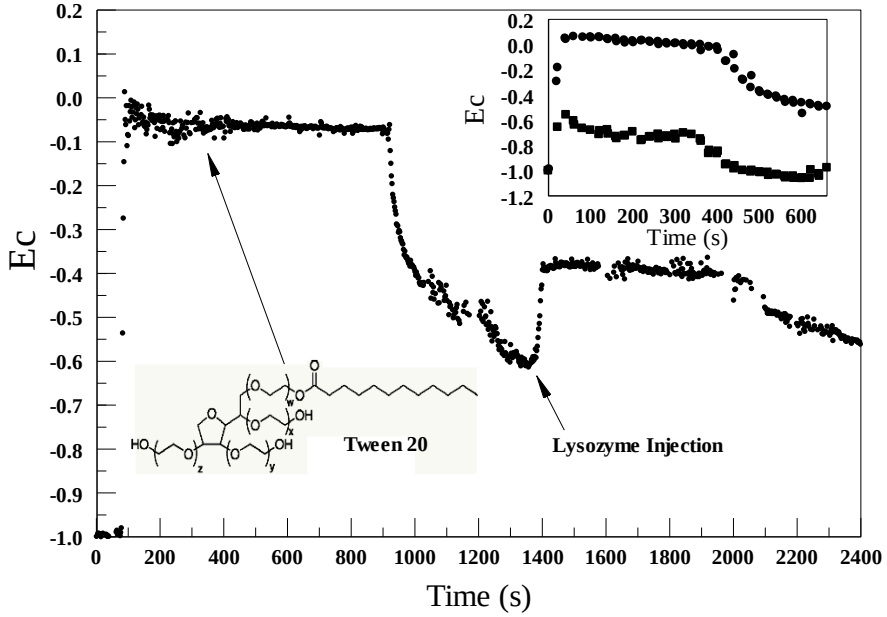

Figure 4.9. Adsorption-desorption cycles for lysozyme 70 nM after previous adsorption of 2% Tween 20 on a COC microchannel. Insert shows adsorption of lysozyme 70 nM on pristine COC (starts) compared with its adsorption on Tween 20 modified COC (squares).

4.4 Conclusions.

In summary, these results show that real-time pulsed streaming potentials generated in plastic microfluidic channels can be used to monitor the kinetics of adsorption and desorption processes between Ly and a plastic surface. Estimation of rate and equilibrium constants can be made by fitting to simple standard models of adsorption. Because most of the proteins tend to adsorb on hydrophobic surfaces, any hydrophobic substrate that can be set up in microchannel configuration could be a platform to study adsorption kinetics of proteins.

By the same token, due to the preconcentration effect on the surface, any type of interaction that can affect the adsorption kinetics could be studied by this method as shown for the case of Ly and phosphate ions. It is envisioned that this approach could be applicable to investigate interactions between bioprobes that require physical contact to express their physiological function (protein, viruses and bacteria) and that are in general difficult to detect. Some of the anticipated advantages of this approach are: the signal is generated without the need of analyte labeling, there are no restrictions to a specific surface because any substrate that can be set up in microchannel configuration can be used, the method is based on very simple and low cost instrumentation, and unlike other approaches the signal arises exclusively from charge interactions. Finally, this method is ideally suited for mircrofluidics because the signal is a result of the interaction of the liquid flow and the surface charge in the microchannel.

4.5 References.

1. Ueda, T.; Tsurumaru, M.; Imoto, T., Kinetic measurement of the interaction between a lysozyme and its immobilized substrate analogue by means of surface plasmon resonance. *J. Biochem.* **1998,** 124, 712-716.
2. Etheve, J.; Dejardin, P., Adsorption Kinetics of Lysozyme on Silica at pH 7.4: Correlation between Streaming Potential and Adsorbed Amount. *Langmuir* **2002,** 18, (5), 1777-1785.
3. Liao, M.-H.; Chen, D.-H., Fast and efficient adsorption/desorption of protein by a novel magnetic nano-adsorbent. *Biotechnol. Lett.* **2002,** 24, 1913-1917.
4. Glomm, W. R.; Halskau, O. J.; Hanneseth, A. D.; Volden, S., Adsorption behaviour of acidic and basic proteins onto citrate-coated Au surfaces correlated to their native fold, stability, and pI. *J. Phys. Chem. B* **2007,** 111, 14329-14345.
5. Chen, Y.-M.; Yu, C.-J.; Cheng, T.-L.; Tseng, W.-L., Colorimetric detection of lysozyme based on electrostatic interaction with human serum albumin-modified gold nanoparticles. *Langmuir* **2008,** 24, 3654-3660.
6. Roulet, J.-C.; Volkel, R.; Herzig, H. P.; Verpoorte, E.; de Rooij, N. F.; Dandliker, R., Performance of an Integrated Microoptical System for Fluorescence Detection in Microfluidic Systems. *Anal. Chem.* **2002,** 74, (14), 3400-3407.
7. Hollards, C. W.; Puls, J.; Bakajin, O.; Olsan, B.; Talley, C. E.; Lane, S. M.; Huser, T., Bio-assay based on single molecule fluorescence detection in microfluidic channels. *Anal. Bioanal. Chem.* **2006,** 385, (8), 1384-1388.
8. Bliss, C. L.; McMullin, J. N.; Backhouse, C. J., Integrated wavelength-selective optical waveguides for microfluidic-based laser-induced fluorescence detection. *Lab chip* **2008,** 8, 143-151.
9. Galloway, M.; Stryjewski, W.; Henry, A.; Ford, S. M.; Llopis, S.; McCarley, R. L.; Soper, S. A., Contact Conductivity Detection in Poly(methyl methacylate)-Based Microfluidic Devices for Analysis of Mono- and Polyanionic Molecules. *Anal. Chem* **2002,** 74, (10), 2407-2415.
10. Liu, Y.; Wipf, D. O.; Henry, C. S., Conductivity detection for monitoring mixing reactions in microfluidics devices. *Analyst* **2001,** 126, 1248-1251.
11. Liu, Y.-S.; Walter, T. M.; Chang, W.-J.; Lim, K.-S.; Yang, L.; Lee, S. W.; Aronson, A.; Bashir, R., Electrical detection of germination of viable mdel *Bacillus anthracis* spores in microfluidics. *Lab chip* **2007,** 7, 603-610.
12. Weng, C.-H.; Yeh, W.-M.; Ho, K.-C.; Lee, G.-B., A microfluidic system utilizing molecularly imprinted polymer films for amperometric detection of morphine. *Sens. Actuators, B.* **2007,** 121, (2), 576-582.
13. Lindsay, S.; Terannie, V.; Egatz-Gomez, A.; Loyprasert, S.; Garcia, A. A.; Wang, J., Discrete microfluidics with electrochemical detection. *Analyst* **2007,** 132, 412-416.
14. Wang, J.; Polsky, R.; Tian, B.; Chatrathi, M. P., Voltammetry on Microfluidic Chip Platforms. *Anal. Chem.* **2000,** 72, (21), 5285-5289.
15. Pu, Q.; Elazazy, M. S.; Alvarez, J. C., Label-Free Detection of Heparin, Streptavidin, and Other Probes by Pulsed Streaming Potentials in Plastic Microfluidic Channels. *Anal. Chem.* **2008,** 80, (17), 6532-6536.
16. Pu, Q.; Oyesanya, O.; Thompson, B.; Liu, S.; Alvarez, J. C., On-Chip Micropatterning of Plastic (Cylic Olefin Copolymer, COC) Microfluidic Channels for the Fabrication of Biomolecule Microarrays Using Photografting Methods. *Langmuir* **2007,** 23, (3), 1577-1583.
17. Norde, W.; Rouwendal, E., Streaming potential measurements as a tool to study protein adsorption kinetics. *J. Colloid Interface Sci.* **1990,** 139, (1), 169-176.

18. Bellmann, C.; Klinger, C.; Opfermann, A.; Bohme, F.; Adler, H.-J. P., Evaluation of Surface Modification by Electrokinetic Measurements. *Prog. Org. Coat.* **2002,** 44, 93-98.
19. Gusev, I.; Horvath, C., Streaming Potential in Open and Packed Fused-Silica Capillaries. *J. Chromatogr. A* **2002,** 948, 203-223.
20. Hunter, R. J., *Zeta Potential in Colloid Science: Principles and Applications*. Academic Press: London, 1981; p 381.
21. Schwarz, S.; Eichhorn, K.-J.; Wischerhoff, E.; Laschewsky, A., Polyelectrolyte Adsorption Onto Planar Surfaces: A Study by Streaming Potential and Ellipsometry Measurements. *Colloids Surf.* **1999,** 159, 491-501.
22. Toshihiko, J.; Mitsuru, H.; Minoura, N.; Akihiko, T., Surface Characterization of Poly(acrylonitrile) Membranes Graft-Polymerized with Ionic Monomers As Revealed by z Potential Measurement. *Macromolecules* **1998,** 31, 1277-1284.
23. Kirby, B. J.; Hasselbrink, E. F. J., Zeta Potential of Microfludic Substrates: 1. Theory, Experimental Techniques, and Effects on Separations. *Electrophoresis* **2004,** 25, 187-202.
24. Kirby, B. J.; Hasselbrink, E. F. J., Zeta Potential of Microfluidic Substrates: 2. Data for Polymers. *Electrophoresis* **2004,** 25, 203-213.
25. Mela, P.; van den Berg, A.; Fintschenko, Y.; Cummings, E. B.; Simmons, B. A.; Kirby, B. J., The Zeta Potential of Cyclo-Olefin Polymer Microchannels and Its Effects on Insulative (Electrodeless) Dielectrophoresis Particle Trapping Devices. *Electrophoresis* **2005,** 26, 1792-1799.
26. Erickson, D.; Li, D., Streaming Potential and Streaming Current Methods for Characterizing Heterogeneous Solid Surfaces. *J. Colloid Interface Sci.* **2001,** 237, (2), 283-289.
27. Pasche, S.; Voros, J.; Griesser, H. J.; Spencer, N. D.; Textor, M., *J. Phys. Chem. B* **2005,** 109, 17545-17552.
28. Wegner, G. T.; Alastir, W. M.; Lee, J. H.; Codner, E.; Saeki, T.; Fang, S.; Corn, R. M., *Anal. Chem.* **2004,** 76, 5677-5684.
29. de Mol, N. J.; Plomp, E.; Fischer, M. J. E.; Ruijtenbeek, R., Kinetic Analysis of the Mass Transport Limited Interaction between the Tyrosine Kinase lck SH2 Domain and a Phosphorylated Peptide Studied by a New Cuvette-Based Surface Plasmon Resonance Instrument. *Anal. Biochem* **2000,** 279, 61-70.
30. Hassenteufel, W.; Jagitsch, R.; Koczy, F. F., *Limnol. Oceanogr.* **1963,** 8, 1952-1956.
31. Tandon, V.; Bhagavatula, S. K.; Nelson, W. C.; Kirby, B. J., *Electrophoresis* **2008,** 29, 1092-1101.
32. Hedström, M.; Galaev, I. Y.; Mattiasson, B., Continuous measurements of a binding reaction using a capacitive biosensor. *Biosens. Bioelectron.* **2005,** 21, (1), 41-48.
33. Svendsen, I. E.; Lindh, L.; Arnebrant, T., Adsorption behaviour and surfactant elution of cationic salivary proteins at solid/liquid interfaces, studied by in situ ellipsometry. *Colloids Surf. B: Biointerfaces* **2006,** 53, (2), 157-166.
34. Malmsten, M.; Siegel, G.; Wood, W. G., Ellipsometry Studies of Lipoprotein Adsorption. *J. Colloid Interface Sci.* **2000,** 224, (2), 338-346.
35. Karlsson, M.; Ekeroth, J.; Elwing, H.; Carlsson, U., Reduction of Irreversible Protein Adsorption on Solid Surfaces by Protein Engineering for Increased Stability. *J. Biol. Chem.* **2005,** 280, (27), 25558-25564.
36. Wertz, C. F.; Santore, M. M., Adsorption and Reorientation Kinetics of Lysozyme on Hydrophobic Surfaces. *Langmuir* **2002,** 18, (4), 1190-1199.
37. Robeson, J. L.; Tilton, R. D., Spontaneous Reconfiguration of Adsorbed Lysozyme Layers Observed by Total Internal Reflection Fluorescence with a pH-Sensitive Fluorophore. *Langmuir* **1996,** 12, (25), 6104-6113.
38. Daly, S. M.; Przybycien, T. M.; Tilton, R. D., Coverage-Dependent Orientation of Lysozyme Adsorbed on Silica. *Langmuir* **2003,** 19, 3848-3857.

39. Yang, J.; Masliyah, J. H.; Kwok, D. Y., Streaming Potential and Electroosmotic Flow in Heterogeneous Circular Microchannels with Nonuniform Zeta Potentials: Requirements of Flow Rate and Current Continuities. *Langmuir* **2004,** 20, (10), 3863-3871.
40. Sun, Y.; Welsh, W. J.; Latour, R. A., Prediction of the Orientations of Adsorbed Protein Using an Empirical Energy Function with Implicit Solvation. *Langmuir* **2005,** 21, (12), 5616-5626.
41. Zimmermann, R., Rein, N., Werner, C., Water ion adsorption dominates charging at nonpolar polymer surfaces in multivalent electrolytes. *Phys.Chem.Chem.Phys.* **2009,** 11, 4360-4364.
42. Vrbka, L.; Jungwirth, P.; Bauduin, P.; Touraud, D.; Kunz, W., Specific Ion Effects at Protein Surfaces: A Molecular Dynamics Study of Bovine Pancreatic Trypsin Inhibitor and Horseradish Peroxidase in Selected Salt Solutions. *J. Phys. Chem. B* **2006,** 110, (13), 7036-7043.
43. Kuehner, D. E.; Engmann, J.; Fergg, F.; Wernick, M.; Blanch, H. W.; Prausnitz, J. M., Lysozyme Net Charge and Ion Binding in Concentrated Aqueous Electrolyte Solutions. *J. Phys. Chem. B* **1999,** 103, (8), 1368-1374.
44. Ethève, J.; Déjardin, P.; Boissière, M., Influence of pH on the adsorption of lysozyme on a sulfonated membrane with and without poly(ethyleneimine). *Desalination* **2002,** 146, (1-3), 111-113.
45. Rabiller-Baudry, M.; Chaufer, B., Small molecular ion adsorption on proteins and DNAs revealed by separation techniques. *J. Chromatogr. B* **2003,** 797, (1-2), 331-345.
46. Karlsson, R.; Roos, H.; Fägerstam, L.; Persson, B., Kinetic and Concentration Analysis Using BIA Technology. *Methods* **1994,** 6, (2), 99-110.
47. Karlsson, R.; Michaelsson, A.; Mattson, L., *J. Immunol. Methods* **1991,** 145, 229-240.

5 A non-fouling surface for protein detection using PSP

This chapter describes the modification of COC microchannels with a composite material which reduces the non specific adsorption of proteins and allows the immobilization of specific receptors to the surface. Real-time Pulsed Streaming Potentials are used along with the modified surface, to detect lysozyme in the presence of cytochrome C as interfering analyte.

5.1 Introduction

Herein, the preparation of a hydrophilic composite surface by UV-photografting of polyethylene glycol acrylate (PEGA) and polyacrylic acid (PAA) films on microchannels fabricated with the plastic cyclic olefin copolymer (COC) is reported.[1] This surface modification allows the easy regeneration of the surface zeta potential which in turn enables consecutive and reproducible detection of protein adsorption in real time by pulsed streaming potentials which are spontaneous ion gradients created when solutions move through microchannels by pressure-driven flow.[2-4]

In the previous chapter, the implementation of a new strategy for sample introduction, which allows the kinetic measurement of Lysozyme (Ly) adsorption in real time on COC was shown.[3] One problem revealed by these kinetic studies, was the non-specific adsorption that prevented regeneration of the original surface charge and made difficult consecutive reproducible measurements using the same microfluidic channel.[3] Also, because these adsorption kinetic studies were performed on pristine COC, the Ly detection did not have any selectivity.[3]

Herein these problems are addressed by preparing a composite hydrophilic film which provides a renewable non-fouling surface and at the same time imparts some degree of specificity by allowing the linkage of Anti-Ly polyclonal antibodies. Furthermore, we used the kinetic monitoring of the surface charge by pulsed streaming potentials to optimize the preparation of the composite film as well as to assess its selectivity and sensitivity. The main significance of this work relies on having developed a surface detection technique of general applicability that

does not require chemical labeling but provides significant mitigation of non-specific adsorption while still providing nanomolar detection limits with some degree of specificity for Ly. Lysozyme is an enzyme that helps natural protection against pathogens and is present in body secretions such as saliva, mucus and tears.[5] Herein Ly is used as a model for developing a protein sensor using pulsed streaming potentials but because binding constants can be obtained, it is also a model for studying protein interactions with immobilized probes.

The understanding of protein interactions like those occurring in protein-peptide binding,[6] pathogen-host interactions[7] and Amyloid formation,[8] is very important to determine biological function and physiological health. Surface based techniques such as Surface Plasmon Resonance (SPR), Quartz Crystal Microbalance (QCM) and Pulsed Streaming Potentials (PSP) are very suitable for such studies because these techniques do not require chemical labeling and allow surface immobilization of one of the targets in the interaction. The surface confinement present in these techniques can better mimic the congregation environment that cellular organelles and membrane macromolecules provide in vivo as opposed to studying interactions in the bulk.[9]

Nonetheless, the investigation of interactions between solution species and immobilized targets on surfaces is difficult because non-specific adsorption (NSA) can obscure the signal of binding events. In hydrophobic substrates, like COC and bare gold, adsorption of proteins occurs spontaneously and is responsible in great part for the NSA and the irreversible fouling observed in such surfaces.[10-12] The challenge for creating platforms to study surface-probe interactions (or surface based sensors) consists in preventing NSA but at the same providing surface receptors

with good specificity. This would improve the sensing performance of the surface and in some cases reduce the cost of analysis by allowing surface regeneration. The immobilization of hydrophilic and non-ionizable films has been the main strategy to circumvent NSA. Approaches such as the immobilization of hydrogels like carboxymethyl dextran has been used on the metallic surface of SPR chips.[13] However, polyethylene glycol is probably the most widely used material to prevent NSA and has been immobilized on almost every surface including silicon,[14] poly(methyl methacrylate),[15] glass,[16] and gold.[17]

In this chapter the surface modification of hydrophobic COC microchannels by sequential photografting of polyethylene glycol acrylate and poly acrylic acid to provide non-fouling properties is described. The attachment of polyclonal anti-Ly was performed to impart some specificity for the adsorption and detection of Ly. Structural and morphological characterization of the composite surface was done by Atomic Force Microscopy (AFM) and FT-IR. Selectivity and fouling evaluation was done with four additional proteins and using Cytochrome C as interfering species.

5.2 Experimental Section.

5.2.1 Chemicals

Double crystallized and dialyzed Lysozyme (Ly) was purchased from Worthington biochemical corporation (Lakewood, NJ). NaCl 99.5%, NaH_2PO_4 and Na_2HPO_4 were obtained from Merck (San Diego, CA). Cytochrome C C from horse heart (CYT), Fibrinogen Fraction I from human Plasma (FIB), Albumin from human serum 97-99% (HSA), Bovine serum albumin (BSA), Poly(ethylene glycol) acrylate (PEGA), 2-(N-Morpholino) ethanesulfonic acid (MES), N-Hydroxysuccinimide (NHS), N-Ethyl-N′-(3-dimethylaminopropyl) carbodiimide (EDC) and acrylic acid anhydrous (AA) were products from Sigma (St. Louis, MO). Rabbit polyclonal antibody to Lysozyme (Ly) was obtained from AbCam (Cambridge, MA).

5.2.2 Surface characterization

The streaming potential (*E*), which is proportional to the liquid pressure, was recorded at different pH for pristine COC and COC-PEGA microchannels and then plugged into the Smoluchowski equation to calculate the zeta potential.[2-4] The zeta potential (ζ) is defined as the potential at the slippage plane of the liquid but it can be considered as the surface charge.[4]

Phosphate buffer solutions of approximately 1.5 mM from pH 2.3 – 10.7 and a constant conductivity of 389 ± 4 μS cm^{-1}, were used to record E. Each solution was pumped into the

microchannels using 10 pulses of 1 s and their average reported as a single value. The viscosity and dielectric constant used for the calculation were those for pure water at 20 ºC.

Spectroscopic characterization of the composite film was performed by attenuated total reflectance (ATR) FTIR of modified COC open plates. PEGA was grafted on a COC plate by covering the surface with a solution of 15% monomer, 0.2% benzophenone and then applying UV illumination for 15 minutes. Subsequently, AA was polymerized using 15% of monomer and 0.2% benzophenone with 15 minutes of UV irradiation. The carboxylate groups in the PAA layer were used to attach polyclonal Anti Ly using 0.4M EDC and 0.1M NHS in 0.1M MES buffer pH 5.1. After each step the surface was thoroughly washed with water and PBS 1X and spectroscopically analyzed by ATR-FT on a Nicolet Nexus 870-FTIR spectrometer using 200 scans with 4 cm^{-1} of resolution. An Avatar Multi-Bounce HATR accessory was used for this purpose and the crystal was ZnSe with an incidence angle of 45°. The different surfaces denoted as COC, COC-PEGA, COC-PEGA-PAA and COC-PEGA-PAA-Anti-Ly were also analyzed by Atomic Force Microscopy (AFM) in tapping mode employing a Veeco ICON dimension instrument.

5.2.3 Sensor response to lysozyme and cytochrome C as interfering species.

The ability of the COC-PEGA-PAA-Anti-Ly microchannels to generate a reproducible and linear response towards Ly with and without interfering species was evaluated using Cytochrome C (CYT). Solutions of Ly in the range of 0.0 to 840 nM were prepared and each concentration sample was introduced in the channel using series of 5 pulses of 1 s each (no still time, between

each series) for 100 seconds. Protein-free buffer was flowed under the same conditions during 100 seconds before introduction of the samples. The average streaming potential of consecutive 5 pulses was divided by the streaming potential value obtained with protein-free buffer and reported as a corrected normalized streaming potential Ec.[3] After adsorption of each protein solution the surface was regenerated by flowing NaCl 0.5 M during 300 seconds and used for the adsorption of the next sample. A second series of samples with the same concentration of Ly but containing 250 nM of CYT were analyzed in three independent chips using the same pulse conditions. Values of the slope (dEc/dt) determined from the linear region (first 30 seconds) of adsorption isotherms Ec vs t per each concentration, were used to prepare calibration curves by plotting (dEc/dt vs [Ly]).[3] All solutions were prepared in phosphate buffer 1.5 mM pH 7.1 and 258 μs cm^{-1}. Details of the photopolymerization of PEGA and PAA on COC as well as the non-specific adsorption experiments for proteins are described in the supporting information.

5.3 Results and discussion.

5.3.1 Preparation, Optimization and Characterization of the Microchannel Surface

The goal of this part of the research was to modify the COC microchannel surface with a composite film that could provide both non-fouling properties and selective receptors for binding Ly. This approach is a model for protein sensors based on pulsed streaming potentials. However it is also a model of a platform for studying protein interactions with immobilized probes, given the fact that this detection technique allows kinetic monitoring of surface adsorption with no need of chemical labeling for the targets under study.

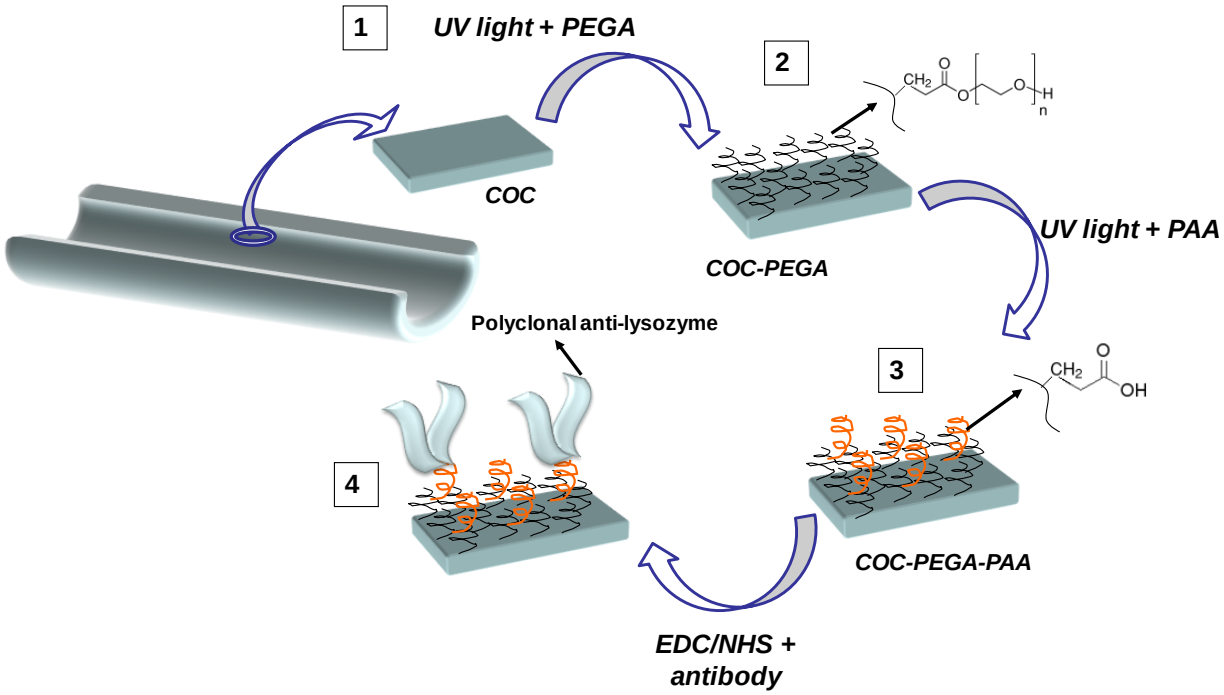

Figure 5.1. Sequence of steps for the production of a non-fouling surface with some selectivity for Ly.

To this end the procedure depicted in Figure 5.1 was devised, first a layer of PEGA was UV-photografted on COC to produce COC-PEGA and then PAA was photopolymerized on top (COC-PEGA-PAA) to provide anchoring groups for the antibody receptors. The last step consisted of attaching the polyclonal antibodies (Anti-Ly) on the activated carboxylate groups of PAA (COC-PGA-PAA-Anti-Ly). Characterization by pulsed streaming potentials, AFM tapping mode and ATR-FTIR was performed at the various steps.

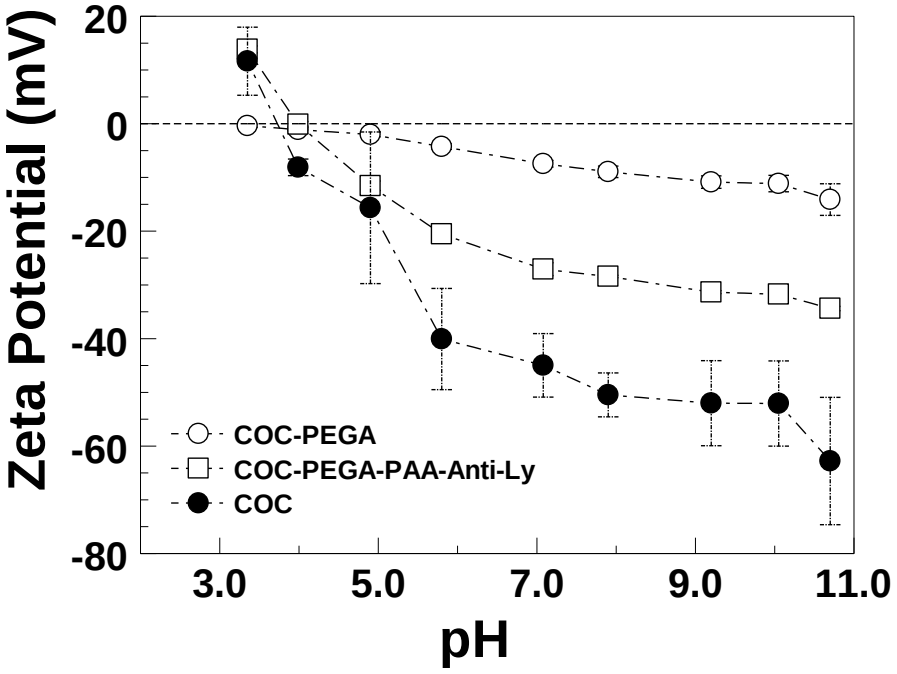

Figure 5.2 Comparison of ζ potential as a function of pH using phosphate buffer solutions between 1.5 and 2.0 mM and 389 ± 4 μS/cm, for COC, COC-PEGA and COC-PEGA-PAA-anti-Ly.

Figure 5.2 shows the zeta potential (ζ) for COC-PEGA, COC-PEGA-PAA-anti-Ly and pristine COC illustrating the decrease in the value of ζ as function of pH observed in the range 3.4 to 10.7. For instance, at pH 3.4 the ζ value for COC-PEGA is ~0.0 mV and it decreases gradually to -15 mV upon increasing the pH to 10.7. On the other hand, COC has a ζ value of +10 mV at pH

3.4 and it reaches a value of -65 mV at pH 10.7. This behavior has been reported before and it has been attributed to anion adsorption, presumably hydroxide ions.[18] Therefore, the smaller variation in ζ observed for COC-PEGA as a function of pH (~15 mV) compared to pristine COC (~70 mV), is seemingly indicative of the lower tendency of PEGA for non-specific adsorption of anions likely due the non-ionic and hydrophilic character of the PEGA film.

This change in zeta potential observed after PEGA immobilization on COC can be analyzed by estimating the charge density for both COC and COC-PEGA using the Gouy-Chapman relationship (Equation 5.1).[19] Where σ is the charge density, ε_o is the vacuum permittivity, ε is the dielectric constant, *R* is the gas constant (8.31 J mol^{-1} K^{-1}), T is the temperature (293 K), *c* it the bulk electrolyte concentration (mol L^{-1}), *z* is ion charge (+1), *F* is the Faraday constant (9.6 x 10^4 C mol^{-1}) and ζ is the zeta potential.

$$\sigma = \sqrt{2\varepsilon\varepsilon_{\circ}RTc}\sinh(zF\zeta / 2RT) \qquad (5.1)$$

Values of charge density estimated using the zeta potential at pH 7.1, show a change from 7.12 x 10^{-5} C cm^{-2} for pristine COC to 10.6 x 10^{-6} C cm^{-2} after modification with PEGA. Assuming that this difference in σ is caused by anions of unit charge (1.6 x 10^{-19} C), this change corresponds to 3.78 x 10^{14} ions cm^{-2} or 6.28 x 10^{-10} mol-ion cm^{-2}, which indicates that the PEGA film is able to reduce anion adsorption in an amount equivalent to approximately one densely packed monolayer. Typical surface density at maximum coverage for self assembled monolayers of alkanethiols on gold has been reported to be ~ 4.5 x 10^{14} molecules cm^{-2}.[20]

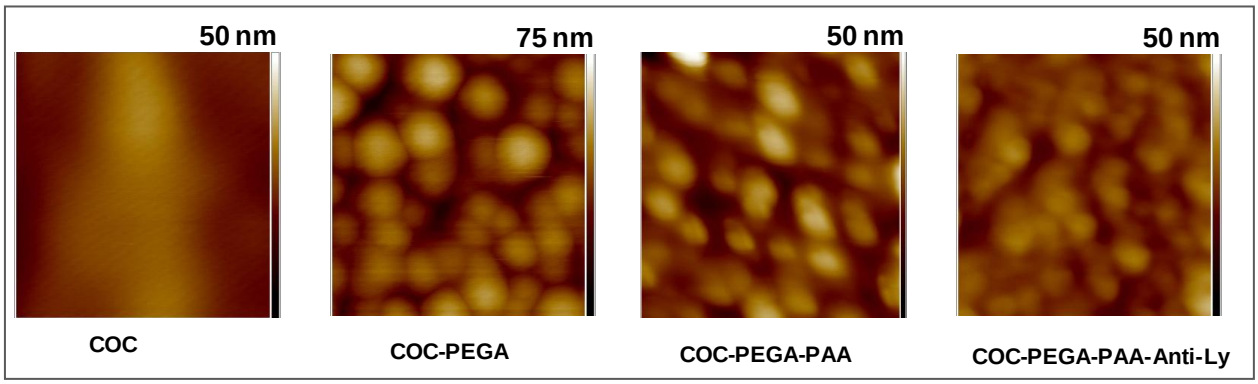

Figure 5.3 Topographic AFM tapping mode images (500 nm x 500 nm) for COC, COC-PEGA, COC-PEGA-PAA, and COC-PEGA-PAA-anti-Ly . The vertical color bar represents height. For COC-PEGA-PAA, 2 min of UV illumination were used for PAA grafting.

Figure 5.3 shows the AFM images in tapping mode for COC and COC-PEGA. The mean square roughness (Rq) determined for COC was 4.15 nm which increased to 7.15 nm after PEGA modification; however, after 2 min of UV induced polymerization to produce COC-PEGA-PAA, the roughness value became ~4.5 nm. This reaction time for PAA modification was the one that produced the best results for Ly adsorption (see below) and it is probably indicative of the similarity in topography between COC-PEGA-PAA and COC-PEGA-PAA-anti-Ly (Figure 5.3).

The morphology of the PEGA film observed is consistent with previous reports where grafted polymers described as polymer brushes adopt globular like structure in their dry state.[21-23] The thickness of the PEGA film determined using a cross-sectional AFM scan between a COC-PEGA region and a pristine COC was found to be 66.2 ± 11.9 nm. This value was used to estimate the grafting density (σ_g) using Equation 5.2,[24] where h is brush thickness; ρ is bulk

density of the brush composition, N_a is the Avogadro's number and M_n, number-average molecular weight.

$$\sigma_g = \frac{(h\rho N_a)}{M_n} \tag{5.2}$$

Using the ρ value of 1.18 g/cm^{3}previously reported for PEGA,[25] and the molecular weight of the (M_n = 375 g mol^{-1}), the graft density was estimated to be 1.3 x 10^2 monomer molecules nm^{-2}. This high amount of monomer molecules per area can be explained by the long time of irradiation used and the formation of hyperbranched structures during the polymerization.[26, 27]

Figure 5.4 shows a series of FTIR spectra at different stages of modification in comparison with the spectrum for pristine COC (Figure 5.4 A) which shows the expected bands for a purely hydrocarbon-based polymer.[1] Figure 5.4 B shows the spectrum for a COC-PEGA surface with the appearance of the C-O ether stretch band at 1095 cm^{-1} and the C=O stretch band, produced by the carboxylic acid in the acryl group at 1720 cm^{-1}.[28, 29] When PAA is grafted on COC-PEGA (Figure 5.4 C), the band for C=O is still maintained but becomes broader consistent with additional source of carboxylate functionalities. The amide groups added when the polyclonal antibodies are attached to produce COC-PGA-PAA-Anti-Ly (Figure S1D), give rise to the amide bands I and II at 1550 and 1650 cm^{-1} respectively as well as the N-H stretch at 3390 cm^{-1}.[30]

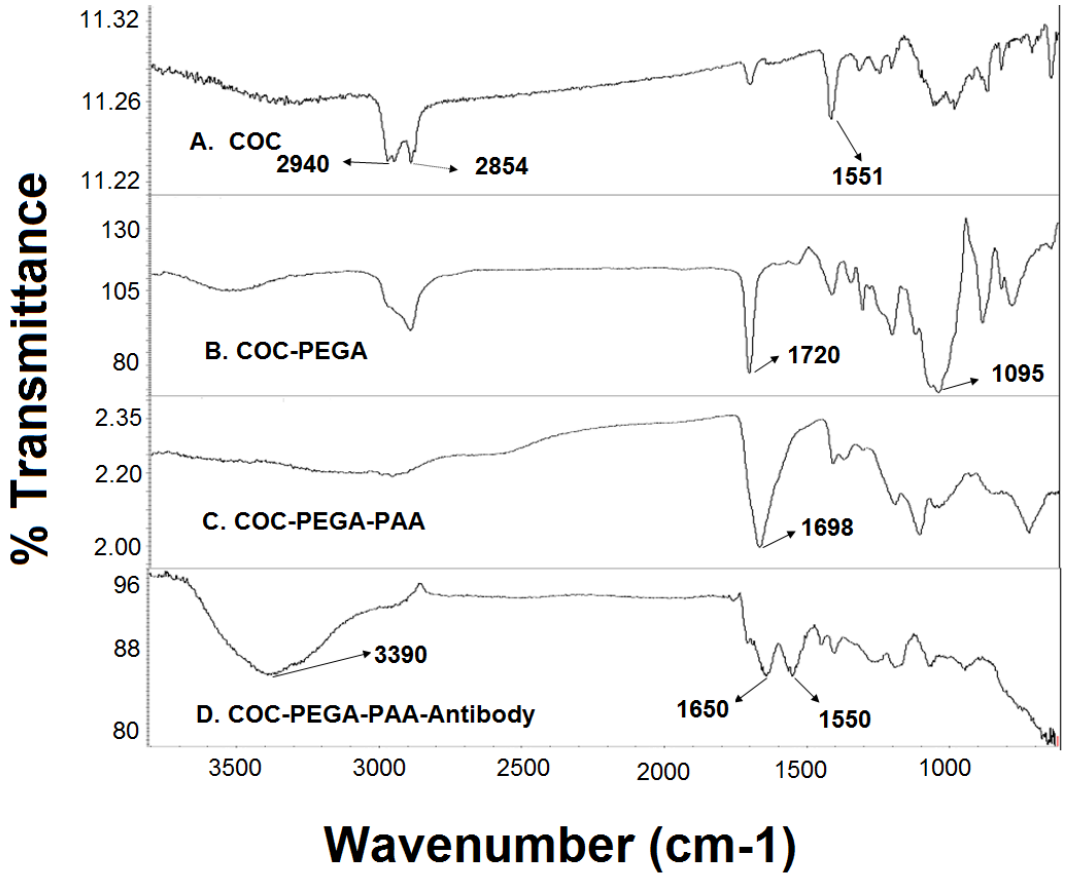

Figure 5.4 . ATR-FTIR spectra for COC at different stages of modification following Figure 5.3

To determine the effect of PEGA in reducing non-specific adsorption of proteins, COC and COC-PEGA microchannels were evaluated by pulsed streaming potentials using six proteins of different size and isoelectric point (pI): lysozyme (Ly), cytochrome C (CYT), fibrinogen (FIB), human serum albumin (HSA), bovine serum albumin (BSA) and IgG (polyclonal anty-ly antibody). Figure 5.5 shows the adsorption and desorption phases for proteins on COC and COC-PEGA. Initially, the microchannels were flowed with protein-free solution for 300 s followed by an injection of the protein solution to monitor adsorption for 600 s. At 900 s another injection of protein-free solution was made to follow desorption. As an example, both FIB and Ly show very low adsorption on COC-PEGA as evidenced by the smaller change in the streaming potential (E)

in comparison to bare COC. The change in E for both COC and COC-PEGA occurs in the same direction though, that is, reducing the negative surface charge of the microchannel upon non-specific adsorption of FIB and Ly[3] as well as the other proteins.

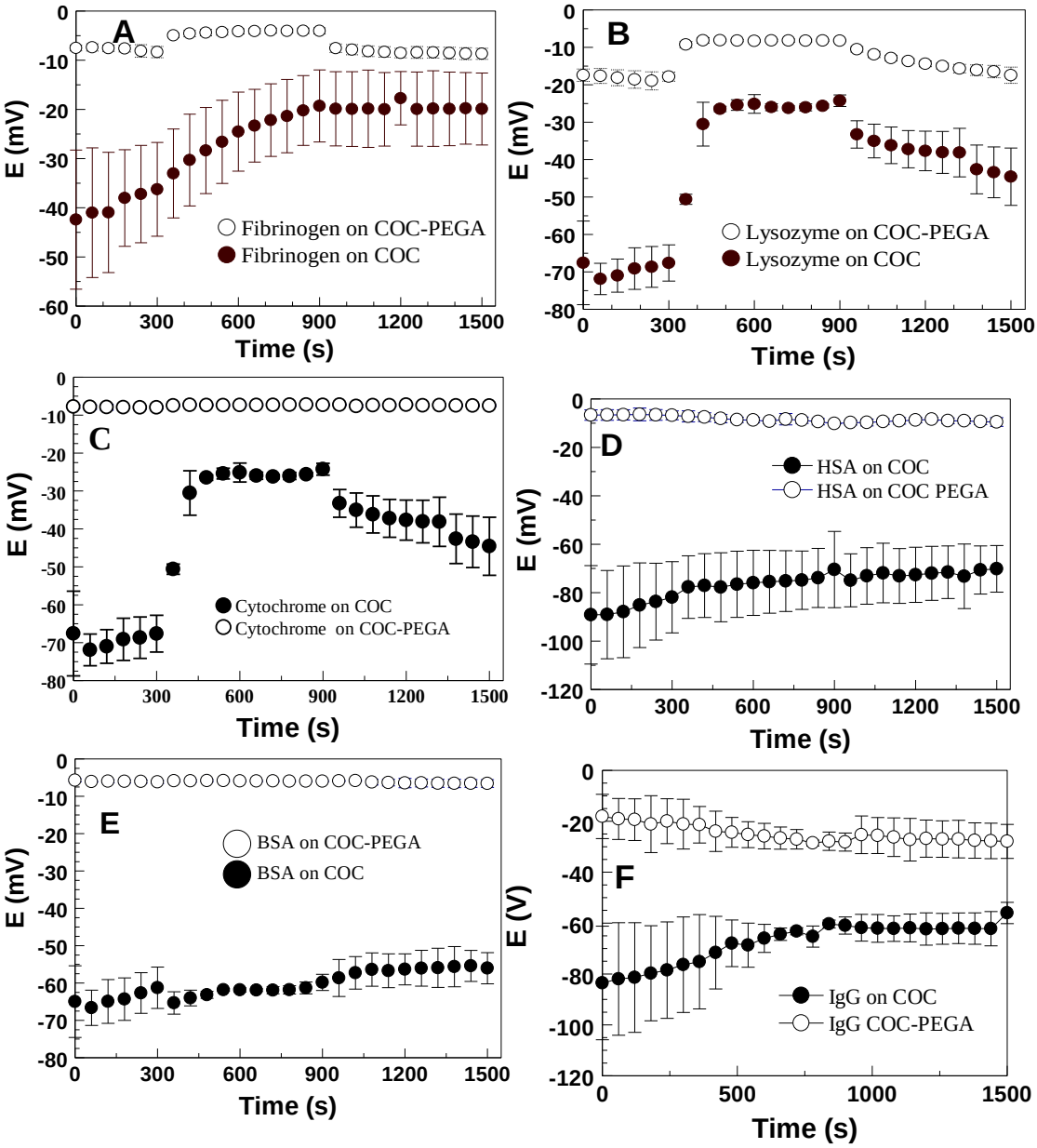

Figure 5.5 Kinetics of adsorption-desorption for several proteins. Protein-free buffer, phosphate 1.5 mM , pH 7.1 and 389 ±3 μS cm^{-1} was injected at 0 s and flowed during 300s. At 300 s protein solutions, 3 μg mL^{-1} in phosphate buffer 1.5 mM, pH 7.1 and 389 ± 3 μS cm^{-1} was injected and flowed for 600 s. At 900 s protein-free buffer was injected again until 1500 s. For fibrinogen, protein solutions and free-protein buffer were 747 μS cm^{-1}.

The magnitude of E and ζ is determined by the average surface charge density (Equations 5.1 and 5.2) inside the microchannels. Therefore, the time dependent behavior of E and ζ depends on the charge density prior to any adsorption and any concomitant change in the charge density as species adsorb on the surface.

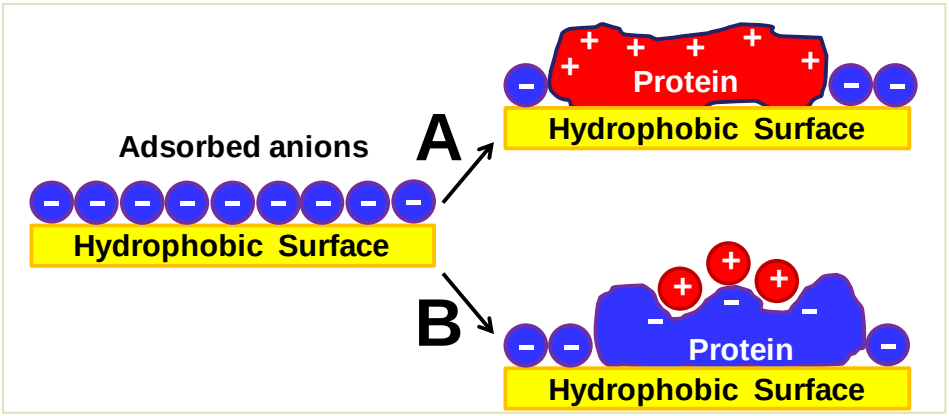

Figure 5.6 Model for the reduction of negative charge by non-specific adsorption of A. a positively charged protein and B. a negatively charged protein with counterion condensation.

In this work it is proposed that the reduction of negative charge density (less negative charge on the surface) can occur through two different mechanisms, presented in Figure 5.6: ***A***, adsorption of a protein with an effective positive charge that simply replace the negative charge on the surface and ***B***, adsorption of a protein with an effective negative charge which is lower than the charge of the anions being replaced on the surface. Proteins contain local regions of high charge density that generate counterion condensation on those local places (Figure 5.6B).[31] Condensed counterions do not contribute to the effective charge because they compensate local charge in the protein and are tightly bound making the net charge of the protein lower than the effective charge.[31] For instance, the net charge of BSA at pH 6.8 is -11.0 but it decreases to -8.4 ± 0.4

because of counterion condensation.[32] Counterions condense when the charge to charge distance within the macromolecule is smaller than the Bjerrum length which is 0.71 nm for water and it increases with the ionic strength.[33] It is conceivable that for Ly and CYT which have pI's of 11.0 and 10.5 respectively (Table 5.1), follow the mechanism in Figure 5.6A because they carry an effective positive charge at pH 7.1. On the other hand, FIB, HSA and BSA which have pI values of 5.8, 4.7 and 4.7, respectively, carry a negative charge at pH 7.1, and therefore the mechanism in Figure 5.6B is likely to be operative. By the same token, because the negative proteins FIB, HSA and BSA are relatively big as indicated by their molecular weight, they provide more room for counterion condensation. For instance the dimensions of BSA are 14 x 4.0 x 4.0 nm^3,[34] which easily allows for the Bjerumm length condition. Another important result from Figures 5.5, is that after adsorption of the proteins on pristine COC the original surface charge was never recovered because of irreversible adsorption of the proteins. In contrast COC-PEGA showed quite renewable behavior of the surface charge under the same conditions of fouling.

Table 5.7 . Protein parameters and non-specific adsorption on COC and COC-PEGA.

Protein	Molecular Weight (KD)	pI	ΔE_{a-d} (mV)	
			COC	COC-PEGA
Ly	14.7	11.0	39.5 ± 12.1	0.4 ± 1.8
CYT	12.0	10.5	23.1 ± 6.6	0.5 ± 0.1
FIB	34.2	5.8	16.3 ± 2.9	-0.3 ± 0.1
HSA	66.7	4.7	11.7 ± 5.1	-0.8 ± 2.2
BSA	66.0	4.7	12.1 ± 3.8	-0.4 ± 0.9

In order to compare the extent of non-specific adsorption between COC and COC-PEGA the difference in streaming potential between the beginning of the adsorption phase and the end of the desorption phase, ΔE_{a-d}, was determined (Table 5.1). The smaller the value of ΔE_{a-d} the smaller the extent of non-specific adsorption occurs and the more renewable the surface becomes. For all the proteins on COC-PEGA, except HAS, the magnitude of ΔE_{a-d} was in the sub-millivolts range whereas for COC, ΔE_{a-d} varied from 12 to 40 mV. This behavior is attributed to the non-ionic and hydrophilic character of COC-PEGA which provides an efficient blocking of the hydrophobic COC surface significantly mitigating non-specific adsorption.

In order to detect Ly using COC-PEGA, functional groups for anchoring the Ly antibodies must be attached. To this end, carboxylic functionalities were incorporated by photografting AA directly on the COC-PEGA microchannel surface following steps 2 and 3 in Figure 5.1. Carboxylates were selected because they are well known to be readily activated with EDC/NHS chemistry.[35]

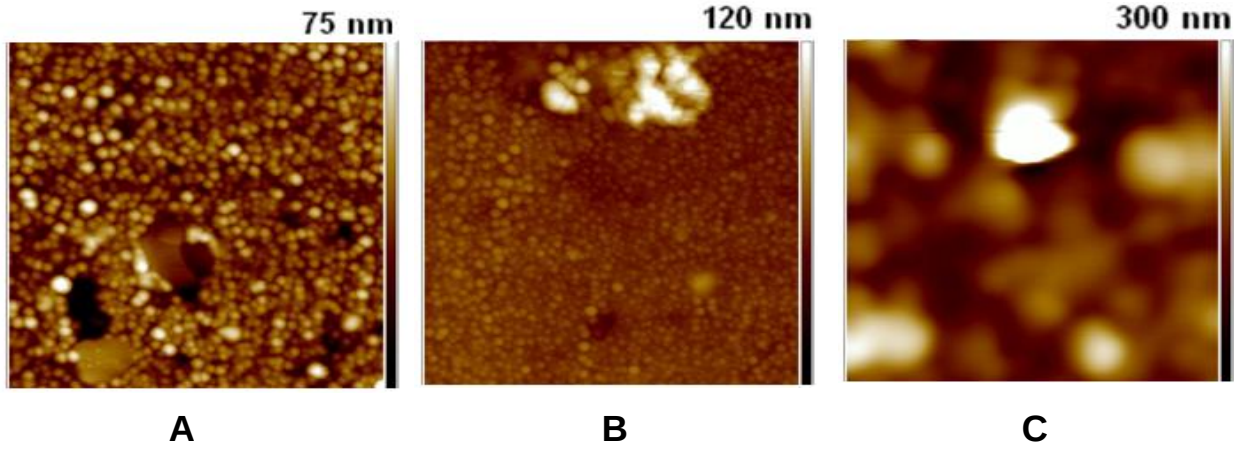

Figure 5.7 AFM topographical image 3μm x 3μm in tapping mode of PAA grafted on COC-PEGA microchannels at different polymerization times (minutes). A. 0, B. 2, and C. 15. Bar color scale on the side represents height.

Figure 5.7 shows three representative AFM topographies at 0, 2 and 15 min of AA UV-initiated polymerization. The roughness (Rq) changes from 8.8 nm, when no PAA is grafted, to 53.8 nm after 15 minutes of polymerization. Interestingly, for 2 minutes of illumination the roughness becomes smaller in magnitude (4.5 nm) than for the original COC-PEGA surface. This result is interpreted as an indication that the initial polymerization of PAA is presumably occurring in the pinholes of the globular PEGA film, creating a smoother surface. As a consequence, reduction in the height of the globular structures of the PEGA film from ~20 to 10 nm was observed (Figure 5.8 A-B). When the polymerization time was 15 min, PAA seems to grow over the COC-PEGA generating a rougher surface with features that reach up to 150 nm in height (Figure 5.8 C).

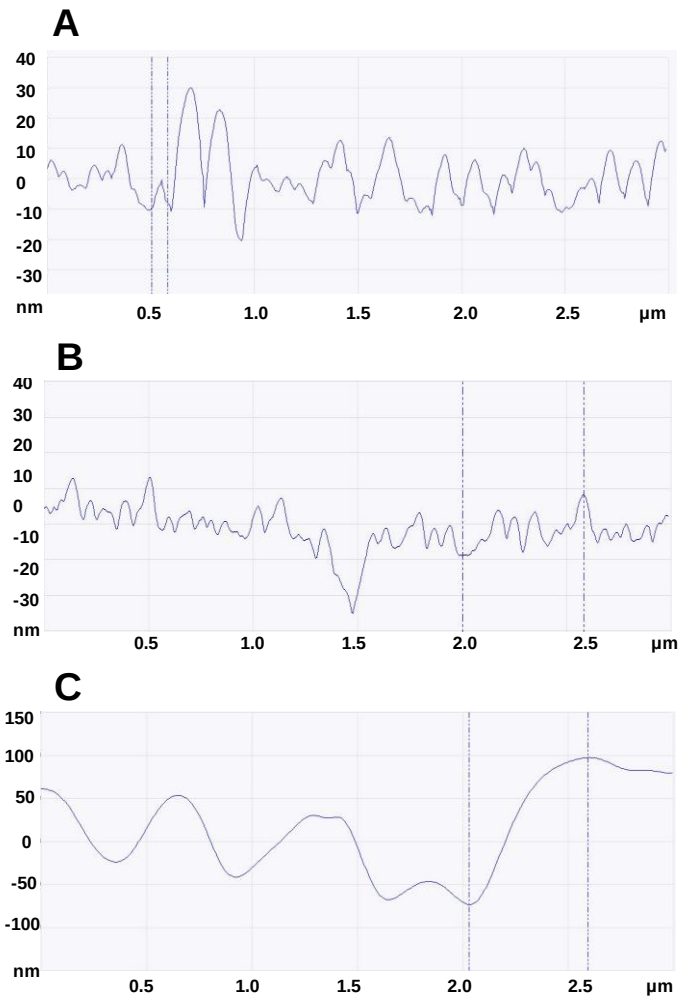

Figure 5.8 AFM sectional analysis of COC-PEGA microchannels after 0 (A), 2 (B) and 15 (C) minutes of PAA photopolymerization.

To establish which PAA polymerization time produces the best surface for Ly detection, Ly antibodies (Anti-Ly) were attached to COC-PEGA-PAA microchannel after activation of the carboxylic groups (Figure 5.1). The time dependent variation (dEc/dt) of the corrected and normalized streaming potential Ec (see experimental section), which can be considered as the initial adsorption rate of Ly, was used as criterion to evaluate Ly adsorption on COC-PEGA-PAA-Anti-Ly.

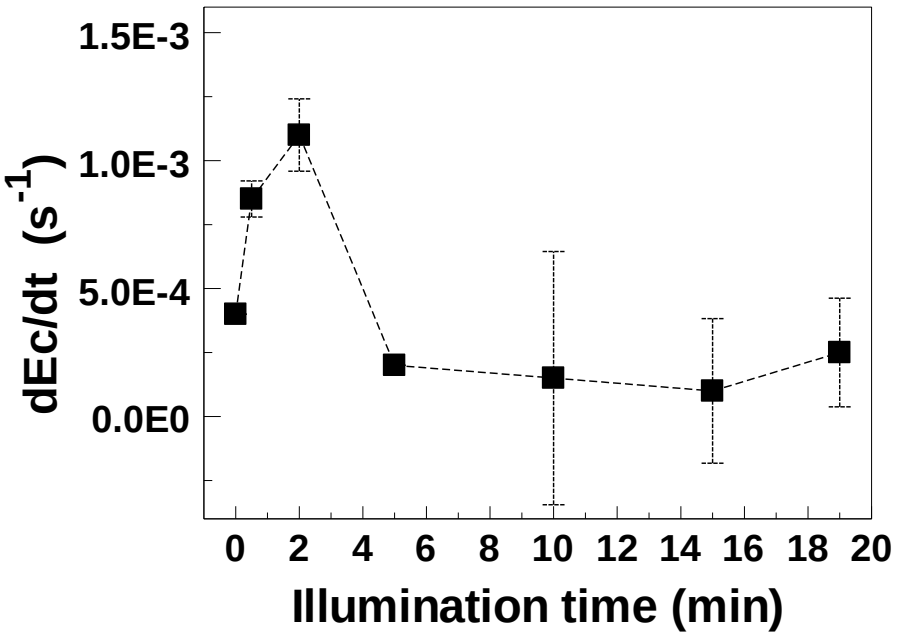

Figure 5.9 Optimization of UV radiation time for polyacrylic acid (PAA) grafting on COC-PEGA modified microchannels. dEc/dt represents the initial velocity of adsorption of lysozyme 210 nM (pH 7.1 , 263 μS cm-1) after PAA grafting and subsequent anti-lysozyme antibody modification with EDC/NHS. Mixture for polymerization was acrylic acid monomer 2% V/V and 0.1% W/V benzophenone as initiator in every case.

Figure 5.9 shows values of dEc/dt at different times of PAA polymerization. The highest adsorption rate for Ly was observed when PAA was polymerized for 2 minutes. However, shorter or longer times (up to 19 min) did not improve Ly detection implying that a higher number of carboxylate groups for anchoring the antibody receptors does not guarantee better detection of Ly. This could mean that at longer polymerization times, the adsorption of the protein probes is compromised by steric crowding effects of the receptors,[36, 37] or by an increased heterogeneity of the film.[38, 39] Such increased heterogeneity was observed by AFM on the films polymerized for more than 5 minutes (Figure 5.8).

5.3.2 Analytical Figures of Merit and Ly-Antibody Interaction

Figure 5.10A shows the corrected and normalized pulsed streaming potential (Ec) vs. time for different concentrations of Ly adsorbed on COC-PEGA-PAA-Anti-Ly. The kinetics of absorption reveals that variations of Ec with time are concentration dependent and higher concentration of Ly produce faster adsorption rates.[3] Also, the linearity of the adsorption rate (dEc/dt) as function of [Ly] (Figure 5.10 B), indicates that the Ly adsorption is limited by mass transport at the initial stages of adsorption.[3] The slope of the plot dEc/dt vs. [Ly] can be taken as the calibration sensitivity and for the condition without interfering species added, the estimated value was 4 x 10^{-5} nM^{-1} s^{-1} (Figure 5.10B). When 250 nM of CYT was added as interfering protein, the sensitivity did not change but the intercept with the ordinate axis was not longer ~0.0. The positive value of the intercept (~+0.011 V) indicates that some CYT adsorption is occurring because this protein is positive at neutral pH (pI = 10.5). The fact that the calibration sensitivity does not change in the presence of CYT, which was added in as much as 30 % of the maximum concentration of Ly (840 nM), implies that the non specific adsorption of CYT does not compromise the specific sites for Ly and quantification is still viable at nanomolar levels even though the precision for some of the points in the curve is lower. When comparing the sensitivity of modified and pristine COC towards the adsorption of Ly, it is clear that COC-PEGA-PAA-Anti-Ly has a sensitivity about one order of magnitude lower than pristine COC (3.9 x 10^{-4} nM^{-1} s^{-1}),[3] which shows that pristine COC has more adsorption sites precisely because of the indiscriminate non-specific adsorption.[3] The dynamic range for Ly detection with COC-PEGA-PAA-Anti-Ly is still in nanomolar concentrations but the polyclonal antibodies provide some level of specificity. This result indicates that this method of monitoring the kinetics of adsorption by pulsed streaming potentials can be used to quantitatively measure analytes and

their interactions with surface bound probes. For instance the equilibrium constant Keq for the adsorption of Ly on COC-PEGA-PAA-Anti-Ly was estimated to 2.7 x 10^6 M^{-1}.

The COC-PEGA-PAA-Anti-Ly surface showed good ability to recover the initial surface charge after NaCl 0.5 M was flowed during 300 seconds**.** In order to produce the calibration curves shown in figure 5.10B three microchannels were regenerated after Ly adsorption (Figure S6, supporting information). Each adsorption-regeneration cycle was repeated 6 times (one per each Ly concentration) and the recovery efficiency was expressed as % R = (E_F / E_I) x 100, where E_I is the pulsed streaming potential of the surface before any Ly adsorption, measured with protein-free buffer and E_F represents the signal with protein-free buffer after regeneration with NaCl. Figure 5.11 shows that average % R per cycle is higher than 97% for each of the six Ly concentrations. This finding demonstrates that the COC-PEGA-PAA-Anti-Ly composite surface is suitable for studying processes where renewal of the original surface is important, like kinetic studies of adsorption interactions with surface bound probes. Additional control experiments showed that in order to achieve these high levels of surface renewal, the presence of PEGA on the composite surface is needed. For instance, when a solution of Ly 320 nM was used for an adsorption-regeneration cycle on COC the % R obtained was 60.9 ± 2.1 and in the case of COC-PAA, the % R was 84.6 ± 25.1.

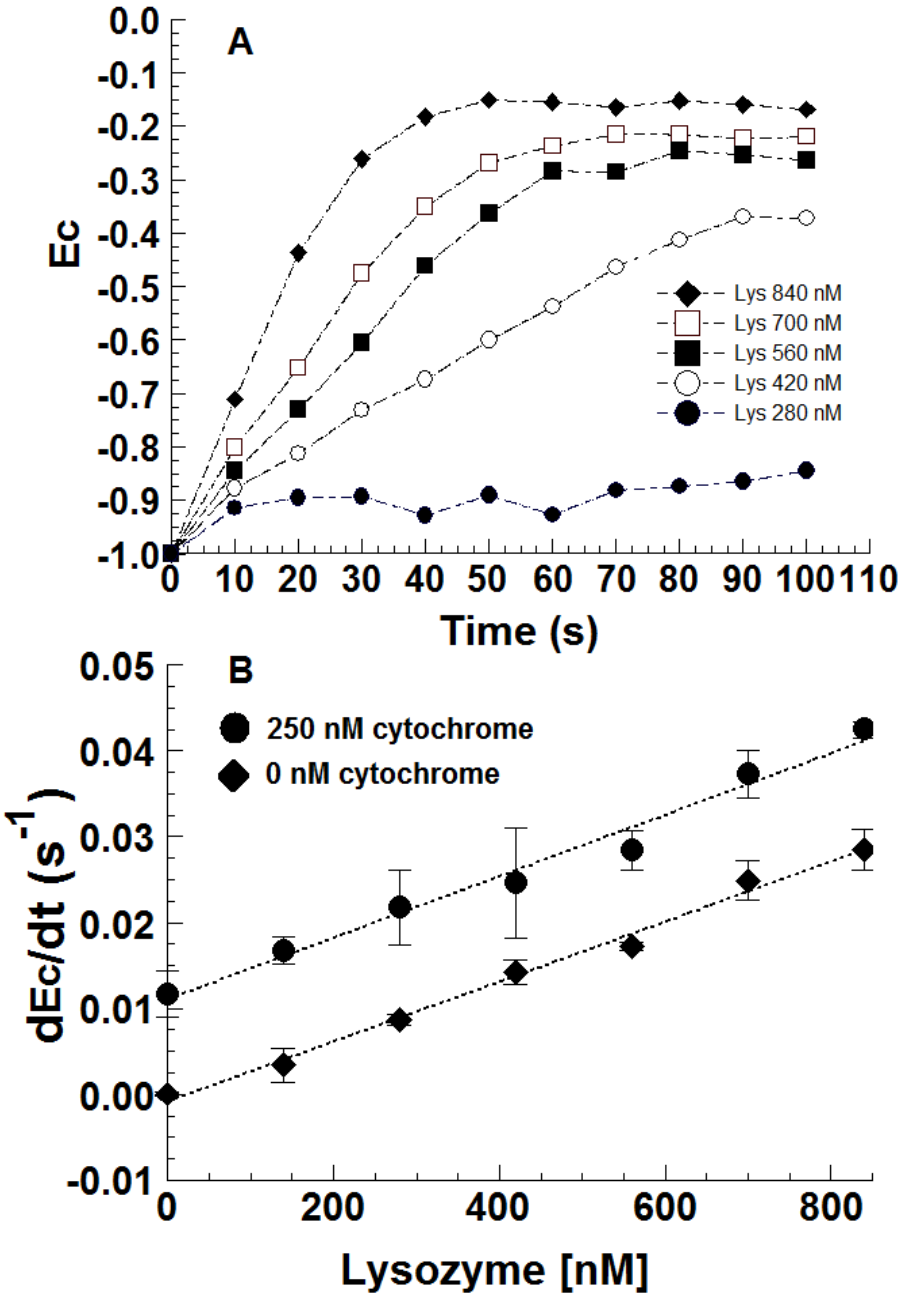

Figure 5.10 A. Adsorption phase for different concentrations of Ly on COC-PEGMA-PAA-Anti-Ly microchannels. Ly solutions had pH 7.1 and 262 μS cm^{-1}. B. Calibration curves for Ly and Ly spiked with 250 nM of CYT. Each curve containing 7 calibration points was produced in the same COC-PEGMA-PAA-Anti-Ly channel after recovery of the initial surface charge. Every point reported is the average of the dEc/dt magnitude for the first 30 seconds of the adsorption phase, obtained for the same concentration in 3 different microchannels. To recover the original surface after Ly adsorption NaCl 0.5 M was flushed for 300 seconds. Dotted lines represent linear regression: $Y= 3.5x10^{-5} X - 0.00082$ ($r^2=0.992$) for Ly and $Y= 2.9x10^{-5} X + 0.011$ ($r^2=0.990$) for Ly(CYT).

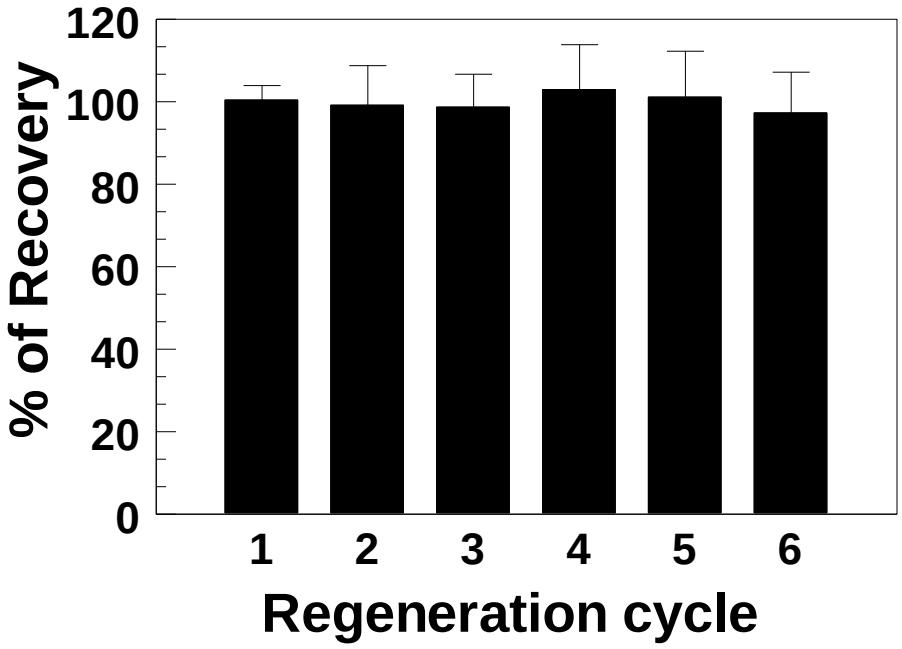

Figure 5.11 Percentage of recovery for 6 different adsorption-regeneration cycles on COC-PEGA-PAA-Anti-Ly. Solutions of different concentration of lysozyme were used for each cycle: 140, 280, 420, 580, 720 and 840 nM of lysozyme were flowed for cycles 1, 2, 3, 4, 5 and 6 respectively. All solutions were in phosphate buffer 1.5 mM pH 7.1 and 258 μs cm-1. Regeneration after adsorption was carried out by flowing NaCl 0.5 M during 300 seconds; followed by protein-free buffer. Error bars correspond to standard deviation of independent measures in three different microchannels.

5.4 Conclusions.

It has been demonstrated the inhibition of non-specific adsorption of proteins after photo grafting of PEGA on COC microchannels. The nonionic and hydrophilic character of PEGA also reduces substantially the surface charge of pristine COC by decreasing the non-specific adsorption of ions. Polyclonal antibodies with affinity for Ly were linked via amide bonds to carboxylate functionalities of PAA grafted on COC-PEGA. The quantification of Ly by pulsed streaming potentials in real time was attained with good linearity in the range 140 – 840 nM, even in the presence of 250 nM of Cytochrome C as interfering species.

The composite film COC--PEGA-PAA-Anti-Ly showed a high renewability of the original surface charge after washing with a regeneration solution of NaCl. This regeneration allowed calibration at different concentrations of Ly on one single microchannel. The major result of this work is the development a surface detection technique of general applicability with low cost and simple instrumentation. The approach does not require chemical labeling and provides significant mitigation of non-specific adsorption while still providing nanomolar detection limits with some degree of specificity for Ly.

5.5 References.

1. Pu, Q., Oyesanya, O., Thompson, B., Liu. S., Alvarez, J.C., On-Chip Micropatterning of Plastic (Cylic Olefin Copolymer, COC) Microfluidic Channels for the Fabrication of Biomolecule Microarrays Using Photografting Methods. **2007,** *23*, 1577-1583.
2. Pu, Q.; Elazazy, M. S.; Alvarez, J. C., Label-Free Detection of Heparin, Streptavidin, and Other Probes by Pulsed Streaming Potentials in Plastic Microfluidic Channels. *Analytical Chemistry* **2008,** *80*, 6532.
3. Luna-Vera, F., Alvarez, J.C., Adsorption kinetics of proteins in plastic microfluidic channels: Real-time monitoring of lysozyme adsorption by pulsed streaming potentials. *Biosens. Bioelectron.* **2010,** *25*, 1539-1543.
4. Hunter, R. J., *Zeta Potential in Colloid Science: Principles and Applications*. Academic Press: London, 1981; p 381.
5. Chen, Y.-M.; Yu, C.-J.; Cheng, T.-L.; Tseng, W.-L., Colorimetric detection of lysozyme based on electrostatic interaction with human serum albumin-modified gold nanoparticles. *Langmuir* **2008,** *24*, 3654-3660.
6. Wegner, G. J., Alastair, W.W., Lee, J.L., Codner, E., Saeki, T., Fang, S., Corn, R.M., Real-Time Surface Plasmon Resonance Imaging Measurements for the Multiplexed Determination of Protein Adsorption/Desorption Kinetics and Surface Enzymatic Reactions on Peptide Microarrays. *Anal. Chem* **2004,** *76*, 5677-5684.
7. Bharadwaj, M., Kohaar, I., Hussain, S., Tiwari, P., Thakur, N., Nasare, V., Das, B.C., Choundhury, S.R., Sarkar, D.P., Genomics of microbial pathogens and host–pathogen interactions. *Genomic Med.* **2008,** *2*, 273-283.
8. Aguilar, M. I., Small, D.H., Surface Plasmon Resonance for the Analysis of β-Amyloid Interactions and Fibril Formation in Alzheimer's Disease Research. *Neurotox res.* **2005,** *7*, 17-27.
9. White, D. A., Buell, A.K., Dobson, C.M., Welland, M.E., Knowles, T.P.J., Biosensor-based label-free assays of amyloid growth. *FEBS lett.* **2009,** *583*, 2587-2592.
10. Lee, V. A., Craig, R.G., Filisko, F.E., Zand, R., Microcalorimetry of the adsorption of lysozyme onto polymeric substrates. *J. Colloid Interface Sci.* **2005,** *288*, 6-13.
11. Dang, F., Hasegawa, T., Biju, V., Ishikawa, M., Kaji, N., Yasui, T., Baba, Y., Spontaneous Adsorption on a Hydrophobic Surface Governed by Hydrogen Bonding. *Langmuir* **2009,** *25*, 9296-9301.
12. Quinn, A., MAntz, H., Jacobs, K., Bellon, M., Santen, L., Protein adsorption kinetics in different surface potentials. *EPL* **2008,** *81*, 56003.
13. Lofas, S., Johnsson, Bo., A Novel Hydrogel Matrix on Gold Surfaces in Surface Plasmon Resonance Sensors for Fast and Efficient Covalent Immobilization of Ligands. *J. Chem. Soc., Chem. Commun.* **1990**, 1526-1528.
14. Zou, X. P., Kang, E.T. Neoh, K.G., Plasma-Induced Graft Polymerization of Poly(ethylene glycol) Methyl Ether Methacrylate on Si(100) Surfaces for Reduction in Protein Adsorption and Platelet Adhesion. *Plasmas Polym.* **2002,** *7*, 151-170.

15. Iguerb, O., Bertrand, P., Graft photopolymerization of polyethyleneglycol monoacrylate (PEGA) on poly(methylmethacrylate) (PMMA) films to prevent BSA adsorption. *Surf. Interface Anal.* **2008,** *40*, 386-390.
16. Zimmermann, R., Norde, W., Cohen Stuart, M.A., Werner, C., Electrokinetic Characterization of Poly(Acrylic Acid) and Poly(Ethylene Oxide) Brushes in Aqueous Electrolyte Solutions. *Langmuir* **2005,** *21*, 5108-5114.
17. Dillon, P. P., Killard, A.J., Daly, S.J., Leonard, P., O`Kennedy, Novel assay format permitting the prolonged use of regeneration-based sensor chip technology. *J. Immunol. Methods* **2005,** *296*, 77-82.
18. Tandon, V., Bhagavatula, S.K., Nelson, W.S., Kirby, B.J., Zeta potential and electroosmotic mobility in microfluidic devices fabricated from hydrophobic polymers: 1. The origins of charge. *Electrophoresis* **2008,** *29*, 1092-1101.
19. Gupta, M. L., Brunson, K., Chakravorty, A., Kurt, P., Alvarez, J.C., Luna-Vera, F., Wynne, K.J., Quantifying Surface-Accessible Quaternary Charge for Surface Modified Coatings via Streaming Potential Measurements. *Langmuir* **2010,** *26*, 9032-9039.
20. Love, J. C.; Estroff, L. A.; Kriebel, J. K.; Nuzzo, R. G.; Whitesides, G. M., Self-Assembled Monolayers of Thiolates on Metals as a Form of Nanotechnology. *Chem. Rev.* **2005,** *105*, 1103-1169.
21. Uhlmann, P., Merlitz, H., Sommer, JU., Stamm, M., Polymer Brushes for Surface Tuning. *Macromol. Rapid Commun.* **2009,** *30*, 732-740.
22. Tsujii, Y., Ohno, K., Yamamoto, S., Goto., Fukuda, T., Structure and properties of high density polymer brushes. *Adv. Polym. Sci.* **2006,** *198*, 1-46.
23. Zhao, B., Brittain, J., Zhou, W., Cheng, S.Z.D., Nanopattern Formation from Tethered PS-*b*-PMMA Brushes upon treatment with Selective Solvents. *J.Am.Chem.Soc* **2000,** *122*, 2407-2408.
24. Brittain, W. J., Minko, S., A Structural Definition of Polymer Brushes. *J. Polym. Sci., Part A: Polym. Chem.* **2007,** *45*, 3505-3512.
25. Lin, H., Van Wagner, E., Swinnea, J.S., Freeman, B.D., Pas, S.J., Hill, A.J., Kalakkunnath, S, Kalika, D.S., Transport and structural characteristics of crosslinked poly(ethylene oxide) rubbers. *J. Membr. Sci.* **2006,** *276*, 145-161.
26. Knoelle, W., Scherzer, T., Naumanov, S., Mehnert, R., Direct (222 nm) photopolymerisation of acrylates. A laser flash photolysis and quantum chemical study. *Radiat. Phys. Chem.* **2003,** *67*, 341-345.
27. Huang, L., Li, Y., Yang, J., Zeng, Z., Chen, Y., Self-initiated photopolymerization of hyperbranched acrylates. *Polymer* **2009,** *50*, 4325-4333.
28. Gao, Z., Henthorn, D.B., Kim, Chang-soo., Enhanced wettability of an SU-8 photoresist through a photografting procedure for bioanalytical device applications. *J.Micromech.Microeng.* **2008,** *18*, 045013 (7pp).
29. Feng, L., Zhou, S., You, B., Wu, L., Synthesis and Surface Properties of Polystyrene-graftpoly(ethylene glycol) Copolymers. *J. Appl. Polym. Sci.* **2007,** *103*, 1458-1465.
30. Rajesh., B., V., Takashima, W., Kaneto, K., An amperometric urea biosensor based on covalent immobilization of urease onto an electrochemicallyprepared copolymer poly (N-3-aminopropyl pyrrole-co-pyrrole) film. *Biomaterials.* **2005,** *26*, 3683-3690.
31. Manning, G. S., Polyelectrolytes. In Selegny, E.; Mandel, M.; Strauss, U. P., Eds. D. Reidel Publishing Company: Dordrecht-Holland, 1974.

32. Bohme, U.; Scheler, U., Effective Charge of Bovine Serum Albumin Determined by Electrophoresis NMR. *Chem. Phys. Lett.* **2007,** *435*, 342-345.
33. Schmitz, K. S., *Macroions in Solution and Colloidal Suspension*. VHC Publishers, Inc.: New York, 1993.
34. Wright, A. K.; Thompson, M. R., Hydrodynamic Structure of Bovine Serum Albumin Determined by Transient Electric Birefringence. *Biophys. J.* **1975,** *15*, 137-141.
35. Grabarek, Z., Gergely, J., Zero-Length Crosslinking Procedure with the Use of Active Esters. *Anal. Biochem.* **1990,** *185*, 131-135.
36. Bonanno, L. M., DeLouise, L.A., Steric Crowding Effects on Target Detection in an Affinity Biosensor. *Langmuir* **2007,** *23*, 5817-5823.
37. Xu, F., Zhen, G., Textor, M., Knoll, W., Surface plasmon optical detection of lactamase binding to different interfacial matrices combined with fiber optic absorbance spectroscopy for enzymatic activity assays. *Biointerphase* **2006,** *1*, 73-81.
38. Hodgkinson, G. N., Hlady, V., How Surface Heterogeneity Affects Protein Adsorption: Annealing of OTS Patterns and Albumin Adsorption Kinetics. *Croat. Chem. Acta* **2007,** *80*, 405-420.
39. Arifuzzaman, S., Ozcam, A.E., Efimenko, K., Formation of surface-grafted polymeric amphiphilic coatings comprising ethylene glycol and fluorinated groups and their response to protein adsorption. *Biointherphases* **2009,** *4*, FA(33-44).

6 Exploration of COC-PEGA-Spheres sensing surfaces for PSP analysis

In this chapter two alternatives are presented for the immobilization of micro and nanoshperes on the surface of COC-PEGA microchannels. The main objective is to provide a derivatizable, hard surface for the binding of specific receptors. XPS and SEM characterization of COC-PEGA, and COC-PEGA-Spheres is provided. Additionally, the ability of fabricated platforms for their use in PSP analysis is provided for the detection of Prostate Specific Antigen (PSA).

6.2 Introduction

Previously, it has been demonstrated that the change in Pulsed Streaming Potentials (PSP) generated on plastic microchannels, after adsorption of proteins, can be used to quantify their concentration in aqueous samples as well as the surface charge of casted polymers.[1,2] Additionally, in previous chapters it has been shown how the monitoring of PSP signal over time can be used to estimate kinetic parameter of protein-surface interactions.[1]

In Chapter 5, an approximation to a sensing surface that provides some degree of selectivity was presented. The approach implemented used the production of carboxylate groups on the sensing surface (*COC-PEGA*) by polymerization of acrylic acid (AA) [3]. Carboxylate groups on the surface were employed later as receptor-binding sites after their previous activation, with EDC/NHS chemistry, against amine coupling. Those experiments showed that even though AA provides the proper chemical functionality to link receptors to the surface, it seems to not produce a high density of receptors that effectively compete against non-specific adsorption.

Data suggested that differences in K_{eq} for the adsorption of lysozyme on surfaces with and without receptors are subtle (2.4×10^{-6} M^{-1} and 4.0×10^{-6} M^{-1}, respectively). Additionally, for the case of *COC-PEGA-PAA-Anti-Ly* almost no signal was produced with a protein concentration below 80 nM after 100 seconds of adsorption. Here, it is speculated that the minor differences in K_{eq} are produced by the high ratio of non specific over specific sites. A high ratio will produce a surface where most of the changes in charge density are still dominated by the adsorption at non-specific sites. The platform *COC-PEGA-PAA-Anti-Ly* is a composite made of the mixture of soft hydrogels having two different regions for the adsorption to take place: the outside layer in direct

contact with the solution and the zone inside the hydrogel. A high abundance of non-specific sites can be reasoned when the double zone structure of the surface is considered. For example, carboxylate activation can take place in both zones, but the outside is most likely to be modified with receptors since antibodies are restricted by diffusion inside the hydrogel as well as size exclusion. Additionally, the modification chemistry used (EDC/NHS) is prone to decomposition of the activated amide intermediate produced, due to the presence of water. Hydrolysis of the activated amide reverses the reaction and regenerates the carboxylate. The combination of these factors is believed to create a high degree of unmodified carboxylates, which behave as non-selective sites for binding of positively charges species.

Moreover, it has been recently demonstrated that ion condensation occurs inside polyelectrolyte hydrogels which is responsible for most of the streaming current observed in electrokinetic experiments with flat cell configurations.[4, 5] This finding implies that when a liquid is flowed tangentially to a hydrogel modified surface, as in PSP measurements; most of the ions removed from the double layer come from the inner side of the hydrogel, despite the low mobility of ions inside polymer brushes. Since most of the ions removed by the flow come from inside the polymer it is expected that the PSP signal from polyelectrolyte soft polymer brushes is due to adsorption phenomena and ion diffusion occurring within the inner zone rather than the from the very outermost layer in contact with the liquid phase.

In this chapter, an exploration for a platform that could overcome the drawbacks identified above due the use of polyelectrolyte hydrogels is presented. The approach herein is the direct attachment of functionalized microspheres to the *COC-PEGA* using the activation of surface

hydroxyls or by just direct adsorption. Spheres are used for attachment of monoclonal antibodies and PSP used to detect Prostate Specific Antigen (PSA).

6.2 Experimental Section

6.2.0 Materials and reagents.

Polyethylene glycol acrylate, benzophenone, trifluoroacetic anhydride (TFAA), N,N'-Carbonyldiimidazole (CDI) and 10X PBS were products from Sigma-Aldrich (Saint Louis, MO) DMSO was obtained from Merck (Gibbstown, NJ). Protein-A coated polystyrene microspheres with a nominal diameter of 1 µm were a product of Bang laboratories (Fishers, IN), aliphatic amino latex nanospheres with nominal diameter of 80 nm were purchased from Invitrogen (Carlsbad, CA) , Bis-*N*-succinimidyl-(pentaethylene glycol) ester ($BS(PEG)_5$) was obtained from Thermo Scientific (Logan, UT).

Monoclonal antibody to Prostate Specific Antigen (PSA), Prostate Specific Antigen (PSA), FITC labeled Goat polyclonal secondary antibody to mouse IgG and mouse monoclonal antibodies to lysozyme were all products from Abcam (Cambrigde, MA).

6.2.1 Modification of COC microchannels with variable PEGA monomer concentration.

Five different Cyclic Olefin Copolymer (COC) micro channels were fabricated following the procedure reported previously[6]. Channels were modified by photo-polymerization of polyethylene glycol acrylate (PEGA); using monomer solutions of 0, 2, 3, 4 and 5% V/V of PEGA and 0.1% W/V of benzophenone in DI water in each case. Each monomer solution was used to modify a different microchannel; BP was dissolved in a small portion of acetone prior to

being mixed with the monomer. Each monomer solution was filtered using filter grade 1 acquired from Whatman and degassed for 15 minutes by application of vacuum. Each microchannel was illuminated for 25 minutes at 5 cm from the light source using a Super Spot MK III UV lamp equipped with a flexible light guide (Lesco, Torrance, CA). The irradiation power, 1.5 W/cm^2 at the end of the light-guide was measured with a calibrated SuperSpot intensity meter from (Lesco, Torrance, CA). After PEGA polymerization, microchannels were removed from the UV-light chamber and cleaned by flowing DI water and dried later with an air stream.

6.2.2 XPS characterization of surface concentration of alcohol (-OH) in COC-PEGA modified microchannels.

Quantification of surface *–OH* groups, on PEGA modified COC, microchannels was performed by the vapor-phase chemical derivatization of *COC-PEGA* with trifluoroacetic anhydride (TFAA)[7, 8]. Both sides of COC chips modified with variable concentration of PEGA were detached and the upper side of the microchannels (side with no groove) was placed on a Teflon holder inside a chamber made with a glass jar (Figure 6.1). Approximately 5 mL of TFAA was dispensed into the glass jar. The jar was capped tightly and vacuum was applied for 20 minutes trough a tiny hole made on the cap and covered with a silicone septum, in order for TFAA to saturate completely the volume of the chamber (Figure 6.1). COC-PEGA chips were allowed to react with TFAA vapor inside the chamber for 12 hours. After reaction, the samples were taken out of the glass chamber and put into a desiccator connected to a vacuum for 4 hours, in order to remove physically adsorbed TFAA.

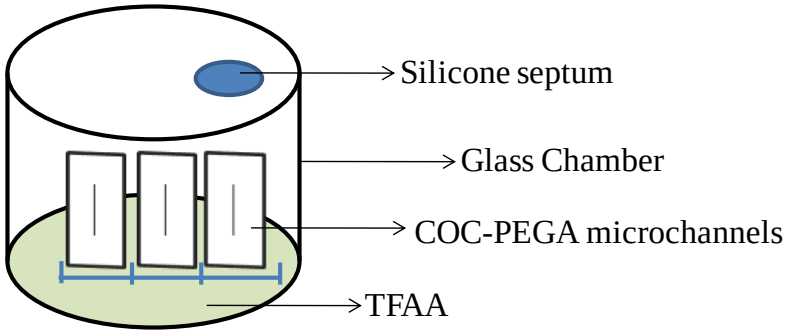

Figure 6.1 Experimental setup for derivatization of COC-PEGA microchannels with TFAA.

The Content of C(1s), O(1s), and F(1s) was analyzed on TFAA derivatized samples using X-ray photoelectron spectroscopy (XPS). XPS analysis was carried out in a ThermoFisher ESCALab 250 spectrometer equipped with an ultra-high-vacuum chamber. Before analysis was initiated, all samples were evacuated in the introductory chamber using a turbo-molecular pump for at least 90 min to ensure removal of all volatile species. Samples were then introduced into the XPS analysis chamber at 10^{-8} Torr. XPS spectra were recorded using the X-ray irradiation from Al Kα (1486.68 eV) anode. All XPS spectra were acquired at 15 kV and spot size of 125 µm. Binding energies were referenced to the CC/ CH2 C(1s) peak at 284.6 eV.

6.2.3. Attachment of protein-A coated polystyrene microspheres to COC-PEGA platforms.

COC microchannels were modified with PEGA as in section 6.2.1, using 4% V/V of monomer. CDI activation of COC-PEGA chips was carried out under argon atmosphere in an Atmostbag glove bag®. Approximately 100 µL of 500 mg of N,N'-Carbonyldiimidazole (CDI) in 2 mL of DMSO, previously dried with molecular sieve, were introduced inside *COC-PEGA* microchannels and the solution was allowed to react with surface hydroxyls for 24 hours. After

that time, channels were thoroughly cleaned with DMSO, removed from the Atmostbag and then dried with a stream of nitrogen. A 1:20 dilution of concentrated (1.975 x 10^{10} microspheres/mL) protein-A coated polystyrene microspheres was made, independently, in pH 8.5 borate buffer and pH 7.4 phosphate buffer. Diluted solutions of microspheres were sonicated for 15 minutes, prior to introduction of approximately 100 µL into activated COC-PEGA microchannels, where they remained for 60 hours. After the reaction was complete, channels were cleaned correspondently with borate or phosphate buffer. Control experiments to evaluate surface charge were carried out following the same procedure described above, but without microspheres, only buffers. Additionally, 0, 50 and 500 mg/mL of CDI activating agent were tested as activating solution using the same procedure to activate *COC-PEGA* microchannels.

Characterization of CDI activated channels and modified with microspheres was carried out by PSP using phosphate buffer of pH 3.1, 7.2 and 11.0. All solutions had a conductivity of 190 ± 1 µS/cm. Pictures of the surface structure of microchannels were taken by Scanning Electron Microscopy (SEM) using a Hitachi FESEM SU-70 ultra high resolution Scanning Electron Microscope. Prior to SEM analysis, COC-PEGA microchannels were separated and the upper side (no groove side) was sputtered with gold for 60 seconds. Before samples were taken in the high vacuum chamber they were grounded to the metallic sample holder using carbon conductive tape in order to reduce charging.

6.2.4. Adsorption of amine modified 80 nm diameter nanospheres on COC-PEGA (COC-PEGA-nanospheres).

Dilutions 1:10 of aliphatic amino latex nanospheres (80 nm in diameter) were made from concentrated solution (7.9 x 10^{13} particles/mL) in phosphate buffer pH 3.1, 7.0 and 11.0 and

citrate buffer pH 3.4, 4.6 and 7.3. After sonication for 15 minutes each solution was introduced inside *COC-PEGA* microchannels (4%V/V monomer) and left for passive adsorption for 48 hours. After adsorption, channels were thoroughly cleaned with the correspondent buffer. The change in the surface charge due to the spheres was investigated by PSP of the surfaces before and after adsorption, using phosphate buffer pH 3.1 with an approximately fixed conductivity of 190 ± 1 µS/cm. Additional surface characterization after nanospheres adsorption was performed by SEM analysis, following the procedure in 6.2.2.

6.2.5. Monoclonal anti-PSA binding to amine modified 80nm diameter nanospheres adsorbed on COC-PEGA.

300 µL of 100 µg/mL mouse monoclonal antibody to Prostate Specific Antigen (PSA) were dialyzed in a Slide-A-Lyzer cassette, 3500 MWCO (Thermo Scientific, Rockford, IL) for 8 hours using borate buffer pH 8.2 as external media. Binding of monoclonal anti-PSA to aliphatic amino latex nanospheres adsorbed on *COC-PEGA* microchannels was carried out in an argon atmosphere, inside an Atmostbag glove bag®. A solution of the amine-reactive crosslinker Bis-*N*-succinimidyl-(pentaethylene glycol) ester ($BS(PEG)_5$) was prepared by addition of 1.3 mL of DMSO, dried in molecular sieve, in the septum capped vial from the vendor, containing 100 mg of ($BS(PEG)_5$). This solution was put inside *COC-PEGA- nanospheres* channels for 4 hours. After reaction, channels were cleaned with abundant DMSO, removed from the Atmostbag and dried with a nitrogen stream. The borate buffer of a dialyzed solution of anti-PSA monoclonal antibodies was exchanged for a 1X phosphate buffers saline (PBS) using an Amicon ultra 0.5 centrifugal filter, 10 kDa (Sigma-Aldrich, St Louis, MO) and 3 cycles of centrifugation-dilution. Additionally, the solution was concentrated to a final volume of 200 µL. The antibody solution

obtained was introduced in *COC-PEGA-nanospheres* channels previously treated with ($BS(PEG)_5$) and left to react for 12 hours in a water saturated atmosphere to avoid evaporation of antibody solution. Controls were carried out with antibody free 1X PBS. After reaction, channels were cleaned with 1X PBS and dried with a nitrogen stream. To quench unreacted crosslikers, a solution 1M of TRIS buffer was put inside channels for 3 hours, after which the channels were again cleaned with 1X PBS and dried with a nitrogen stream.

Confirmation of anti-PSA monoclonal antibodies binding to the *COC-PEGA-nanospheres* microchannels was performed by observation of fluorescence after exposure of channels to FITC labeled Goat polyclonal secondary antibodies to mouse IgG. A 1:10 dilution of secondary antibodies in 1X PBS, from concentrated solution (2.00 mg/mL), was introduced in anti-PSA modified *COC-PEGA-microspheres* channels and left to react for 4 hours in the dark. Controls were carried out by adsorption of a secondary antibody in channels where anti-PSA was not linked. After reaction, microchannels were cleaned with 1X PBS. Fluorescence of channels was observed in a Lesco System Fluorescence microscope using 400 mS of exposure and 60X of magnification.

Real time Pulsed Streaming Potential experiments for the detection of PSA on COC-PEGA-microspheres channels modified with anti-PSA Ab were performed by flowing solutions of 1.1 and 14 µg/mL in phosphate buffer pH 7.0 and 196 ± 8 µS/cm, after 100 seconds of free-protein buffer flow for conditioning of the surface.

6.3 Results and discussion.

6.3.1 Analysis of available surface binding sites on COC-PEGA platforms

In previous experiments the high degree of non-specific adsorption observed on polyelectrolyte polymer brushes in modified microchannels reduced the ability of the PSP system to detect specific interactions. The direct attachment of antibodies to the COC-PEGA layer, which was identified previously as good protein fouling inhibitor[3], was proposed as a first approach to circumvent the use of hydrogels, like polyacrylic acid (PAA). The only functionality for binding of receptors in PEGA is the terminal hydroxyl group (-OH) at the end of the polymer chain (Figure 6.2). One of the most important characteristic for specific interactions with surfaces is the density of bonded receptors.[9-11] Therefore the amount of hydroxyls available for binding was investigated before any attachment of antibodies to the COC-PEGA substrate was performed.

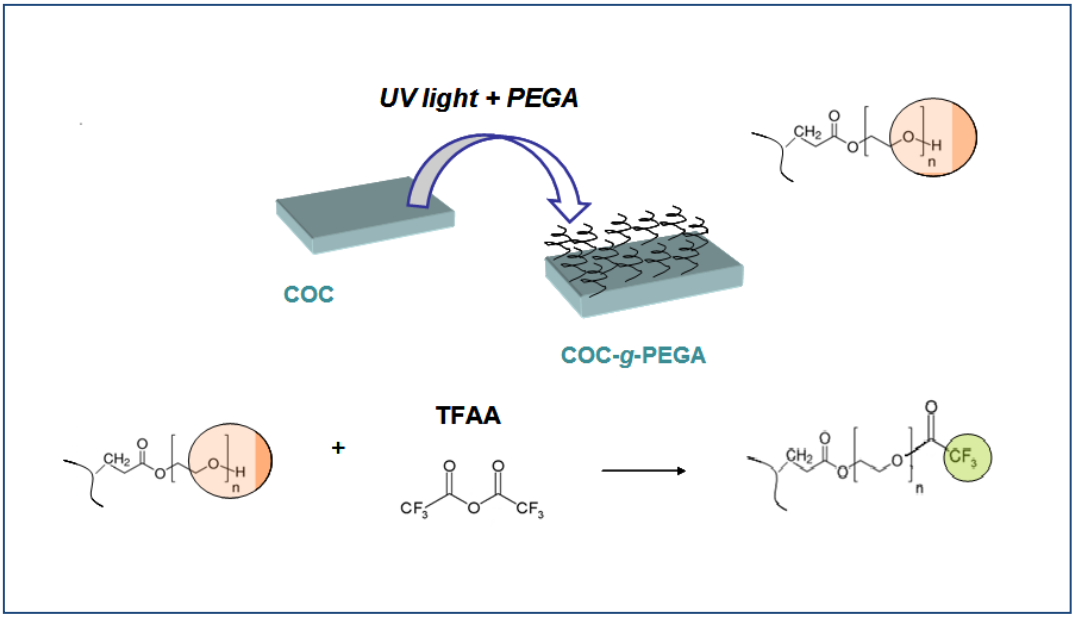

Figure 6.2 General strategy for derivatization of surface hydroxyls on COC-PEGA substrates.

Assessment of hydroxyl percentage was carried out by the following strategy depicted in Figure 6.2, which consists of selective reaction of hydroxyls with TFAA[7, 8] and the later quantification of Fluorine atoms by XPS. The amount of fluorine (F1s) in XPS is directly related to the content of –OH and by stoichiometry of the reaction their relative amount is calculated. Figure 6.3 shows the XPS spectrum for COC microchannels modified with 5% PEGA monomer with and without of TFAA treatment. Typical peaks for C and O in the region of 282.5 and 530 eV, respectively, are found for both samples as expected for a PEGA substrate which contains a back bone made entirely of carbon and oxygen (Figure 6.3 B). In derivatized samples (Figure 6.3 A) a prominent peak for F was observed at 687 eV which shows the successful attachment of TFAA to the COC-PEGA platform. Additionally, a clear increment of the oxygen signal was observed (530 eV), probably due to the carboxylate (-C=O) introduced after TFAA derivatization.

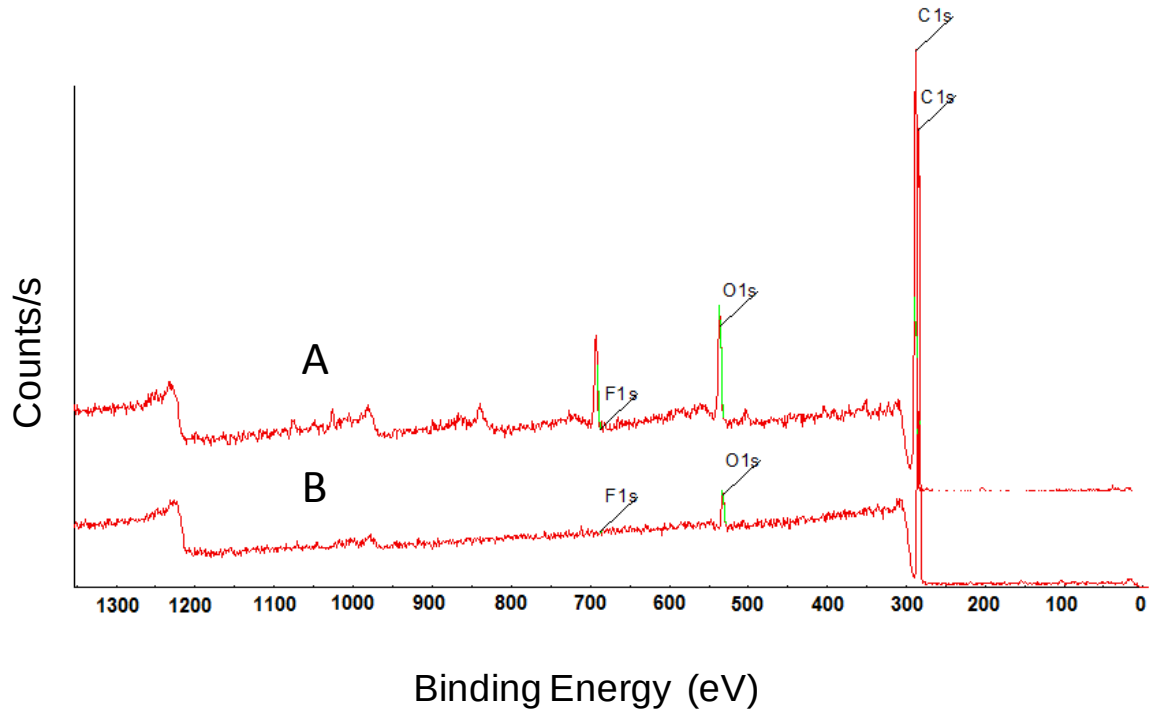

Figure 6.3. XPS spectrum of COC-PEGA microchannels derivatized (A) and underivatized (B) with TFAA. 5% of monomer was used for polymerization of PEGA on COC channels.

The XPS methodology shown, was found to be useful for the efficient in situ characterization of microchannels after chemical modification. Line scans across microchannels, using a X-ray size spot of 120 µm, accurately reproduced the chemical profile of regions inside and outside channels. Figure 6.4 shows, for example, the distance profiles for C, O and F in COC and COC-PEGA samples, both treated with TFAA. As expected, COC shows an almost constant content of C trough the 400 µm region studied, since the material is homogenously COC. However, a constant signal for O and F provides evidence of some residual TFAA adsorbed on COC. For the case of COC-PEGA microchannel it is evident a gradient of C, which shows a depletion in the middle region, where the PEGA modified region is located. That depletion of the C content is expected when the line scans cross the channel and surveys regions of pure hydrocarbon (COC), go later to a reduced C area which contain a high content of oxygen and finally goes back to COC regions. Fluoride (F1s) and Oxygen (O1s) showed the expected profile with regions of high concentration of F1s and O1s at the imprinted channel area (middle zone of the distance profile) corresponding to the PEGA polymerized regions.

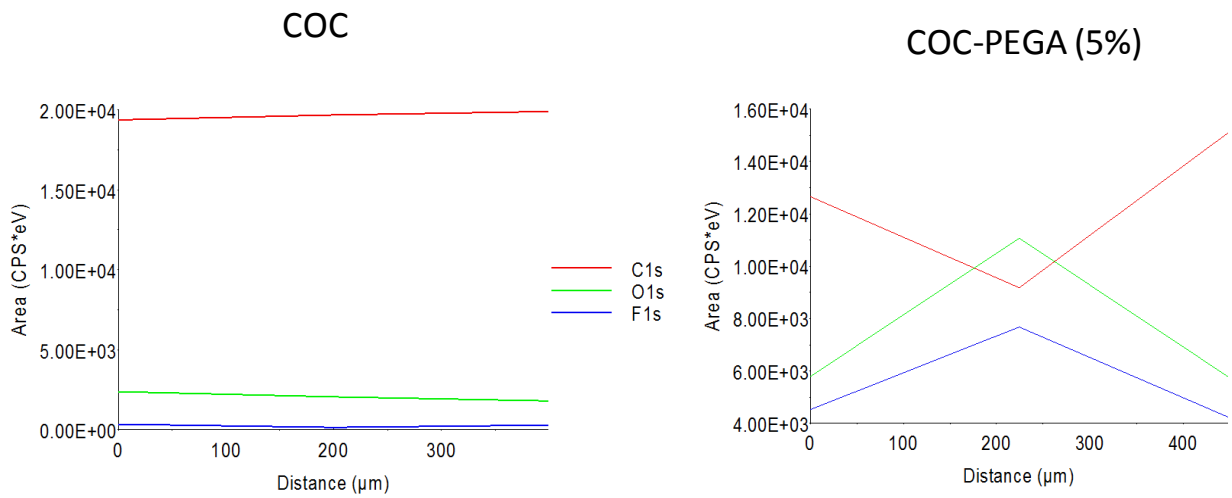

Figure 6.4. XPS line scan profile across COC and COC-PEGA microchannels after treatment with TFAA

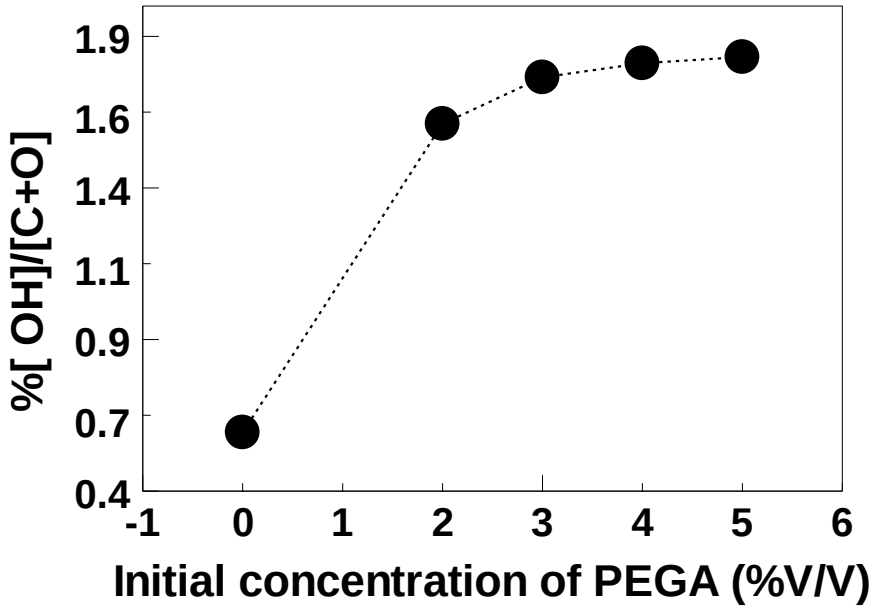

Figure 6.5. Percentage of surface hydroxyls on COC microchannels after photo-grafting with variable concentrations of initial PEGA monomer.

Percentage of hydroxyl abundance was evaluated in COC-PEGA samples prepared by using increased concentrations of PEGA monomer (0-5%) in order to evaluate its relevance in controlling –OH surface availability. Percentage of hydroxyls, in TFAA derivatized COC-PEGA microchannels, were calculated relative to the abundance of carbon and oxygen in un-derivatized samples. In every case, abundance was related to the peak area for each individual element, after correction with appropriate response factors. Extension of the TFAA reaction with PEGA was assumed to be 100%. Figure 6.5 shows the calculated hydroxyl percentage found in COC-PEGA platforms prepared with variable initial concentration of PEGA. Results show a small increase in the abundance of surface hydroxyls as the PEGA monomer increases, from about 1.60% when 2% initial PEGA was used to 1.85% with 5% of PEGA monomer. This result shows that there is not a notable gain in the amount of surface –OH, relative to the whole amount

of atoms available on the surface, due to the initial monomer used in photo-polymerization. Additionally this result shows that the maximum abundance remains under 2%, which is less than the ~3.5% theoretical amount of –OH available in the PEGA monomers used.

Additional characterization of COC-PEGA at variable initial monomer was performed by PSP at three different pHs values. Figure 6.6 shows the results of PSP characterization. The PSP (E) becomes highly reduced with increased monomer concentration, from ~ 250 mV on pristine COC (0% at pH 11.0) to ~ 50 mV when 5% PEGA was used. This reduction of potential is interpreted as a reduced ability of hydroxyl anions to absorb on the underlying COC substrate. Since the surface abundance of –OH appeared to be approximately constant; this steady reduction of PSP (Figure 6.6) is interpreted as a constant increment of the PEGA layer height, which hinders the passage of electrolyte solution ions to COC. However, this implies that the polymer grows producing a constant relative abundance of hydroxyls at the interface.

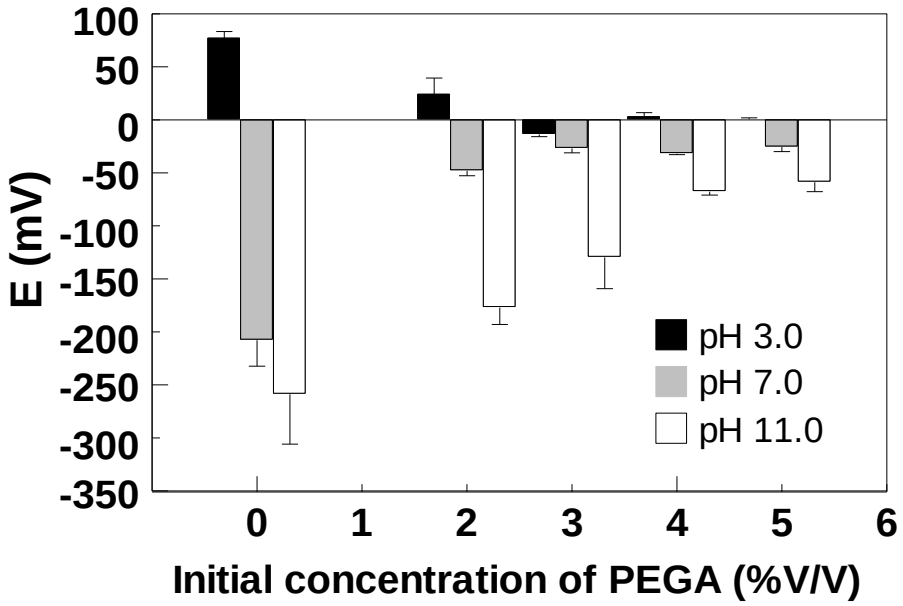

Figure 6.6. Pulsed Streaming Potential of COC grafted with variables concentrations of PEGA monomer. Different pH solutions were produced with phosphate buffer at approximately constant conductivity of 191 ± 5 µS/cm

In general, the abundance of surface hydroxyls in COC-PEGA platforms was very low, around 1.7% of total population of surface atoms. This abundance is believed to be inadequate to produce a reliable sensing surface by direct binding of receptors on the PEGA layer, since this surface will result in a very low coverage of antibodies (< 2%). This values is below the optimal densities found in other label-free detection systems where receptors cover about a 25% of a well pack monolayer[9, 12]. In this light, no further efforts were performed to attain direct attachment of antibodies to COC-PEGA platforms.

6.3.2 Assessment of protein-A coated microspheres linked to COC-PEGA to increase binding site density for antibodies.

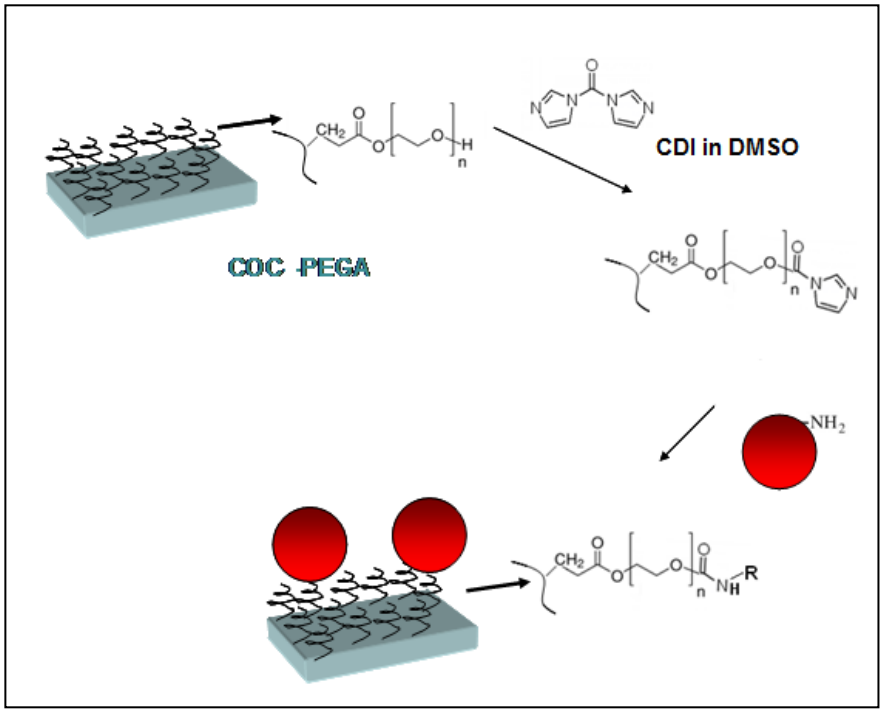

Figure 6.7. General strategy for binding of polystyrene microspheres coated with protein A, to the surface of COC-PEGA microchannels.

As an alternative to increase the surface area available for binding of receptors to the COC-PEGA platform, it was proposed to link polystyrene microspheres coated with protein A to

available surface hydroxyls on the PEGA layer. Activation of surface hydroxyls was carried out following the strategy depicted in Figure 6.7, in which N,N'-carbonyldiimidazole (CDI) is used for activation of surface hydroxyls. CDI has been shown to be efficient in the activation of terminal –OH groups for the attachment of proteins on silica[13] and polyethylene glycol[14]. Additionally, CDI chemistry is much less sensitive to water than the activating agents used for the activation of carboxylates (EDC/NHS)[15]. In this strategy, amine groups present in protein-A were expected to react with activated surface hydroxyl groups.

Table 6.8 Differences in Pulsed Streaming Potentials after binding of polystyrene microspheres coated with protein-A to COC-PEGA microchannels using CDI activation

	Number of Spheres Adsorbed	$\Delta E_{binding}$ pH 3.1 (mV)	$\Delta E_{binding}$ pH 7.2 (mV)	$\Delta E_{binding}$ pH 11.0 (mV)
Microspheres pH 7.4. CDI activated	25 ± 7	102 ± 1	11 ± 1	-85 ± 1
Microspheres pH 8.5 CDI activated	338 ± 244	93.8 ± 0.6	1.0 ± 0.4	-99 ± 1
Microspheres pH 7.4. NO CDI activated	17 ± 24	28 ± 4	-1 ± 1	-19 ± 1
Microspheres pH 8.5 NO CDI activated	21 ± 34	4 ± 0.1	1 ± 1	-29 ± 3
No spheres. Only 50 CDI/mL activation.	-----	95 ± 3	-20.2 ± 0.4	-35.4 ± 0.1
No spheres. Only 500 CDI/mL activation.	-----	81 ± 2	-14.5 ±0.6	-32.2 ± 0.1
No spheres. No activation.	-----	-11 ± 1	-11.7 ± 0.3	-2.8 ± 0.3

Table 6.1 shows PSP characterization at three values of pH, for microsphere linking to COC-PEGA microchannels, through CDI activation. The difference between PSP before and after binding was referred as $\Delta E_{binding}$ for each condition studied: phosphate buffer pH 7.4 and borate buffer pH 8.5.

Results show a high $\Delta E_{binding}$ after binding of spheres for both, phosphate and borate buffer, exhibiting changes close to 100 mV and -100 mV for pH 3 and 11 respectively (Table 6.1). Control experiments were performed by adsorption of microspheres without any CDI activation. Those controls showed a comparatively small $\Delta E_{binding}$, ranging from ~ 20 mV to – 29 mV for pH 3 and 11 respectively (Table 6.1). Additionally, a control carried out with no spheres and no CDI activation showed small changes ranging from ~ -11 to -3 mV for pH 3 and 11. These findings suggest that binding of particles occurs when CDI activation is used, which explain the high changes in PSP. On the contrary, small $\Delta E_{binding}$ when no CDI activation was used could imply a small adsorption of spheres.

In order to confirm these predictions, direct observation of bonded microspheres to the COC-PEGA substrate was performed using Scanning Electron Microscopy (SEM). For each experiment and control, 10 sections of ~ 40 µm x 30 µm along microchannels were observed and number of particles counted manually each time. The results of number of surface spheres are reviewed in Table 6.2. Figure 6.8 presents examples of SEM images obtained for binding of protein-A coated microspheres when borate buffer pH 8.5 was used. Figures 6.8 A, C and E represent control experiments without CDI activation. Figures 6.8 B, D and F show experiment with CDI activation. These results revealed an average of 21 ± 34 particles for the case of no-CDI activation, whereas, the CDI activated channel produced a value of 338 ± 244 particles. Despite the high variance between different spots analyzed along each microchannel, the results show that the use of CDI activation, in the case of borate buffer, produces an increase in the number of particles allocated on the COC-PEGA surface. Borate buffer CDI activation results in a higher number of spheres allocated on the COC-PEGA surface than just passive adsorption. The surface structure of channels after adsorption of spheres at pH 8.5 shows a channel highly

covered with spheres (Figure 6.8 F) with regions of organized packing of spheres (Figure 6.8 D) and regions of less dense, more random distribution (Figure 6.8 F). This shows a good agreement between the number of allocated particles in channels and $\Delta E_{binding}$ obtained for the case of borate buffer pH 8.5.

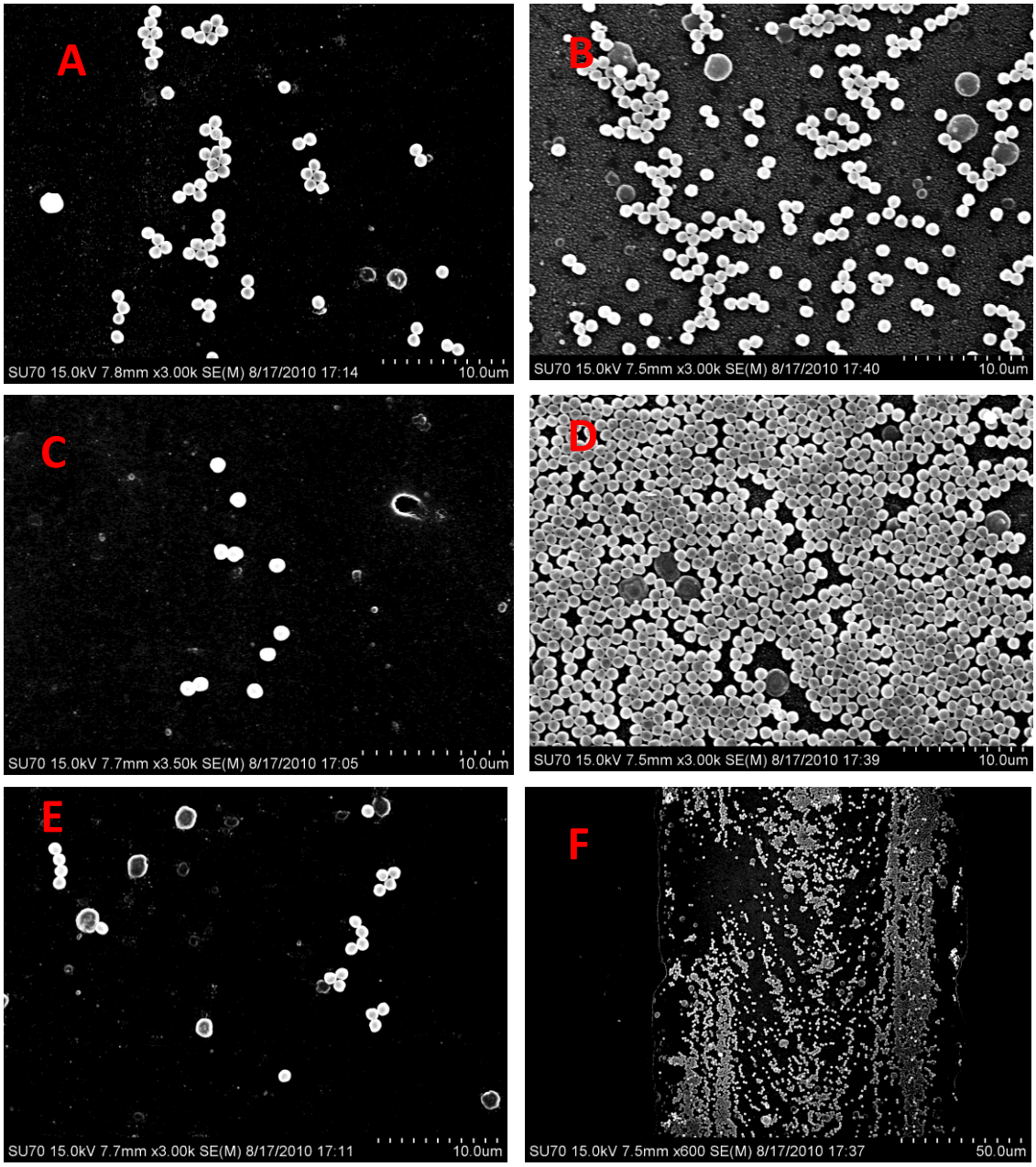

Figure 6.8. SEM images of COC-PEGA microchannels with (B, D, F) and without (A, C, D) CDI activation prior to treatment with protein A coated polystyrene microspheres. Buffer for binding was borate at pH 8.5. Nominal size of the spheres was 0.93 µm. Samples were gold sputtered for 60 seconds prior to SEM imaging.

However, experiments with phosphate buffer (pH 7.4) revealed that even though $\Delta E_{binding}$ is still high (~ 100 mV at pH 3, Table 6.1) the average number of particles bound, 25 ± 7, was in the same range of controls without CDI activation, 17 ± 24. Figure 6.9 shows SEM images for experiments with and without CDI activation using phosphate buffer for the binding step.

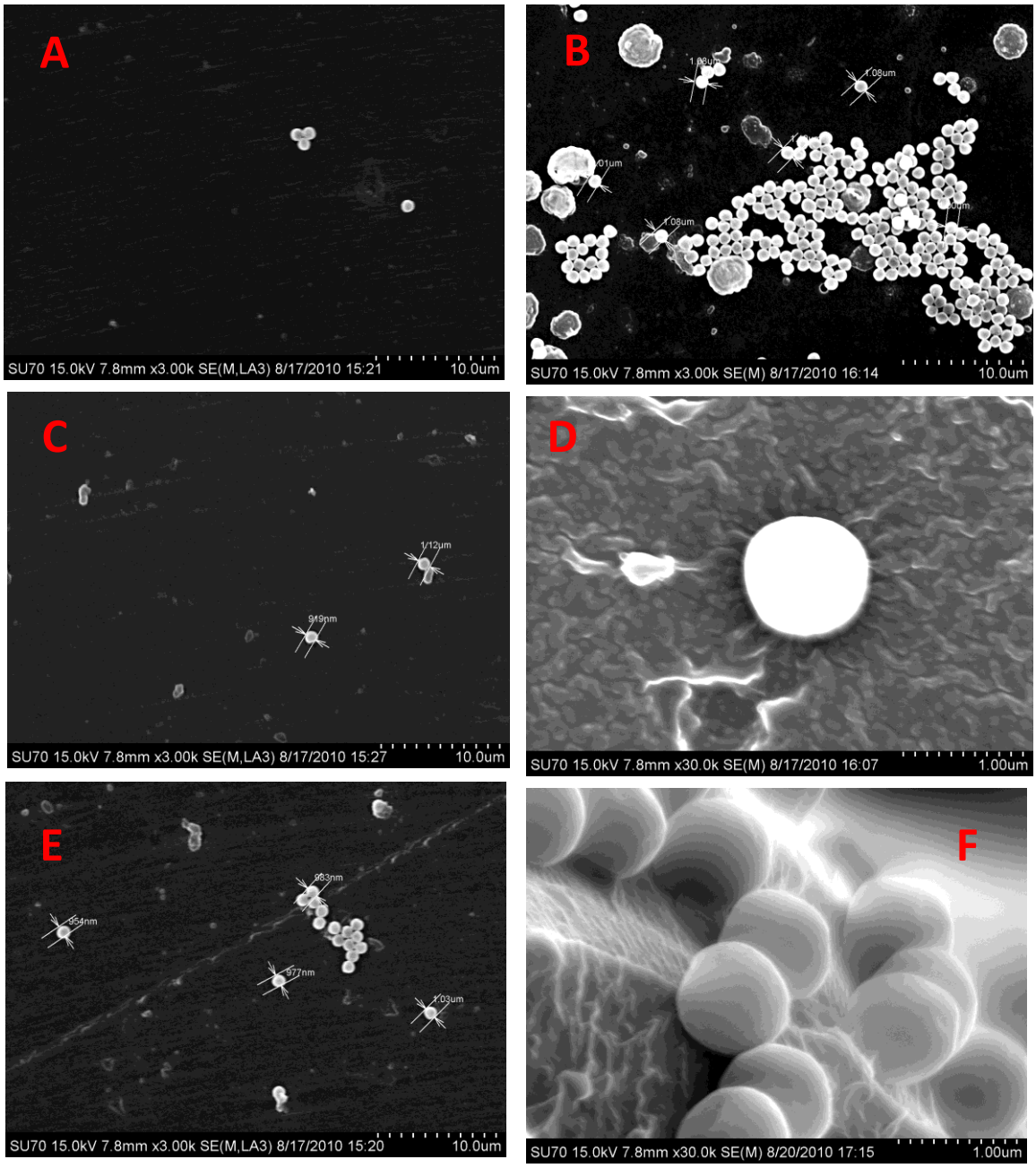

Figure 6.9. SEM images of COC-PEGA microchannels with (B, D, F) and without (A, C, D) CDI activation prior to treatment with protein A coated polystyrene microspheres. Buffer for binding was phosphate at pH 7.4. Nominal size of spheres was 0.93 µm. Samples were gold sputtered for 60 seconds prior to SEM imaging.

SEM pictures show just a few adsorbed particles when no CDI was used (Figure 6.8 A, C, D) as well as for the case of CDI activated microchannels with exceptional spots, which show aggregation of spheres (Figure 6.8 B). Detailed pictures show the substrate PEGA layer with a characteristic worm-like shape, demonstrating the manner in which the protein-A spheres are attached to the COC-PEGA surface (Figure 6.8 D). Additionally, some adsorption of spheres is observed in regions where only COC is present, like in the outlets and inlets of microchannels (Figure 6.8 F).

The result found after analysis of SEM pictures using buffer at pH 7.4, which shows that only few microspheres were bound even after CDI activation, reveals a discrepancy between $\Delta E_{binding}$ and number of allocated particles. As shown before, it turned out that channels with approximately the same number of particles showed four-fold differences in $\Delta E_{binding}$ (spheres with and without CDI activation, pH 7.4, Table 6.1). This evidence points out that surface charge observed with PSP, after -OH activation of PEGA and binding of spheres, is not controlled by linked microspheres. In order to find the source of the huge charge observed, additional control experiments were carried out. Two concentration of CDI, 50 and 500 mg/mL, were used to activate COC-PEGA microchannels but no binding of microspheres was performed. Activated substrates were in contact with microspheres free phosphate buffer for the same period of time used previously for binding. Results shown in Table 6.1 for these experiments reveal that just activation with CDI produces a high $\Delta E_{binding}$. This result reveals that most of the PSP signal at pH 3, for those cases when spheres where linked, can be explained as consequence of the use of CDI. For example, binding of spheres at pH 7.4 on activated COC-PEGA produced a $\Delta E_{binding}$ of

102 mV at pH 3 (Table 6.1), but only CDI activation produced already a $\Delta E_{binding}$ of 95 mV, which explains 93% of the change in PSP at pH 3. Above pH 7 CDI seems to not be the most influential in setting up the surface charge. At pH 11 for example, only CDI produced a $\Delta E_{binding}$ of -35.4 mV which explains 41% of the signal obtained from microspheres binding. The surface charge produced by CDI could be explained by the formation of a very stable carbamate with the PEGA substrate (Figure 6.7), which are not hydrolyzed after the binding period and not used for liking of spheres. Carbamates with a pending imidazole end can be easily protonated a produce the high PSP observed at low pH.. The resistance of this carbamates to hydrolysis, after CDI activation has been reported previously and explained by the slow dynamics of the reaction under phosphate buffer conditions[13, 16]. Here, electrokinetic evidence of this phenomenon has been provided.

In general, the above results show that binding of polystyrene coated with protein-A on COC-PEGA platforms is achievable using CDI activation and borate buffer pH 8.5 for the binding step. However, in this kind of substrate the charge density seems to be controlled by a combination of imidazole pending groups, from CDI, and to a small extent by ~1 µm diameter surface allocated microspheres. Since the objective of using spheres was to eliminate the possibilities of non-specific adsorption, it is believed that CDI activation is not the best option, Since carbamates can be protonated, which produces the option for electrostatic non-specific interactions.

6.3.3 Assessment of passive adsorbed latex amine-coated nanospheres linked to COC-PEGA for binding of antibodies.

The passive adsorption of latex nanoparticles, coated with aliphatic amines, on COC-PEGA platforms, was studied as an alternative method to produce receptor binding sites, without the formation of functionalities on the non-fouling PEGA layer. Table 6.2 shows values of the PSP difference, between COC-PEGA microchannels before and after adsorption of nanospheres ($\Delta E_{adsorption}$). Six different conditions of pH were studied. Results show that low pH ~ 3.0, using citrate and phosphate buffers, produced an appreciable $\Delta E_{adsorption}$ of > 80 mV. Also, citrate buffer pH 4.6 and phosphate buffer pH 11 produced $\Delta E_{adsorption}$ > 100 mV. However, when nanoparticles were dissolved in buffers having a pH close to neutral values, the magnitude of $\Delta E_{adsorption}$ was relatively small, ranging from 25 to 32 mV for phosphate and citrate, respectively.

Table 6.9 Change in PSP for COC-PEGA microchannels after passive adsorption of amine coated latex nanospheres using variable pH for adsorption. pH 3 phosphate buffer , 191 µS/cm was used for PSP determination

$\Delta E_{adsorption}$ Phosphate Buffer pH 3.0 (mV)	$\Delta E_{adsorption}$ Citrate Buffer pH 3.4 (mV)	$\Delta E_{adsorption}$ Citrate Buffer pH 4.6 (mV)	$\Delta E_{adsorption}$ Phosphate Buffer pH 7.0 (mV)	$\Delta E_{adsorption}$ Citrate Buffer pH 7.3 (mV)	$\Delta E_{adsorption}$ Phosphate Buffer pH 11.0 (mV)
131 ± 11	79 ± 3	111 ± 1	25 ± 3	32 ± 1	105 ± 8

Since only nanospheres were used in the adsorption, it is expected that values of $\Delta E_{adsorption}$ correlate with the amount of spheres adsorbed. SEM images of microchannels after passive adsorption of nanoparticles carried out at neutral pH are shown in Figure 6.10. Observation of the surface obtained after 48 hours of contact with amino modified nanosphere dissolved in phosphate buffer pH 7.0 (Figure 6.10 A, B and C) reveal very poor adsorption and the

appearance of the aggregation particles. This aggregation is believed to occur in solution not at the surface, due to the lack of electrostatic repulsion between spheres at neutral pH.

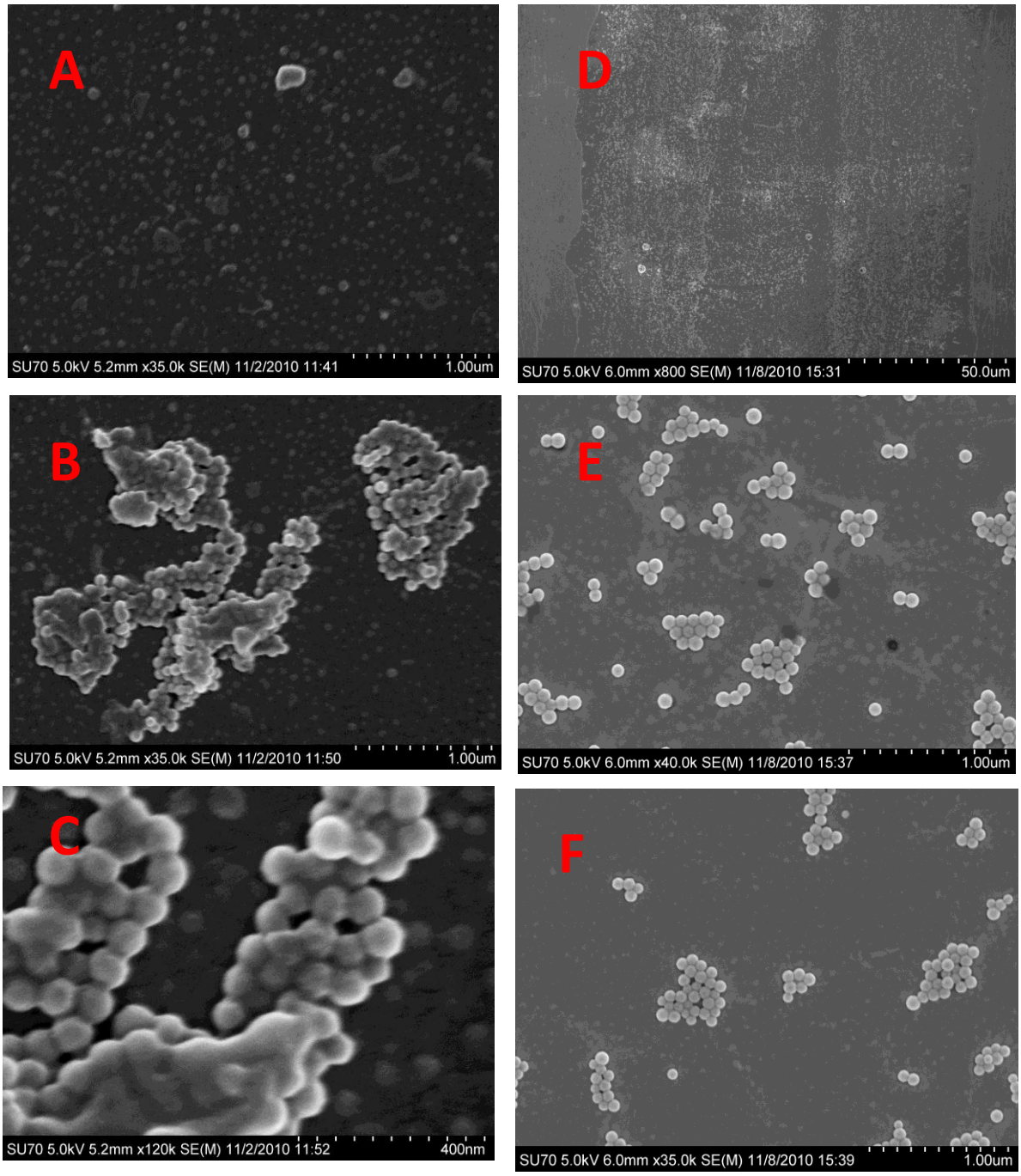

Figure 6.10 . SEM images of COC-PEGA microchannels after passive adsorption of ~ 80 nm nanospheres in phosphate buffer pH 7.0 (A, B C) and citrate buffer pH 7.3 (D, E, F). Time of adsorption was 48 hours. Samples were gold sputtered for 60 seconds prior to SEM imaging.

When citrate buffer pH 7.3 is used as solvent for passive adsorption, a more homogenous distribution of particles is obtained in the COC-PEGA microchannel (Figure 6.10 D). However, a low coverage is still obtained and aggregation of small groups of particles, which does not cover more than 15% of the area studied (Figure 6.10 E and F) is evident. In general, this low adsorption of particles is in agreement with the low values of $\Delta E_{adsorption}$ obtained for neutral pH.

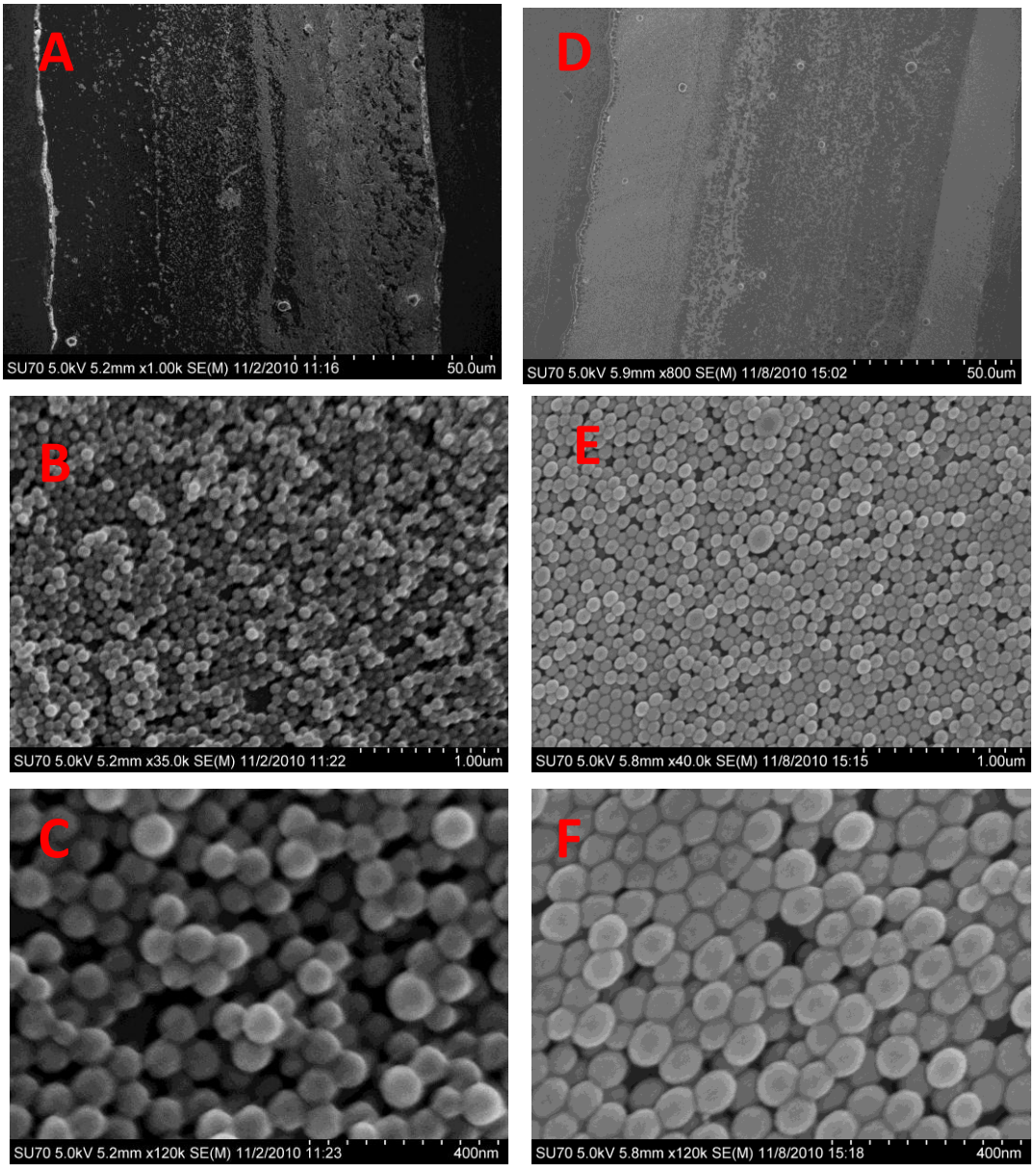

Figure **6.11**. SEM images of COC-PEGA microchannels after passive adsorption of ~ 80 nm nanospheres in phosphate buffer pH 11.0 (A, B C) and citrate buffer pH 4.6 (D, E, F). Time of adsorption was 48 hours. Samples were gold sputtered for 60 seconds prior to SEM imaging.

In contrast, pH conditions which allow the development of appropriated electrostatic repulsion, like pH 11 and 4.6, were demonstrated to produce a high coverage on the COC-PEGA microchannels (Figure 6.11). In the case of phosphate buffer pH 11, complete coverage of large zones inside microchannels with the formation of multilayers was evident (Figure 6.11 A-C). Samples where citrate buffer pH 4.6 was used as solvent for adsorption showed a similar behavior. However, a more homogeneous arrangement seems to be achieved. This high density of particles on the sensor platform is in accordance with the high values of $\Delta E_{adsorption}$ obtained by PSP (Table 6.2)

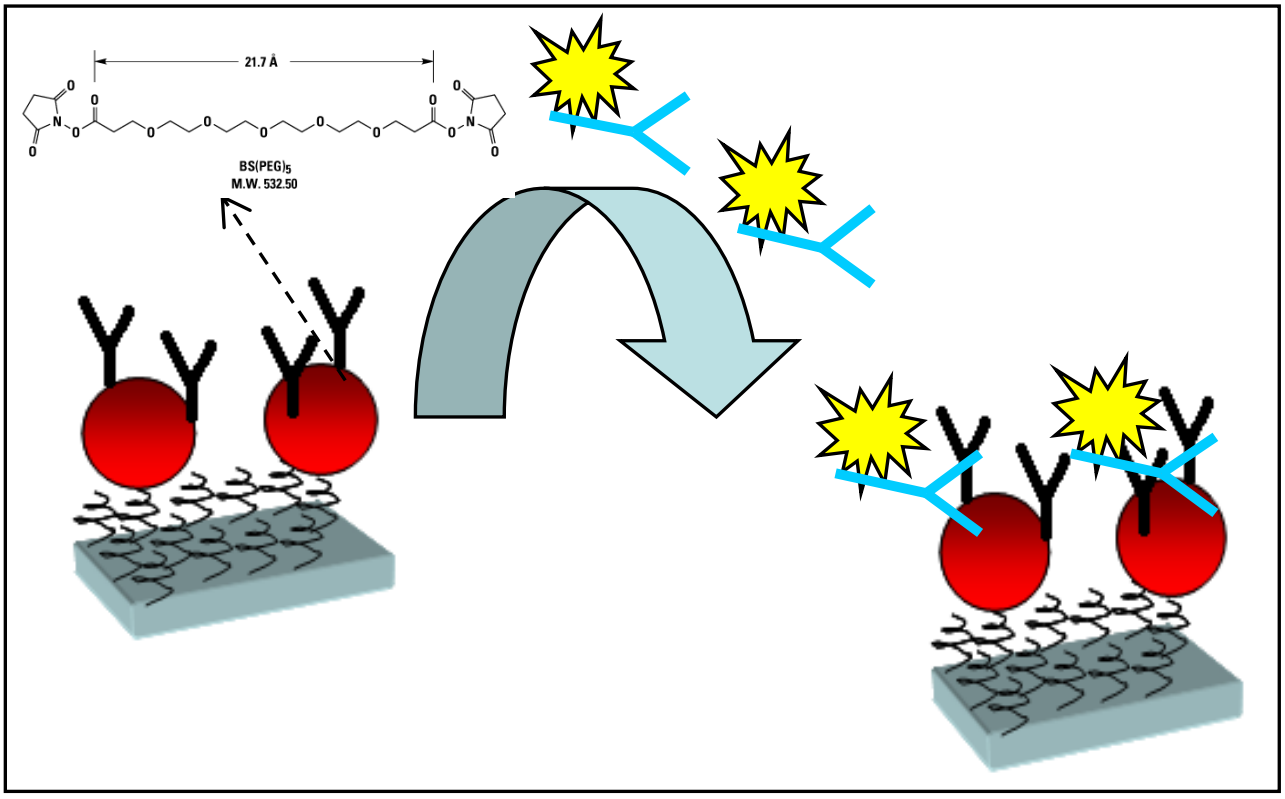

Figure 6.12. General strategies for the attachment of antibodies to amine coated latex nanospheres adsorbed on COC-PEGA microchannels and their recognition with fluorescent label secondary antibody.

This finding provides strong evidence that in the case of ~ 80 nm nanospheres allocated on COC-PEGA microchannels, control over surface charge is held exclusively by charge brought by

nanospheres. This fact allows speculation that this dual surface made of hydrogel-nanospheres is compatible with PSP measurements since adsorption of specific targets on nanospheres will change the overall charge. Following that concept, high coverage of nanoparticles were used later to bind antibodies to the amine groups present on their surface. In order to avoid direct contact of receptors to the nanosphere, which could hinder and damage their detection capabilities, the homobifunctional cross linker ($BS(PEG)_5$) was used (Figure 6.12).

This cross linker is able to attach one of its sides to the aliphatic amine groups on nanospheres and the free end to amine groups in the antibody. The general strategy of attachment is depicted in Figure 6.12, which was carried out in COC-PEGA-Nanospheres platforms obtained using phosphate buffer pH 3 and 11 and citrate pH 4.6 as solvents for passive adsorption. Figure 6.12 also describes the method used to evaluate the efficiency of antibody attachment, which consists in the use of a secondary, fluorescent (FITC) labeled antibody which recognizes the Fc section of mouse monoclonal antibodies linked to nanoparticles.

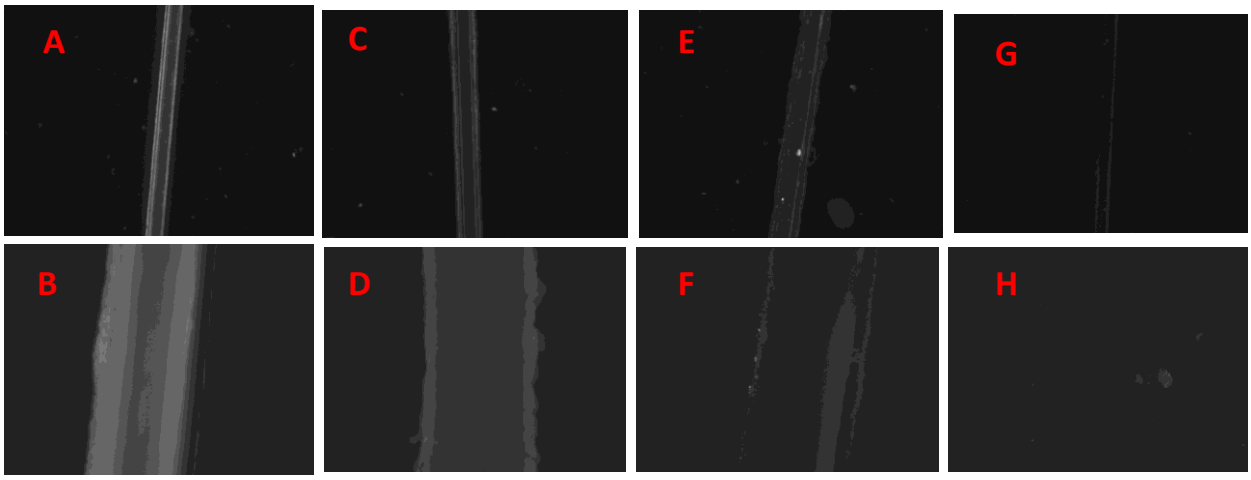

Figure 6.13. Fluorescence developed after application of secondary FITC labeled antibody on COC-PEGA-Nanoparticles platforms linked with monoclonal anti PSA. Platforms contain 80 nm amine-coated latex nanopheres passive adsorbed using citrate buffer pH 4.6 (A-B), phosphate buffer pH 3.0 (C-D) and phosphate buffer pH 11.0 (E-F),. Panels G-H show fluorescence in control experiment for channels where no anti-PSA was linked.

Results of fluorescence experiments, after application of labeled FITC secondary antibodies, show a successful binding of monoclonal anti-PSA antibodies to the COC-PEGA-Nanospheres surface (Figure 6.13). Additionally, the highest fluorescence was obtained with citrate pH 4.6 buffer, whereas phosphate buffers pH 3.0 and 11.0 gave a faded signal. Control experiments, where no anti-PSA antibodies were bound to spheres, revealed that a very low non-specific adsorption of secondary antibody took place on COC-PEGA-Nanosphere (Figure 6.13 G-H). This last finding showed additionally that fluorescence was due to the specific recognition of anti-PSA antibodies on the microchannel surface.

These results showed that it is possible to create a high coverage of amine-coated latex nanospheres on COC-PEGA microchannels by simple passive adsorption. Additionally, results showed that it was possible to use the allocated nanoparticles on COC-PEGA platforms to anchors receptors to the microchannel.

6.3.4 Detection of Prostate Specific Antigen (PSA) and Lysozyme by PSP on COC-PEGA-Nanoparticles-Antibody platforms.

The COC-PEGA-Nanoparticle platform with bound antibodies was evaluated as a sensing surface for real time Pulsed Streaming Potentials detection of the prostate cancer biomarker PSA. Figure 6.14 shows the real time profile adsorption-desorption of 504 nM PSA as well as the adsorption phase for 40 nM PSA. Results show a clear detection of both concentrations of PSA. As expected, the signal was manifested as a rise in the value of Ec, which resulted in a change from -1 to ~ -0.91 and -0.86 for 504 and 40 nM PSA, respectively. Even though PSP signals were small it is worth mentioning that the hydrogel-nanosphere platform produce some differentiation between PSA concentrations. This differenciation is obvious even at conditions

were a very low charge or no charge at all is expected to be developed on the protein, since the pH used for real time PSP (7.0) was almost the reported isoelectric point of PSA (6.9)[17]. Additionally, the control experiment, where no antibody was linked to nanospheres showed a depletion of Ec, instead of an increment, after adsorption of 504 nM of PSA. This finding shows that the signal produced on antibody modified spheres is due to specific interactions, since non-specific interaction obtained in no-linked receptor platform leads to the opposite time profile (Figure 6.13). This implies a high increment of signal/noise ratio and points out that selectivity could be enhanced in PSP measurements when studied targets are analyzed at a pH close to their isoelectric point so electrostatic, non-specific interactions can be inhibited.

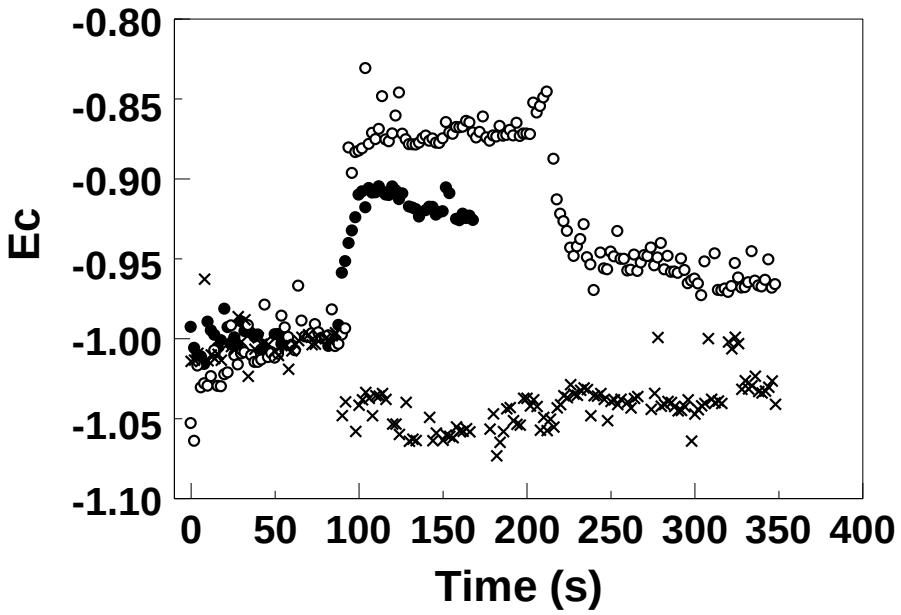

Figure 6.14. Real time Pulsed Steaming Potentials for adsorption of 40 nM (black dots) and 504 nM (open dots) of PSA on COC-PEGA-Nanoparticles platform where mouse monoclonal anti-PSA was bound using homobifunctional crosslinker $BS(PEG)_5$ through amine-coated nanospheres. Adsorption of 504 nM PSA was also performed in a platform without linked antibody (equis x). Adsorption was carried out in phosphate buffer pH 7.0 and 196 ± 8 µS/cm

However, in terms of limits of detection PSP measurement of PSA are far beyond of clinical relevant concentrations for diagnosis which are in the range 15-36 pM. [18] This points out in general the need for a investigation of an amplification mechanism compatible with label-free Pulsed Streaming Potentials.

6.6 Conclusions.

It has been demonstrated that microchannels modified with a non-fouling PEGA layer have a small surface concentration of potentially derivatizable hydroxyls, useful for direct binding of selective receptors at its surface. However, amine coated nanospheres, passively adsorbed on PEGA layers, were demonstrated to be an alternative way to link antibodies to microchannels. Passive adsorption was demonstrated to be the best method to put spheres on the channel, when compared with chemical bonding of spheres, since no functionalities are created at the surface and non-specific adsorption is reduced. Platforms made using this dual, hydrogel-nanospheres, surface were proven to be useful for detection of Prostate Specific Antigen (PSA) using monoclonal anti-PSA antibodies and Pulsed Streaming Potentials. In general, adsorbed nanospheres on non-fouling layers are shown to be an option for sensing platform to PSP analysis, which requires further research.

After development of real-time Pulsed Streaming Potentials as a viable method for the label-free study of adsorptive processes between biomolecules and sensing surfaces in microchannels, it is envisioned that further fundamental understanding of the mechanisms of PSP detection, will provide a cost-efficient alternative for current label-free detection methods. Under the light of the results here disclosed, it is suggested that further development should focus on three principal topics: the determination of the relationship between the amount of adsorbed molecules and PSP, the amplification of the PSP signal for low or non-charged molecules and the fabrication of

platforms with reduced non-specific adsorption and controlled surface configuration of specific receptors.

6.5 References.

1. Luna-Vera, F., Alvarez, J.C., Adsorption kinetics of proteins in plastic microfluidic channels: Real-time monitoring of lysozyme adsorption by pulsed streaming potentials. *Biosens.Bioelectron.* **2010,** 25, 1539-1543.
2. Gupta, M. L., Bruson, K., Chakravorty, A., Kurt, P., Luna-Vera, F., Alvarez, J.C., Wynne, K.J., Quantifying surface-accessible quaternary charge for surface modified coatings via streaming potential measurements. *Langmuir* **2010,** 26, (11), 9032-9039.
3. Luna-Vera, F., Ferguson, J.D., Alvarez, J.C., Real time detection of lysozyme by pulsed streaming potentials using polyclonla antibodies immobilized on a renewable nonfouling surface inside plastic microfluidic channels. *Anal.Chem* **2011,** 83, (6), 2012-2019.
4. Zimmerman, R., Norde, W., Martien, A.C.S., Werner, C., Electrokinetic characterization of poly(acrylic acid) and poly(ethylene oxide) brushes in aqueous electrolyte solutions. *Langmuir* **2005,** 21, 5108-5114.
5. Dukhin, S. S., Zimmermann, R., Werner, C., Electrokinetic phenomea at grafted polyectrolyte layers. *J.Colloid. Interf. Sci.* **2005,** 286, 761-773.
6. Pu, Q., Oyesanya, O. Thompson, B., Liu, S., Alvarez, J.C., On-chip micropatterning of plastic (cyclic olefin copolymer, COC) microfluidic channels for the fabrication of biomolecule microarrays using photografting methods. *Langmuir* **2007,** 23, (3), 1577-1583.
7. Langley, L. A., Villanueva, D.E., Fairbrother, H., Quantification of surface oxides on carbonaceous materials. *Chem. Mater.* **2006,** 18, 169-178.
8. Sutherland, I., Sheng, E., Brewis, D.M., Heath, R.J., Studies of vapour-phase chemical derivatisation for XPS analysis using model polymers. *J.Mater.Chem.* **1994,** 4, (5), 683-687.
9. Zhu, H., Dale, P.S., Caldwell, C.W., Fan, X., Rapid and label-free detection of breast cancer biomarker CA15-3 in clinical human serum samples with optofluidic ring resonator sensors. *Anal.Chem* **2009,** 81, 9858-9865.
10. Carter, J. A., Mehta, S.D., Mungillo, M.V., Striemer, C.C., Miller, B.L., Analysis of inflamatory biomarkers by arrayed imaging reflectometry. *Biosens.Bioelectron.* **2011,** In press, (In press).
11. Daniels, J. S., Pourmand, N., Label-free impedance biosensors: opportunities and challenges. *Electroanalysis* **2007,** 19, (12), 1239-1257.
12. Peluso, P., Wilson, D.S., Do, D., Venkatasubbaiah, M., Quincy, D., Heidecker, B., Pointdexter, K., Tolani, N., Phelan, M., Witte, K., Jung, S.L., Wagner, P., Nock, S., Optimizing antibody immobilization strategies for the construction of protein microarrays. *Anal.Biochem.* **2003,** 312, 113-124.

13. Crowley, S. C., Chan, K.C., Walters, R.R., Optimization of protein immobilization on 1,1'-carbonyldi-imidazole-activated diol-bonded silica. *J.Chromatogr.* **1986,** 359, 359-368.
14. Beauchamp, C. O., Gonias, S.L., Menapace, D.P., Pizzo, S.V., A new procedure for synthesis of polyethylene glycol-protein adducts; Effects on function, Receptor recognition, and clearance of superoxide dismutase, lactoferrin and a_2-Macroglobulin. *Anal.Biochem.* **1983,** 131, 25-33.
15. Hermanson, G. T., *Bioconjugate Techniques*. 2 ed.; Elsevier Sciences: London, UK, 2008; p 1323.
16. Bethell, G. S., Ayers, J.S., Hearn, M.T.W., Hancock, W.S., *J.Chromatogr.* **1981,** 219, 353.
17. Chu, M. T., Prostate-specific antigen in screening of prostate cancer. *J.Clin.Lab.Anal* **1994,** 8, 323-326.
18. Waggoner, P. S., Varshney, M., Craighead, H.G., Detection of prostate specific antigen with nanomechanical resonators. *Lab. Chip* **2009,** 9, 3095-3099.

Vita

Fernando Luna Vera was born on January 1, 1979, in Bogotá, Colombia, and is a Colombian citizen. He graduated from San Bartolomé la Merced High School, Bogotá, Colombia in 1996. He received his Bachelor of Sciences in Chemistry from Universidad Nacional de Colombia, Bogotá, Colombia. Subsequently he worked as researcher in the Centro Control Contaminación del Pacifico, Tumaco, Colombia and later he was lab manager at Daphnia Ltda, Bogotá, Colombia. He was the recipient of the Mary E. Kapp service award in spring 2011.